INFLAMMATORY STRESS IN THE CEREBELLUM: IMPLICATIONS FOR NUTRITIONAL INTERVENTION IN ALCOHOL-MEDIATED CNS DAMAGE

By

Mary Barile Hogan

RECOMMENDED:

Advisory Committee Chair

(William Simpson)

Chair, Department of Chemistry

APPROVED:

Dean, College of Natural Science and Mathematics

Dean of the Graduate School

March 27, 2012

Date

INFLAMMATORY STRESS IN THE CEREBELLUM: IMPLICATIONS FOR NUTRITIONAL INTERVENTION IN ALCOHOL-MEDIATED CNS DAMAGE

A

THESIS

Presented to the Faculty

of the University of Alaska Fairbanks

in Partial Fulfillment of the Requirements

for the Degree of

MASTER OF SCIENCE

By

Mary Barile Hogan, B.S.

Fairbanks, Alaska

May 2012

Abstract

Presently there are no effective disease-modifying treatments to combat neurodegeneration among chronic alcoholics. Alcohol abuse imparts a sustained presence of oxidative stressors, including pro-inflammatory cytokine TNFα, in the brain. A persistent presence of TNFα leads to an accumulation of reactive oxygen species, which promotes oxidative damage, subsequent neurodegeneration, and ultimately permanent cognitive changes in afflicted individuals. Our laboratory has demonstrated the potency of ursolic acid, isolated from Alaskan blueberries, to abolish TNFα mediated neurotoxicity in human neuroblastoma cells. Our current study investigated the neuroinflammatory effects of ethanol and TNFα on dissociated neurons and glia cells cultured from embryonic chicks while quantitatively evaluating the preventive and therapeutic effectiveness of blueberry extracts. We compared both CNS and PNS neurons to examine correlations to clinically indicated neurodegeneration. Our results clearly revealed a particular sensitivity of cerebellar neurons to oxidative stress; however, supplementation with blueberry extracts rescued neuronal health by up-regulating antioxidant defenses, suppressing TNFα secretion, blunting lipid peroxidation, restoring cytoskeleton organization, modulating lipid rafts and altering the lipid environment of ion channels. Implementation of blueberries into the diet may offer an inexpensive and safe means to improve quality of life and reduce future health care costs associated with alcohol abuse and neurodegenerative disease.

Table of Contents

List of Figures

Page

Chapter 2

Chapter 3

Chapter 5

Appendix A: Additional Figures

List of Tables

Appendix B: Additional Statistical Data

List of Appendixes

List of Abbreviations

BAC	Blood Alcohol Content
BBB	Blood Brain Barrier
BBX	Crude Blueberry Extract
BCA	Bicinchoninic Acid
BHT	Butylated Hydroxytoluene
BLK	Blank (diluent only)
BSA	Bovine Serum Albumin
C	Cortical Forebrain
Cal	Calbindin-D-28K (Purkinje marker)
CAM	Cellular Adhesion Molecules
Cb	Cerebellum
CD14	Cluster of differentiation group of cell surface marker proteins (14)
COX-2	Cyclooxygenase - 2
CNS	Central Nervous System
DHA	Docosahexaenoic acid
DMEM	Dulbecco's Modified Eagle Medium
DRG	Dorsal Root Ganglia
E35	Ethanol concentration (35mM)
ED	Embryonic Day
EDTA	Ethylenediaminetetraacetic acid

ELISA	Enzyme Linked Immunosorbent Assay
FBS	Fetal Bovine Serum
FdUr	Fluorodeoxyuridine
FITC	Fluorescein Isothiocyanate
G	Glia (cerebellar origin)
GFAP	Glial Fibrillary Acidic Protein (astrocyte marker)
GM1	Ganglioside-1 (LR marker)
GPI	Glycosylphosphatidylinositol
HBSS	Hank's Balanced Salt Solution
H2DCFDA	2',7'-Dihydrodichlorofluorescein Diactate
HRP	Horseradish Peroxidase
LPS	Lipopolysaccharide
LR	Lipid Raft
MAPK	Mitogen-activated Protein Kinase
MBCD	Methyl-B-Cyclodextrin
MDA	Malondialdehyde
MTT	3-(4,5-Dimethylthiazol-2-yl)-2,5-Diphenyl Tetrazolium Bromide
NADPH	Nicotinamide Adenine Dinucleotide Phosphate
Nav	Voltage-gated Sodium Ion Channel
NF	Neurofilament (Neuron marker)
NF-kB	Nuclear Factor Kappa-light-chain-enhancer of Activated B Cells
NGF	Nerve Growth Factor

NOX	NADPH Oxidase
NP	Non-polar BBX Fraction
nSMase	Neutral Spingomyelinase
NT	No Treatment Negative Control
OA	Oleanolic Acid
OB	Olfactory Bulb
P	Polar BBX Fraction (5ug/ml)
PBS	Phosphate Buffered Saline
PBST	Phosphate Buffered Saline with Tween 20
PNS	Peripheral Nervous System
RNS	Reactive Nitrogen Species
ROS	Reactive Oxygen Species
S	Spine
SDS	Sodium Dodecyl Sulfate
SF	Serum-Free
TBS	Tris-Buffered Saline with Tween 20
TBST	Tris-Buffered Saline with Tween 20
TJ	Tight Junctions
TLR	Toll-like Receptor
TNFα	Tumor Necrosis Factor Alpha
TRITC	Tetramethylrhodamine-5-(and 6)-isothiocyanate
UA	Ursolic Acid from BBX

Acknowledgements

This thesis research was supported in part by the Alaska Experimental Program to Stimulate Competitive Research through the National Science Foundation grant **(EPSCoR NSF grant - EPS-0701898)** awarded for the spring semester of 2011.

I would sincerely like to express my thanks to the Department of Chemistry and Emily Reiter for training me and entrusting in me the important task of teaching undergraduate students the fundamentals of chemistry in the lab. I may have learned more than they did.

Other people's hard work set the foundation for my own research. I would like to thank Colin McGill for developing the fractionation technique that produced the blueberry extracts my study hinged on. Additionally, I would like to thank Kriya Dunlap and Sally Gustafson for their work on neutral sphingomylinase (nSMase), nicotinamide adenine dinucleotide phosphate oxidase (NADPH oxidase or NOX), and lipid rafts in neuroblastoma cells. You were my introduction to biochemistry in the laboratory.

I'd like to thank my committee members, Kriya Dunlap and Sarah Ying, for their support and guidance in my graduate studies and research. To my advisor, Tom

Kuhn, thank you for allowing me to follow my interests and investigate freely. I especially appreciate your confidence in me and my work.

Most importantly, I'd like to thank my husband, Mike, and our three daughters for their unwavering support of me in my return to school, and ultimately to my Creator and Savior Jesus Christ for saving my life and providing strength for today and security for tomorrow.

Chapter 1: Purpose of Research

1.1 Significance

This study identified possible nutritional therapies capable of negating chronic neuroinflammation and degeneration due to alcohol abuse. Analysis compared different regions of the central and peripheral nervous systems to the cerebellum. Although the cerebellum comprises only ten percent of the brain's volume, it houses half of the brain's neurons and has been shown to be particularly vulnerable to alcohol abuse (Baker et al. 1999). Because the cerebellum is implicated in a broad spectrum of disorders including autism, schizophrenia, depression, and multiple movement disorders, the results of this study are applicable to many neurological and inflammatory disorders compounded and possibly induced by alcohol abuse. Oxidative stress is a common thread in the complex diseases associated with alcohol abuse and therefore interventions that disrupt the neuroinflammatory cascade are critical to the prevention of irreparable neuronal damage and degradation. Ursolic acid, isolated from natural products, has shown great promise in abutting oxidative stress in the liver and cardiovascular system, but very little is known about its ability to confer neuroprotection in the 8.1 million alcoholics living in America today (Saraswat et al. 2000, Mahadik et al. 2001, Saravanan et al. 2006, Saravanan and Pugalendi 2006). Ursolic acid and other blueberry biomolecules may stymie development of future neurodegenerative disease as well as inflammation associated with metabolic syndromes and arteriosclerosis prevalent

in alcoholics. This study advances our understanding of the neuroinflammatory effects of alcohol and provides a novel nutritional approach through blueberry supplementation to improve the overall health of alcoholics and unborn babies subject to maternal alcohol abuse.

1.2 Innovation

This research utilized an *in vitro* model system that concordantly determined neuron and glia specific alterations in the brain, spine, and dorsal root ganglia due to ethanol and TNFα exposure. Additionally, this study determined the effectiveness of preventive and intervening blueberry therapies on subsequent neuroinflammation and oxidative stress. Our approach gave a unique picture of how oxidative stress presents in cerebellar neurons and glia, as compared to other regions of the central and peripheral nervous systems. The embryonic chick model was used for dissociated neuronal and glial studies. Not only did it provide insight into the cellular mechanisms of alcohol abuse, but it could be further manipulated to examine the vulnerability of the developing cerebellum in cases of fetal alcohol syndrome. Since blueberry extracts drastically reduced oxidative stress and inflammatory cytokine release in our cellular model they may also confer protection to abusing mothers, thus sparing developing babies many dire consequences of maternal alcohol use.

1.3 Specific Aims

1.3.1 Summary of Specific Aims

The goal of this research was to determine whether natural products derived from wild Alaskan blueberries could effectively blunt the chronic neuroinflammatory cycle induced by alcohol abuse. Excessive alcohol intake, even sporadically, results in a sustained presence of inflammatory stressors in the brain (Crews et al. 2006). Increasing evidence has linked neuroinflammation with neuronal death attributed to alcoholism, Parkinson's disease, Alzheimer's disease, multiple sclerosis, cerebellar ataxia, and other chronic disorders, either as the primary cause or compounding factor (Frank-Cannon et al. 2009). Therefore, interventions that disrupt the neuroinflammatory cascade are critical to the prevention of irreparable neuronal damage and degeneration.

Alcohol abuse, coupled with a dietary shift to more processed foods, may increase chronic inflammation and predispose individuals to neurodegenerative disease. Here in Alaska, the alcohol mortality rate in rural Alaska Native communities stands at ten times the national average and is coupled with the poorest nutrition and highest obesity rates within the state (Ehrlander 2010, Fenaughty et al. 2009). We proposed that supplementation of blueberries, highly enriched in the traditional Alaska Native diet, would potentially mitigate inflammatory stress and thus reduce the irreversible neurodegenerative effects of alcohol abuse.

1.3.2 Hypothesis

Chronic exposure to ethanol will induce oxidative stress, critically altering neuronal membranes and cytoskeleton dynamics, which in turn will produce permanent morphological changes and lasting behavior and motor impairment to such individuals. We hypothesized that natural compounds isolated from wild Alaska blueberries would blunt the inflammatory effects of ethanol by restoring neuronal and glial membrane and cytoskeleton dynamics, reducing oxidative stress, and ultimately preventing irreversible neurodegeneration.

1.3.3 Aim 1

Using the embryonic chick model, we defined the inflammatory response of dissociated neurons and glia to increasing concentrations of ethanol over time and determined the effectiveness of preventive/therapeutic strategies utilizing blueberry extracts (BBX) and the isolated compound, ursolic acid (UA), on neuroinflammation.

Ethanol neurotoxicity was assessed by quantifying oxidative stress through reactive oxygen species (ROS) production, tumor necrosis factor alpha (TNFα) production, metabolic viability, antioxidant capacity, lipid peroxidation, and cytoskeletal integrity in dissociated neurons and glia of the cerebellar cortex, forebrain cortex, spine, dorsal root ganglia (DRG), and olfactory bulb.

1.3.4 Aim 2

Using the embryonic chick model, we defined the inflammatory response of dissociated neurons and glia to TNFα over time and determined the effectiveness of preventive/therapeutic strategies of BBX and UA supplementation on neuroinflammation.

TNFα neurotoxicity was assessed by quantifying oxidative stress through ROS production, metabolic viability, antioxidant capacity, lipid peroxidation, and cytoskeletal integrity in dissociated neurons and glia of the cerebellar cortex, forebrain cortex, spine, DRG, and olfactory bulb.

1.3.5 Aim 3

Using the embryonic chick model, we quantified lipid raft modifications in dissociated neurons and glia of the cerebellum, forebrain, and DRGs due to increasing doses of ethanol and intervention with BBX and UA. Lipid rafts were assessed through microscopy and through quantifiable fluorescence.

1.3.6 Aim 4

Using the embryonic chick model, we quantified lipid raft modifications in dissociated neurons and glia of the cerebellum, forebrain, and DRGs due to insult with TNFα and intervention with BBX and UA. Lipid rafts were assessed through microscopy and quantifiable fluorescence.

1.3.7 Aim 5

Using the embryonic chick model, we determined the effects of ethanol and blueberry compounds on voltage-gated sodium ion channels and their association with lipid rafts in cerebellar neurons. Sodium ion channels were assessed through microscopy, quantifiable fluorescence and enzyme linked immunosorbent assays (ELISA).

Chapter 2: General Introduction

2.1 Neuroinflammation

The central nervous system (CNS) possesses a dynamic immune and inflammatory response to a variety of insults such as trauma, stroke, infection, and toxin exposure (Rivest 2009). Typically, an acute neuroinflammatory response ensues from such insults wherein microglia are activated and inflammatory mediators (i.e. cytokines and chemokines) are released. Although oxidative stress is also triggered, this temporary condition is unlikely to detrimentally affect long-term neuronal survival and is thus deemed beneficial to the CNS (Frank-Cannon et al. 2009). Chronic neuroinflammation however, elicits a long term self-perpetuating neuroinflammatory response that outlives the initial insult or injury. The continual activation of microglia and sustained release of inflammatory mediators exasperates the CNS's ability to handle oxidative stress (Tansey et al. 2007). Chronic neuroinflammation no longer serves the protective role brought on by acute responses and may expose the brain to breeches of the blood brain barrier (BBB) (Rivest 2009).

2.2 Oxidative Stress

Oxidative stress refers to the steady state of oxidative damage caused by the reactive oxygen species (ROS). Oxidative stress can be isolated at the molecular level or affect an entire organism. ROS is composed of free radicals

and peroxides that are derived from oxygen metabolism and therefore inherently exist within all aerobic organisms. Due to unpaired electron(s), free radicals are highly unstable and can extract electron(s) from nearby molecules eliciting oxidative damage to DNA, lipids, and proteins which cause drastic cellular changes that can affect the entire organism (Beal 1995). Free radical production is ideally balanced by its consumption by antioxidants. Oxidative stress therefore occurs when the balance of antioxidants is outweighed by pro-oxidants (Seis 1991).

2.3 Microglia

The microglia are the macrophages of the CNS and primary mediators of neuroinflammation. In a healthy brain, microglia dynamically sample their microenvironment through continual extension and retraction of their processes (Nimmerjahn et al. 2005, Raivich 2005). When activated, microglia transform their structure to fill functional protective and repair roles (Tansey et al. 2007, Tansey and Wyss-Coray 2008). These activated microglia now act as phagocytes that scavenge cellular debris, dying cells and neurotoxins. They also secrete trophic factors that promote neuronal survival and a variety of inflammatory mediators (*cytokines*: TNFα and interleukins IL-1B and IL-6; *chemokines*: macrophage inflammatory protein MIP-1a, monocyte chemo-attractant protein MCP-1, interferon IFN, and inducible protein IP-10) that promote the inflammatory state (Frank-Cannon et al. 2009, Schmidt et al. 2009).

In addition to environmental insults, genetic mutations may produce toxic proteins that unceasingly promote microglial activation and lead to aberrant responses to subsequent insults as illustrated in Fig 2.1 (Frank-Cannon et al. 2009). Neuroinflammation is the brain's required response to clear cellular debris, limit tissue damage, and contribute to wound repair within the CNS. It is critical to distinguish the inflammatory factors and mechanisms that lead to neurotoxicity and death from the neuroprotective effects of microglia (Liu et al. 2003).

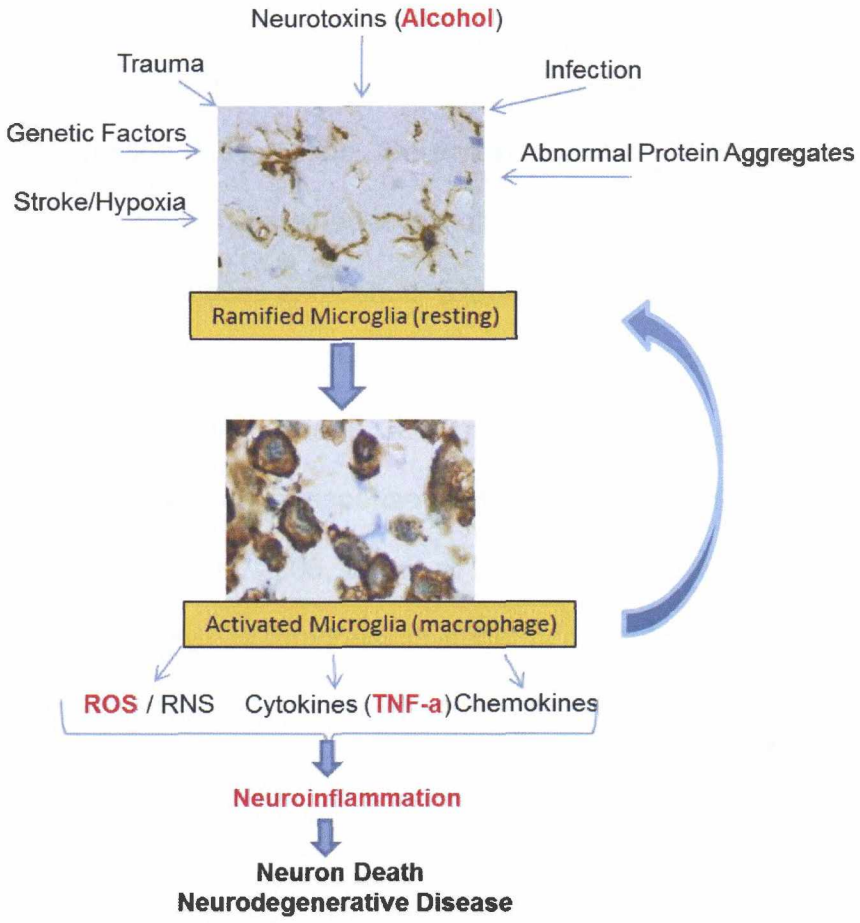

Fig 2.1 Neuroinflammatory Pathways may Lead to Neurodegeneration
Chronic neuroinflammation may lead to neuronal dysfunction and ultimately to neurodegeneration. A myriad of triggers transform microglia from the resting state to the amoeba-shaped activated macrophage form. Lectin proteins, stained by horseradish peroxidase (HRP), help illustrate the transformation of microglia in an injured rat cortex. The sustained production of neuroinflammatory mediators leads to a chronic self-propagating neuroinflammatory cycle. The continued demise of neurons creates cellular debris that causes microglia to remain in the activated macrophage state. Microglia photos were obtained from *Wikipedia Commons, Mikroglejl_1.jpg and Mikroglejl_2.jpg (Dec 2011).* Content adapted from *Frank-Cannon et al. 2009.*

2.4 Inflammatory Cytokines

Tumor necrosis factor-alpha (TNFα) is secreted by glia cells in response to acute inflammation and infection. Deregulated production of TNFα results in chronic inflammation and sustained levels of ROS, hallmarks of many neurodegenerative diseases and cancer (Dowlati et al. 2010, Swardfager et al. 2010, Locksley et al. 2001). Additionally, research at the Bowles Center for Alcohol Studies (University of North Carolina, Chapel Hill), has demonstrated increased TNFα production in response to ethanol at the cellular and systemic level, Fig 2.2, (Crews et al. 2006, Qin et al. 2008). TNFα activates two membrane bound enzymes (magnesium-dependent neutral sphingomeylinase and NADPH oxidase), which further compound oxidative stress (Li et al. 2009, Wheeler et al. 2009).

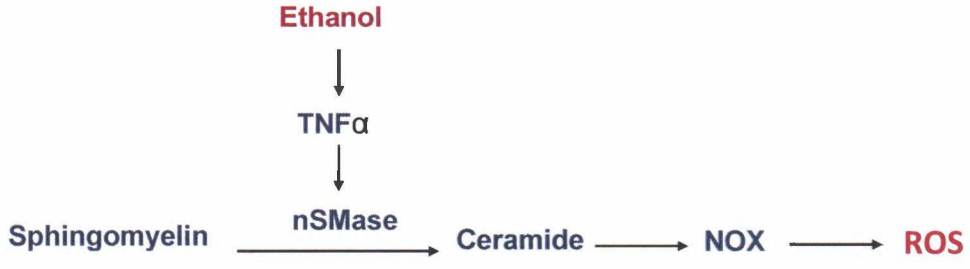

Fig 2.2 Ethanol Exposure Increases Enzymatic Production of ROS
Membrane sphingomyelin is converted to ceramide upon activation of membrane bound nSMase. Ceramide production initiates subunit assembly of NOX in lipid rafts. NOX activation generates ROS.

Recent work in our laboratory has demonstrated the ability of ursolic acid, isolated from blueberries, to block the activation of neutral spingomeylinase (nSMase), and the functional assembly of NADPH oxidase (NOX) (Gustafson et al. 2012, *in press*). Therefore, it is feasible to propose that ursolic acid and other blueberry compounds may blunt oxidative stress induced by up-regulated TNFα production due to ethanol abuse. Easily administered dietary modifications that can blunt TNFα secretion may break the tragic cycle of inflammation that deteriorates the health of individuals suffering from a far reaching spectrum of disorders, including alcoholism.

2.5 Antioxidants in Blueberries

Antioxidants are substances namely found in fresh fruits and vegetables that scavenge and stabilize free radicals and thereby prevent oxidative damage. High levels of antioxidant anthocyanins are found in the skins of Alaskan blueberries which defend against light stress invoked by the long daylight hours encountered in high latitudes. Bioavailability studies of anthocyanins indicate that these highly pigmented compounds can localize in the brains of rats fed blueberries thus suggesting blood brain barrier (BBB) permeability (Andres-Lacueva et al. 2005). Studies also reveal that blueberries exhibit potent neuroprotective qualities that alleviate cognitive decline and even improve cognitive abilities and motor skills in the aging population (Joseph et al. 1999,

Youdim et al. 2000, Lau et al. 2007). We believe supplementation of blueberries into the diet will potentially mitigate inflammatory stress.

2.6 Ursolic Acid and Oleanolic Acid

Our laboratory has demonstrated that ursolic acid isolated from the nonpolar lipophilic fraction of Wild Alaska Bog Blueberries blunts inflammatory stress induced by TNFα by stabilizing the integrity of lipid rafts and cytoskeletal organization within human neuroblastoma cells (Gustafson et al. 2012, *prepared for submission*). Ursolic Acid (UA) and its isomer, oleanolic acid (OA), are pentacyclic triterpenes (Fig 2.3) with demonstrated anti-inflammatory, hepatoprotective, anti-hyperglucemic, and anti-tumor protective capabilities (Brieskorn and Klinger 1961, Liu 1995, Schneider et al. 2009). Both UA and OA have identical molecular weights and differ only in the positioning of one methyl group (Schneider and Hosseiny 2009). The triterpenes found in fruits typically reside in the waxy outer protective layer of the skin (Orban and Kozak 2009).

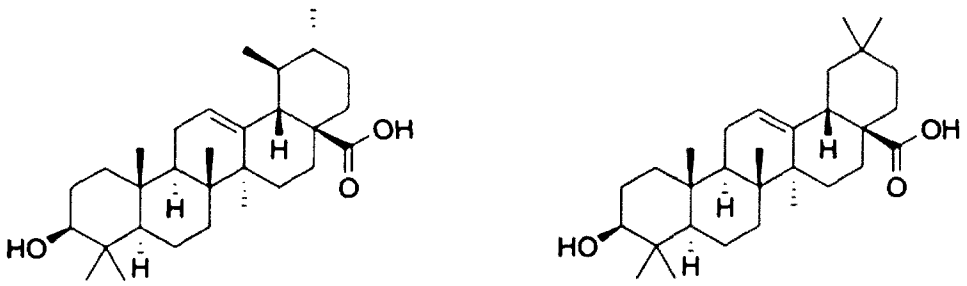

a. Ursolic Acid b. Oleanolic Acid

Fig 2.3 Chemical Structures of Ursolic and Oleanolic Acids
Ursolic acid and Oleanolic Acid are pentacylclic triterpene acids found in plants, particularly in many herbs, berries, and apple peels (de Queiroz et al. 2011). Structures were obtained from *Wikipedia Commons Ursolic acid.png and Oleanolic acid.png (Dec 2011)*.

It is unknown whether the colorless blueberry fraction containing ursolic acid (UA), can definitively cross the BBB. Encouraging studies however demonstrate that UA, derived from natural products such as blueberries, can attenuate oxidative damage and ameliorate cognitive deficits in mice (Lu and Zheng 2007) and rats (Shih et al. 2004) against induced neurotoxicity. These results suggest that blueberry extracts and ursolic acid may offer novel therapeutic treatments against neurodegeneration caused and exacerbated by oxidative stress in individuals suffering from a myriad of neurodegenerative diseases.

Recent work with both UA and OA isolated from glossy privet fruit and hawthorn fruit has also revealed their capability to effectively suppress the formation of two glycative products (pentosidine and carboxymethyllysine –

CML), formed from reactive carbonyl compounds and proteins (Yin and Chan 2007). It is well documented that these glycative products enhance the progression of glycation associated diseases such as Alzheimer's disease (AD), diabetes, atheroscolerosis, osteoarthritis, inflammatory arthritis, and cataracts (Monnier et al. 2005, Bar et al. 2003, Mera et al 2005, Reddy and Beyaz 2006). Since UA and OA may provide significant antiglycative and antioxidant protection, UA/OA supplementation may also delay progression of these diseases (Yin and Chan 2007).

2.7 Lipid Rafts

Lipid rafts are highly dynamic microdomains residing within fluid cellular plasma membranes (Fig 2.4). Their distinct and ordered lipid composition is essential for spatial and temporal signal modification between neurons (Simons and Toomre 2000, Harder and Engelhardt 2004). Well-ordered lipid raft platforms are rich in cholesterol and sphingolipids and found to provide scaffolding for signaling and redox events (Klopfenstein et al. 2002, Vilhardt and Van Deurs 2004, Yang and Rizzo 2007). Alterations to lipid raft composition may therefore alter lipid and protein interactions necessary for signaling molecules to functionally assemble.

Cholesterol depleting compounds, such as methyl-beta-cyclodextrin (MBCD), are shown to obliterate lipid raft formation (Gustafson et al. 2012, *prepared for submission*). Interestingly, preventive treatment with ursolic acid

hinders the functional assembly of nSMase and NOX expected to form in lipid rafts due to TNFα insult. It is proposed that the structural similarity of UA (Fig 2.3) to cholesterol (Fig 2.5) may allow UA to displace cholesterol and modulate lipid rafts (Gustafson et al. 2012, *prepared for submission*). Lipid rafts (Fig 2.4) now present as a therapeutic target to mitigate neuroinflammatory signaling events.

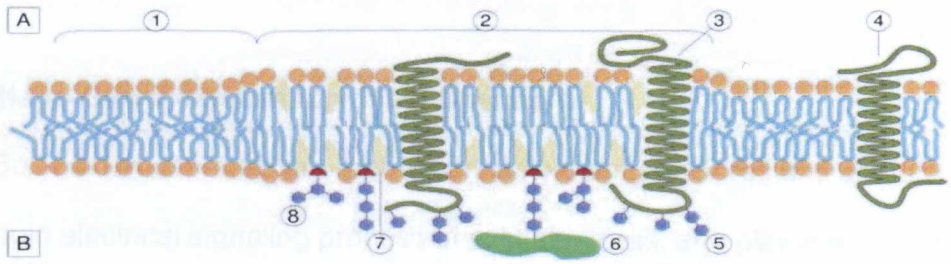

Fig 2.4 Lipid Raft Diagram

A. Intracellular space / cytosol
B. Extracellular space
1. Non-raft plasma membrane (non-ordered and detergent soluble)
2. Lipid raft (ordered and detergent resistant)
3. Lipid raft associated transmembrane protein
4. Non-raft membrane protein
5. Glycosylation modifications (on glycoproteins and glycolipids)
6. GPI-anchored protein
7. Cholesterol
8. Glycolipid

Wikimedia Commons: Lipid Raft Organization scheme.SVG (Dec 2011)

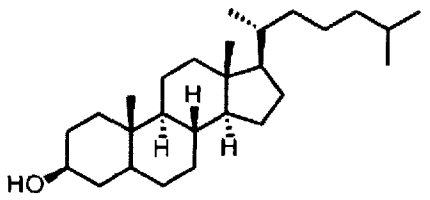

Cholesterol

Fig 2.5 Chemical Structure of Cholesterol
Cholesterol is integral to lipid raft structure (Fig 2.4).
Wikipedia Commons: Cholesterol.SVG (Dec 2011)

2.8 Voltage-Gated Sodium Ion (Nav) Channels

Sodium ion channels are embedded in lipid raft structures and are integral to the rapid electrical signaling process of excitable cells, and play a role in the molecular basis of tolerance (Pietrzykowski and Treistman 2008). Oxidative stress and ethanol exposure induce formation of large lipid raft signaling platforms that may elicit significant changes in the electrical potential of such cells (Dai et al. 2005). Instances of epileptic seizures, a disorder of sodium ion channel function, are increased in alcoholics (Frucht et al. 2000). Taken together, an important correlation between oxidative stress, lipid rafts, sodium ion channel function, and alcohol abuse needs to be elucidated.

Voltage gated sodium ion (Nav) channels are heteromeric membrane proteins composed of alpha and beta subunits with a molecular weight of about 260 kDa (Goldin 2001). Ten isoforms of the Nav channel alpha subunit are encoded by ten different genes in mammals (Schaller and Caldwell 2003). The

large alpha subunit controls channel gating through four homologous domains which consist of the sodium ion conduction pore and the voltage sensor (Fig 2.6). This subunit exerts control over the sodium flux into the cell upon membrane depolarization and channel activation. The alpha subunit undergoes both glycosylation and phosphorylation during post-translational modification (Schaller and Caldwell 2003). The smaller auxiliary beta subunits then fine tune the voltage dependence and kinetics of the channel gating (Goetz et al. 2009). Intracellular protein interactions with Nav channels are essential for both function and proper subcellular location (Peles and Salzer 2000). Because sodium channel pathogenesis is involved in epilepsy, cardiac arrhythmias, neuropathy, multiple sclerosis, and cerebellar ataxia (SCA27), it is a very important target for drug therapy (Wittmack et al. 2004).

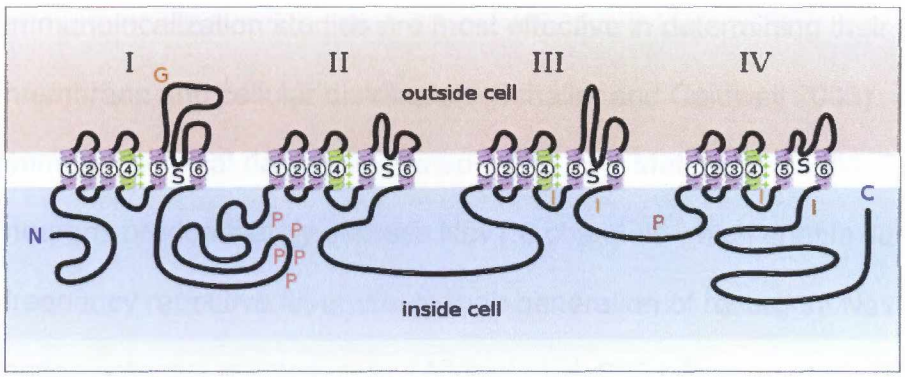

Fig 2.6 The Voltage-gated Sodium Ion (Nav) Channel

The four homologous transmembrane domains of the Nav channel alpha subunit are indicated (I – IV). The domains associate in the membrane to form a Na+ permeable pore. The intercellular loop between domains III and IV forms the inactivation gate of the channel. The positive (+) charges in S4 provide a means to sense voltage and the S5-6 loop lines the channel pore.

Wikimedia Commons: sodiumchannel.svg (Dec 2011)

Expression of the alpha and beta subunits is tissue and cell specific. Four of the Nav alpha subunits (Nav1.1, 1.2, 1.3, and 1.6), are expressed in both the CNS and PNS; three are expressed in the PNS only (Nav1.7, 1.8, and 1.9); and two are expressed in the muscle and heart (Nav1.4 and 1.5). All three beta subunits (NaB1, 2, and 3) are expressed in the brain and heart, whereas only NaB1 and NaB2 are found in the muscle (Meisler and Kearney 2005).

2.9 Nav Channel Distribution in the Cerebellum

Four voltage gated sodium ion channels are expressed in the cerebellum: Nav1.1, Nav1.2, Nav1.3 (development only), and Nav1.6. These channels are all tetrodotoxin (TTX)-sensitive and are difficult to differentiate electrically; therefore

immunolocalization studies are most effective in determining their regional membrane and cellular distribution (Schaller and Caldwell 2003). A composite of immunochemical data is illustrated in Fig 2.7. Mature cerebellar Purkinje neurons predominately express Nav1.6 channels which enable sustained high frequency repetitive firing due to their generation of resurgent Nav current during action potential repolarization (Afshari et al. 2004, Raman et al. 1997). Nav1.6 labeling also reveals both presynaptic and postsynaptic membrane localization in the parallel fibers and the dendritic spines of Purkinje neurons (Caldwell et al. 2000). The ability of Nav1.6 to reside in multiple locations suggests differential interaction with modulating proteins. Additionally, intracellular labeling of Nav1.6 is prominent in Purkinje dendrites indicating the possibility of pooled Nav1.6 that can be quickly recruited to active synapses and play a role in synaptic plasticity (Caldwell et al. 2000). Nav 1.6 channels are also expressed in the cerebellar granule cells (parallel fibers) that communicate directly with Purkinje neurons. Labeled parasagittal sections of the rat brain reveal heavier labeling of Nav1.6 in the granule cells of the posterior lobe opposed to those of the anterior (Schaller and Caldwell 2003).

Sodium channels, Nav1.1 and Nav1.2, have been found to be responsible for fast kinetics within the cerebellum. Nav1.1 is found in Purkinje soma and dendrites, interneurons of the molecular layer, and within deep cerebellar neurons (Fig 2.7). Nav1.2 is found in the unmyelinated granule cell axons and in the interneurons of the molecular layer (Fig 2.7) (Schaller and Caldwell 2003).

Interestingly, the aging process has recently revealed a shift in expression of Nav channels in the cerebellum of aged rats. This study demonstrates an age related increase in Nav1.1 immunoreactivity in Purkinje cell bodies and a simultaneous decrease of Nav1.1 in granule cells. Additionally, in the cerebellar nuclei of aged rats, Nav1.1 and Nav1.2 expression was selectively increased in cerebellar output neurons. This research for age related changes in Nav channel expression of the cerebellum will help explain alterations in synaptic transmission during aging (Chung et al. 2003).

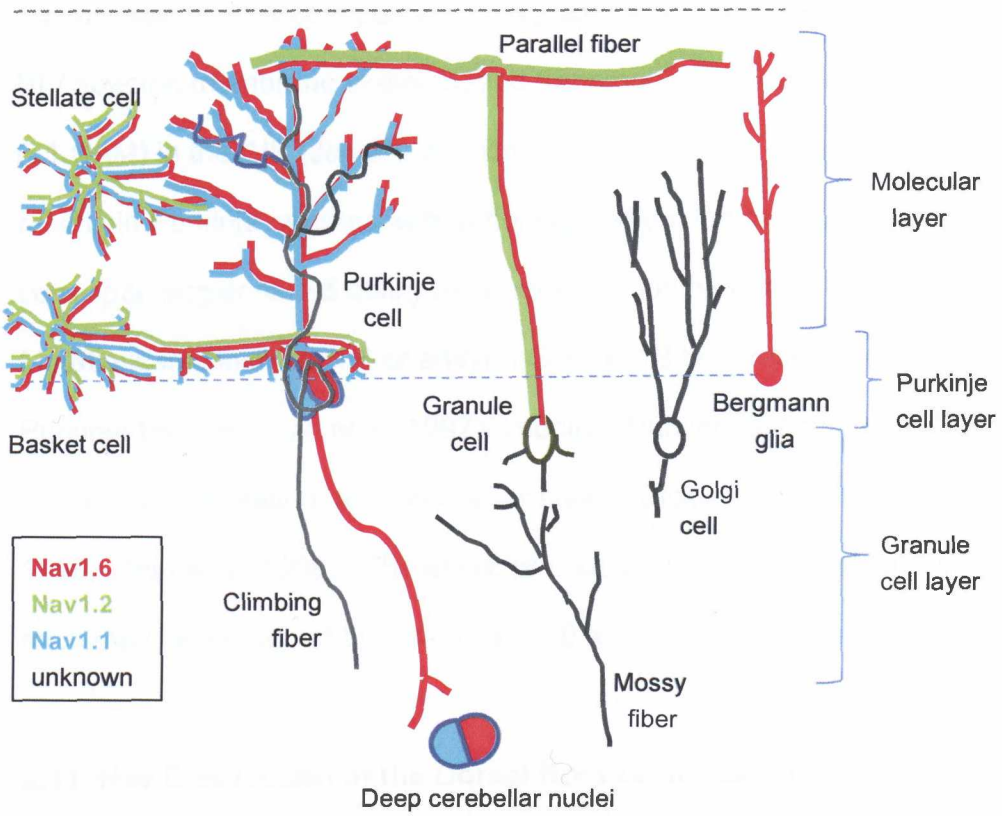

Fig 2.7 Sodium Channel Distribution in the Cerebellum

Sodium channel distribution in the rat cerebellum was determined by immunolocalization studies and is color coordinated to represent Nav1.6 (red), Nav1.2 (green), and Nav1.1 (blue) in specific neuronal cells. It is unknown what isoforms of sodium ion channels are present in the cells illustrated in black. *Adapted from* (Schaller and Caldwell, 2003).

2.10 Ankyrin-G and Nav Channels in Purkinje Initial Segments

The axon initial segment (AIS) is an excitable membrane responsible for integrating neuronal inputs and initiating action potentials. The AIS is highly

enriched with Nav1.6 channels in mature cerebellar Purkinje neurons. Ankyrin-G coordinates the physiological assembly and clustering of Nav1.6 channels, the BIV spectrin membrane skeleton, and transmembrane cell adhesion molecules (L1 CAM) in the AIS (Jenkins and Bennett 2001). Lack of ankyrin-G expression results in Purkinje neurons with abnormal sodium ion channel distribution and corresponding impaired ability to generate action potentials (Zhou et al. 1998). Mutations in either Nav1.6 or ankyrin-G exon 1B both result in decreased Purkinje firing (Raman et al. 1997), impaired Purkinje action potential generation, Purkinje degeneration, and cerebellar ataxia (Dick et al. 1985, Kohrman et al. 1996, Zhou et al. 1998). The ataxic phenotype exhibited in ankyrin-G knockout mice may be explained by loss of Nav1.6 at the AIS (Jenkins and Bennett 2001).

2.11 Nav Distribution in the Dorsal Root Ganglias (DRGs)

As in other neurons, cytosolic proteins regulate the trafficking and function of the Nav channels in DRGs of the PNS. Nav1.6 is highly expressed at the nodes of Ranvier and along the unmyelinated fibers of the PNS. One of the fibroblast growth factors, FGF13, is found to collocate with Nav1.6 channels in DRGs. Their association with Nav1.6 channels significantly increases peak amplitude thereby causing a depolarizing shift of voltage-dependent inactivation of the channel. Interestingly, FGF13 is not expressed in the ventral root motor axons. This preferential expression of FGF13 for the sensory neurons as opposed to the motor neurons may explain physiological differences reported in

the sodium currents within the PNS (Wittmack et al. 2004). The axons of sensory neurons are more likely to fire repeatedly in response to continuous stimulus than those of motor neurons (Erlanger and Blair 1938). Sensory neurons are also sensitive to different injuries and neuropathies which may be indicative of both variable sodium channel expression and regulatory protein interaction (Wittmack et al. 2004). Through research on diabetic rats, evidence suggests that reduction of Nav1.6 at the nodes of Ranvier in large DRGs leads to slowed nerve conduction velocity (Kearney et al. 2002) that contributes to diabetic sensory neuropathy (Hong and Wiley 2006). It is unknown whether neuroninflammation may promote sensory peripheral neuropathy through Nav channel dysfunction. This study will take the first steps to investigate this question by determining changes in Nav channel densities due to inflammation.

2.12 Nav1.6 and Resurgent Sodium Current in Purkinje and DRG Neurons

Resurgent sodium currents are produced by unusual gating behavior of TTX-sensitive Nav channels. Like other channels, upon depolarization, channels activate and inactivate, but a repolarizing current of only -50 to -60 mV causes a transient surge of sodium where other sodium channels would remain closed to recover from inactivation. Resurgent current equates to unusually rapid recovery from inactivation and priming of the channel to promote a second action potential (Raman and Bean 1997, Bean 2005). The high-frequency firing of Purkinje neurons is due to resurgent current.

The unique resurgent sodium current critical for determining the firing patterns of the cerebellar Purkinje neurons (Raman and Bean 1997) has also been recorded in native DRG neurons. Nav1.6 is found to underlie the resurgent current generation in both Purkinje and DRG neurons (Cummins et al. 2005). Resurgent sodium current in Purkinje neurons is nearly obliterated in Nav1.6-null mice (Raman et al. 1997). Minimal amounts of resurgent current are probably produced through Nav1.2 expression (Cummins et al. 2005). Importantly, although Nav1.6 is present in both small and large DRG neurons, resurgent current is not observed in the small DRGs (Black et al. 2002). Differentially expressed factors involved in Nav1.6 function may determine the ability of this channel to generate resurgent currents (Cummins et al. 2005). Likewise, Nav1.6 is expressed in the hippocampus (Raman and Bean 1997) and spine (Pan and Beam 1999) without producing resurgent current. The role of sensory neuronal excitability due to the generation of resurgent sodium current by Nav1.6 channels in DRGs begs further investigation.

2.13 Sodium Ion Channel Disorders

Sodium ion channel disorders are caused by a myriad of factors and intercellular proteins that influence channel function and timing. Another fibroblast growth factor, FGF14, differentially modulates interaction with several Nav-alpha (pore forming) subunits including Nav1.1, Nav1.2, Nav1.5 (heart), and Nav1.6 (Lou et al. 2005). FGF14 is also collocated with Nav1.6 and particularly

enriched at the axonal initial segments which are critical for action potential generation and propagation in the CNS and PNS (Kaplan et al. 2001, Clark et al. 2005). Intriguingly, a mutation in the human SCN8A gene that encodes Nav1.6 was recently found to lead to cerebellar atrophy, ataxia, and mental retardation strikingly similar to individuals possessing a FGF14 mutation in spinocerebellar ataxia 27 (SCA27), (Trudeau et al. 2006). Clinical assessments of these patients and immunochemical data point to the unique function of Nav1.6 in the cerebellum.

A growing number of sodium ion channel mutations have been identified in other cases of neurological disease. Epilepsy results in almost 200 of these mutations and illustrates the particularly sensitivity of the nervous system to sodium ion channel aberrations. Persistent sodium current, deregulation, or loss of function may result in serious neurological disease. Symptoms of Nav channel dysfunction may include seizures, ataxia, paralysis, pain resistance, dystonia, learning deficits, and psychiatric disease (Meisler and Kearney 2005). The increased occurrence of seizures during acute alcohol intoxication and withdraw leads us to investigate ethanol's influence on Nav channel dysfunction.

2.14 Cerebellum

Historic views of the cerebellum limit its function to the coordination of voluntary movement, gait, posture, speech, and motor function (Ghez and Fahn 1985). Current studies however, reveal its role in higher cognition, behavior and

psychiatric illness to include autism, schizophrenia, dementia, and alcohol dementia (Schmahmann 2004, Rapoport et al. 2000). Although not generally considered to be of cerebellar origin, Alzheimer's disease also causes a significant decline in the cerebellar Purkinje neurons (Rapoport et al. 2000).

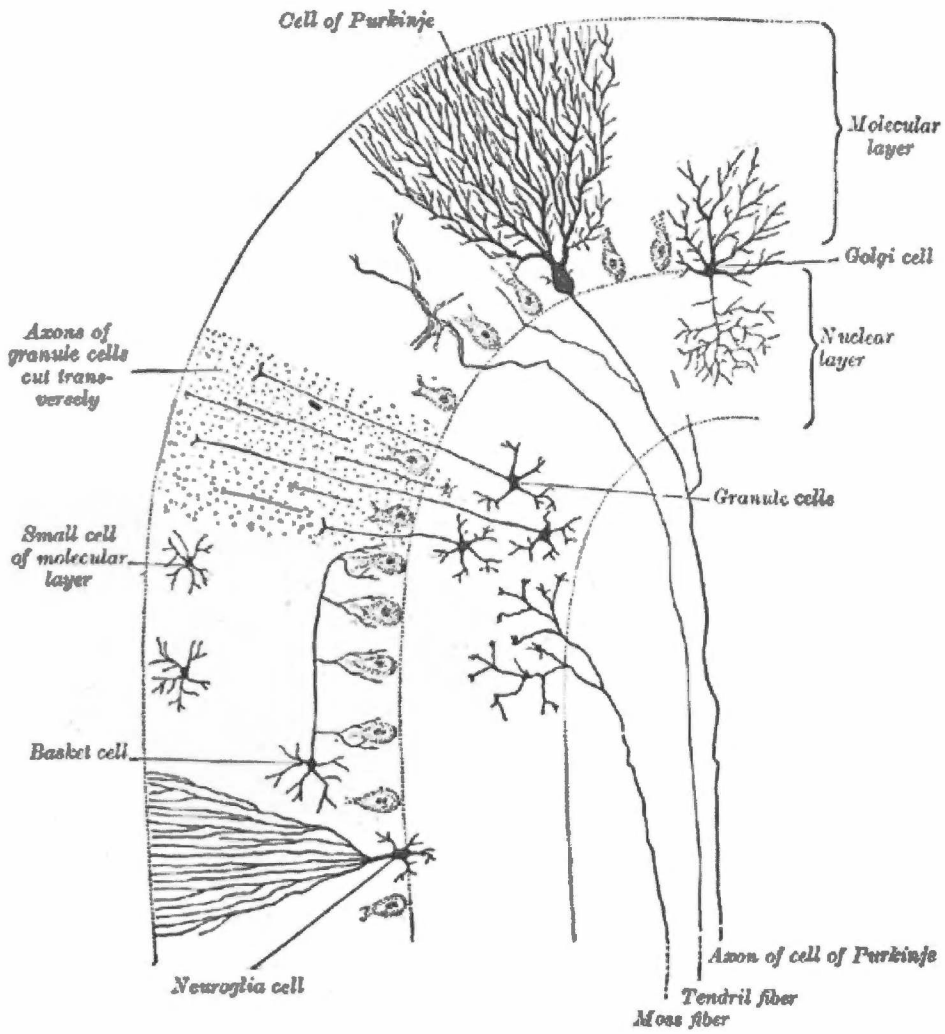

Fig 2.8 The 1918 Sketch of the Cerebellum

Wikimedia Commons Gray706.png, Gray's Anatomy 1918, accessed (Dec 2011).

Purkinje cells are the largest neurons in the brain and are easily identified by their elaborate dendritic arbors (Fig 2.8). Each dendritic tree interacts with nearly 200,000 parallel fibers that form 500 granule-Purkinje cell synapses per climbing fiber. Purkinje cells also receive inhibitory GABA inputs from basket cells (at axon initial segments) and stellate cells (on the dendrites), Fig 2.7. The Purkinje coordinates all these inputs and produces the sole inhibitory output of the cerebellar cortex to the deep cerebellar nuclei (Wadiche and Jahr 2001, Tyrrell and Willshaw 1992). Purkinje dysfunction is therefore catastrophic to the cerebellum which houses half the brain's neurons and orchestrates inputs from all over the brain (Rapoport et al. 2000). Consequently, its influence on functions held primarily in other regions is very likely.

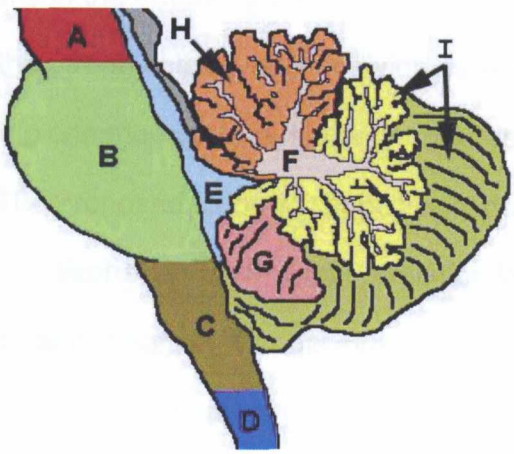

Fig 2.9 The Cerebellum and Surrounding Regions
The regions include: A) midbrain, B) pons, C) medulla, D) spinal cord, E) fourth ventricle, F) arbor vitae, G) tonsil, H) anterior lobe, I) posterior lobe.
Figure from *Wikimedia Commons: CerebellumRegions.jpg (Dec 2011).*

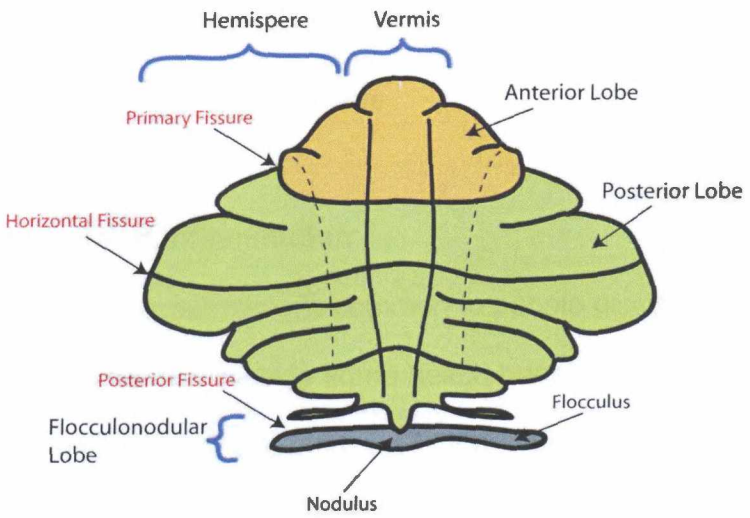

Fig 2.10 Major Subdivisions of the Cerebellum

The diagram illustrates the cerebellum from the superior view when laid out two dimensionally. *Wikimedia Commons: CerebellumDiv.png (Dec 2011)*

Imaging studies of the alcoholic brain reveal obvious cerebellar atrophy, particularly in the anterior lobe and vermis (Sullivan et al. 2006). This pattern mimics the atrophy observed in individuals with degenerative cerebellar ataxia suggesting common pathways or vulnerabilities (Schmahmann and Caplan 2006). The proposed study will specifically determine how the cerebellum is affected by alcohol abuse and its correlation to observable changes in behavior and motor performance. We believe supplementation with blueberries will drastically mitigate inflammatory stress and prevent neurodegeneration due to alcoholism and other chronic conditions marked by increased oxidative stress.

Chapter 3: Alcohol Abuse Triggers Dynamic Alterations in Neuronal Membranes via Oxidative Stress

3.1 Alcohol and Inflammation

Alcohol consumption is common to people groups worldwide. Although moderate intake may provide some health benefits, excess consumption leads to systemic inflammation and increased morbidity (Vasdev et al. 2006). On the cellular level, alcohol abuse is marked by oxidative stress and lipid peroxidation of cellular membranes (Nordmann et al. 1990a&b). Lipid peroxidation reduces membrane bilayer fluidity and potential, thereby altering lipid raft formation and subsequent signaling and synaptic events (Szabo et al. 2007). Additionally, ethanol dramatically suppresses immunological and antioxidant defense systems thus amplifying the delirious effects of free radicals and creating a continued cycle of oxidative stress (Szabo 1997, Wilson 1997, Dringen et al. 2000). Collectively, this cascade of events may lead to cellular dysfunction and death. Interventions that block this chronic inflammatory response provide potential therapeutic avenues for limiting the impact of oxidative stress in cases of alcohol abuse and other inflammatory and degenerative diseases. Although, alcohol exerts its affects through a myriad of mechanisms and produces a wide spectrum of responses throughout the body, this chapter will focus primarily on the pathways that ultimately lead to impaired brain function through altered membrane dynamics and oxidative stress.

3.2 Ethanol's Path through the Body

To examine the effects of alcohol on the brain we must first review the path it takes to get there. Upon consumption, ethanol is minimally metabolized in the stomach and quickly absorbed through the gastrointestinal (GI) tract. Chronic alcohol consumption leads to a breakdown of the GI mucosal barrier whereby resident microbes may enter into the bloodstream. Lipopolysaccharide (LPS), a potent endotoxin making up gram-negative bacteria cell walls, is therefore frequently elevated in alcoholics due to their 'leaky guts'. Once LPS enters the bloodstream, it stimulates activation of leukocytes through ligand binding to membrane associated toll like receptors (TLRs) that recognize pathogen-associated molecular patterns. Interaction with CD14, a glycosylphosphatidylinositol (GPI) linked protein, then amplifies TLR4 signaling through complex clustering and co-localization within lipid rafts. At physiologically relevant doses of ethanol (10-50mM equivalent to 0.05-0.24 blood alcohol content), ethanol mimics LPS in TLR4 complex assembly and concurrently triggers downstream signaling pathways of NF-kB and mitogen-activated protein kinase (MAPK) to up-regulate expression of inflammatory cytokines, such as TNFα, IL-1B, IL10, and NO in the blood stream (Fernandez-Lizarbe et al. 2007).

3.3 Ethanol and Lipid Rafts

Strikingly, at high doses of ethanol (greater than 50mM as seen in extreme binge drinking), ethanol inhibits TLR activation by disrupting lipid raft formation. It is clear that ethanol can differentially affect the formation of lipid rafts and TLR activation dependent on its concentration. Furthermore, recent studies indicate that recruitment of various receptor molecules to lipid rafts via actin polymerization can be inhibited by ethanol (Szabo et al. 2007). Activation of TLRs is necessary to clear pathogens but must be tightly regulated in both intensity and duration in order to prevent chronic inflammatory states. Deregulation of the immune system contributes to the pathogenesis of inflammatory diseases common in alcoholics: liver disease, arteriosclerosis, arthrosclerosis, diabetes, irritable bowel syndrome, neuropathy, neuroinflammation and degeneration. Additionally, a strong correlation exists between alcohol consumption and the risk of infections such as pneumonia, tuberculosis, ARDS, Hepatitis-C, HIV, and HIV-dementia (Szabo 1997). The cycle of endothelial breakdown, pathogen entry, immune response, cytokine release, inflammation and oxidative stress is common throughout the body, to include the central nervous system (CNS).

3.4 Ethanol – the Liver and Beyond

Kupffer cells, the specialized resident endothelial macrophages of the liver, produce a significant proportion of the TNFα found in the serum, which in

turn propagates the production of more TNFα in other tissues. Chronic ethanol feeding studies on rats demonstrate how ethanol exaggerates the LPS stimulated release of inflammatory cytokines in the liver and further generates reactive oxygen species (ROS) through assembly and activation of the lipid raft associated complex NADPH oxidase, (NOX) (Han et al. 2008, Thakur et al. 2006). Ethanol and ROS work in concert to hyper-sensitize Kupffer cells to LPS, hence amplifying the inflammatory response and increasing oxidative stress beyond the bounds of the liver.

3.5 Ethanol Metabolism

The liver handles the primary responsibility of metabolizing ethanol but can only do so at a rate of 0.25 ounces per hour. Alcohol ingested in excess of this rate will therefore be metabolized by other cells in the body. Ethanol is metabolized through two different processes dependent on its concentration (see Fig 3.1). These pathways hold the key to whether alcohol is beneficial to health by providing an anti-inflammatory environment or detrimental by increasing oxidative stress. At low doses, ethanol is metabolized by alcohol dehydrogenase to acetaldehyde and then by aldehyde dehydrogenase to acetate, where NADH is produced in both reactions. NADH is part of the electron transport chain and possesses a high reducing potential that regenerates vitamin radicals back to their reduced forms, thereby increasing antioxidant capacity (see Fig 3.2). Conversely, at high doses, ethanol is metabolized to toxic acetaldehyde by

producing NADP+ which creates an oxidative environment and reduces antioxidant capacity (Vasdev et al. 2006).

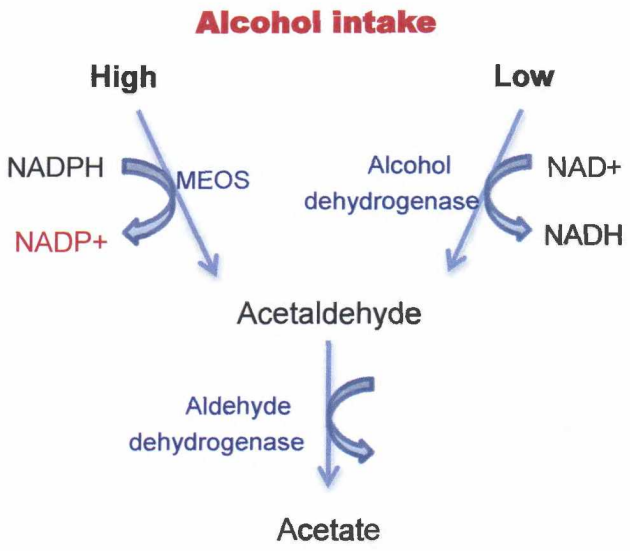

Fig 3.1 Differential Ethanol Metabolism

Adapted from (Vasdev et al. 2006).

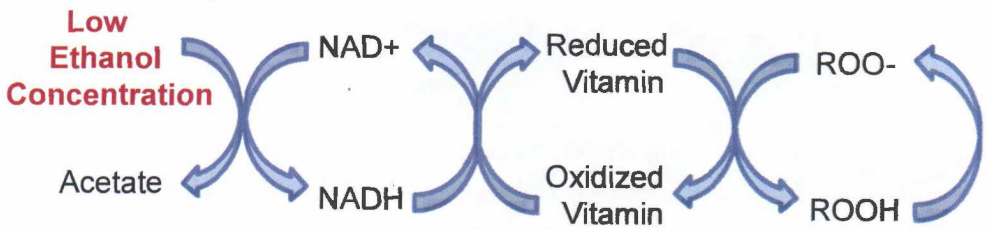

Fig 3.2 Low Ethanol Concentrations Reduce Vitamin Radicals

Adapted from (Vasdev et al. 2006).

3.6 Astrocytes and the Blood Brain Barrier

The brain holds a privileged position in the body and is highly protected by the blood brain barrier (BBB), but as with the other endothelial linings of the body, it too is disrupted by inflammation induced by alcohol (Weiss et al. 2009, Haorah et al. 2007, Haorah et al. 2005a). The BBB is created by tight junctions (TJ) of endothelial cells within vessels of the brain that are then completely surrounded by astrocytes as seen in Fig 3.3. This unique arrangement restricts entrance through the BBB by tightly controlling permeability to plasmatic compounds and ions.

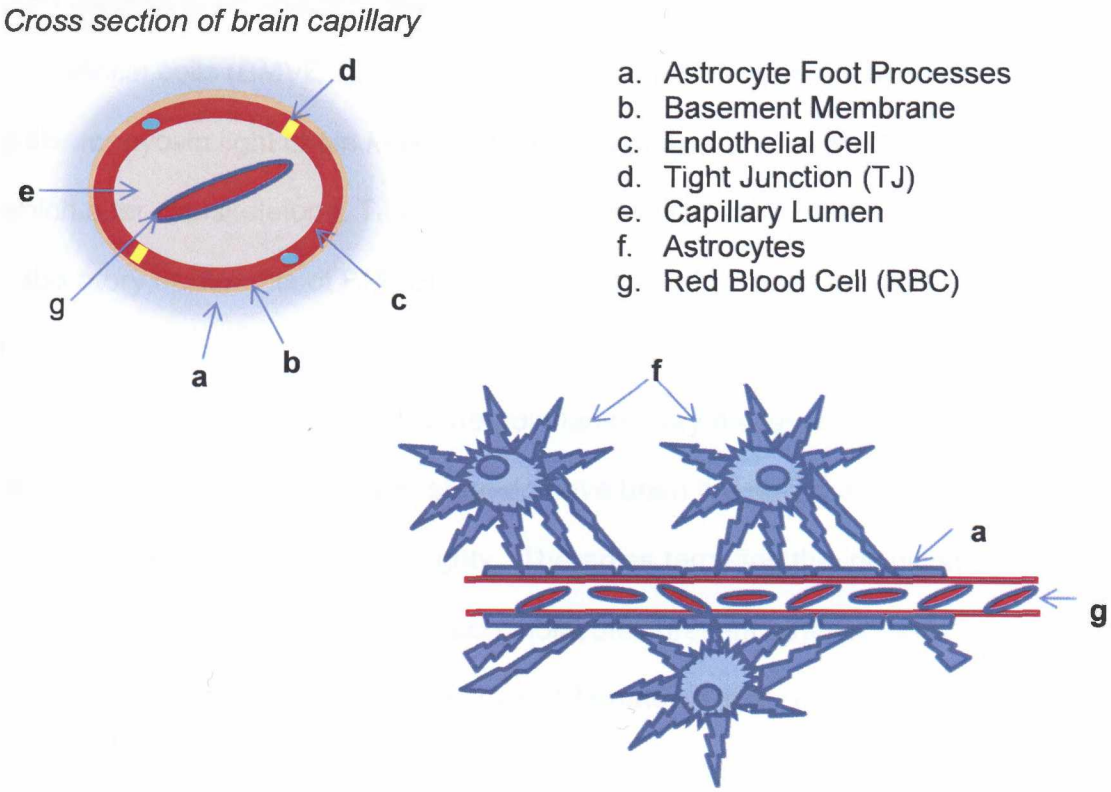

Fig 3.3 Astrocytes are Integral to the Blood Brain Barrier (BBB)

3.7 Blood Brain Barrier Transmigration

Increased levels of serum inflammatory cytokines dramatically alter the expression of surface adhesion molecules in leukocytes and CNS vascular endothelial cells. Mediation of adhesion molecules in leukocyte-endothelial cell interactions leads to ROS generation and TJ disruptions (Haorah et al. 2005a). Circulating leukocytes can now transmigrate through the BBB by way of these adhesion molecule interactions, a discovery that challenges the former concept of the brain as an immune privileged organ (Weiss et al. 2009). Upon entry into the brain, leukocytes stimulate a resident immune response from microglia which then initiates brain specific inflammation. Additionally, brain microvascular endothelial cells (BMVEC), can metabolize alcohol into acetaldehyde (AA) and activate myosin light chain kinases (MLCK) to phosphorylate MLC/TJ proteins which alter cytoskeletons, TJ integrity, and promote monocyte transmigration. Laboratory treatments of BMVEC with antioxidants has been shown to prevent BBB leakiness and underscores the role of oxidative stress in BBB impairment common to alcoholism and other neuroinflammatory diseases (Haorah et al. 2005a&b). Generally however, steroids have been the only prescribed treatment option used to improve BBB integrity. Therapies targeting the inhibition of inflammatory cytokines and adhesion molecules present other potential approaches to mitigate BBB breakdown (Stamatovic et al. 2008).

Circulating serum inflammatory cytokines, such as TNFα and IL-1, quickly cross the BBB but appear to have a significantly longer lasting presence in the

brain than in the liver or bloodstream. Excessive alcohol intake, even sporadically, produces continued up-regulation of inflammatory stressors in the brain that may last over a week. The sustained presence of cytokines further up-regulates membrane enzyme NADPH oxidase (NOX) which results in increased ROS production perpetuating the cycle of oxidative stress (Crews et al. 2006, Thakur et al. 2006).

3.8 Glial Activation due to Inflammation

A hallmark of neuroinflammation in the brain is glial cell activation, particularly that of microglia and astrocytes (Blanco et al. 2006). Glia cells undergo morphological changes and proliferate in response to alcohol induced brain damage as determined by post-mortem analysis on alcoholic brains (Crews and Nixon 2009). It has also been observed that cerebellar microglia proliferation precedes ethanol-induced atrophy of the anterior vermis of the cerebellum, most noted for degeneration in chronic alcoholics (Riikonen et al. 2002). Glia also produce a variety of inflammatory cytokines that when left unchecked induce chronic inflammation and sustained levels of reactive oxygen species (ROS) common to neurodegenerative diseases and cancer (Dowlati et al. 2010, Swardfager et al. 2010, Locksley et al. 2001). Up-regulation of inflammatory mediators by alcohol triggers downstream activation of NF-kB and further amplification and sustainment of inflammation through inducible nitric oxide synthase (iNOS), IL-1B, TNFα, and COX-2. Contrary to the fore-stated

neurotoxic pathway, astrocytes are also programed to provide trophic and metabolic support to neurons by supporting axonal regrowth and enhancing the antioxidant environment (Valles et al. 2004).

3.9 Alcohol Impairs Antioxidant Defense of Astrocytes

Under intense oxidative stress, astrocytes become functional impaired and lose their ability to fulfill their protective role to neurons, leaving both cell types more vulnerable to dysfunction and eventual death (Valles et al. 2004). The human brain utilizes a disproportionate 20% of the body's oxygen intake. Metabolism of oxygen produces a continual level of ROS whereby the brain must defend against the toxic effects of ROS. This role is primarily filled by the astrocytes which provide antioxidant glutathione precursors and reduced vitamin C to the neurons (Dringen et al. 2000, Wilson 1997). Alcohol may compromise the astroglial glutathione system that is integral to the brain's defense against ROS.

3.10 Lipid Peroxidation

The brain's cellular membranes contain a very high proportion of polyunsaturated fatty acids, which are greatly susceptible to lipid peroxidation induced through oxidative stress. Lipid peroxidation is a chain of events mediated by free radicals that leads to membrane deterioration. Alcohol abuse enhances lipid peroxidation, particularly in the cerebellum. Ethanol has also

been shown to reduce antioxidant defenses, not only in the astroglial glutathione system, but also in neuronal superoxide dismutase (SOD), alpha-tocopherol (vitamin E), ascorbate (ester of vitamin C), and selenium (Nordmann et al. 1990a&b). Interestingly, the cerebellum shows the lowest concentration of a-tocopherol (Meydani et al.1986) in the brain and is particularly sensitive to its deficiencies (Le Bel et al.1989). Injury to the cellular membranes leads to decreased fluidity, modification of synaptosomes, and alterations of neurotransmitter metabolism, all of which could contribute to tolerance and dependence on alcohol (Zaleska et al. 1989, Nordmann et al. 1990a&b).

3.11 Tolerance and Alterations to Cellular Membranes

The disordering effect of ethanol *in vitro* is overcome by increases in cholesterol *in vivo,* providing a possible molecular basis of alcohol tolerance (Sun and Sun 1985, Pietrzykowski and Treistman 2008). Behavioral tolerance to the effects of alcohol entails complicated molecular processes that buffer the impact of acute alcohol intoxication. That being said, neuronal membrane-bound ion channels present a common mode of action for these interrelated pathways (Pietrzykowski and Treistman 2008). Numerous studies have sought to better understand the elusive molecular mechanism of ethanol-channel interactions in voltage gated sodium and potassium channels, chloride and calcium channels, acetylcholine, NMDA-glutamate, and GABA(A) systems (Peoples and Weight 1997). Alterations in channel structure and function are imparted by the

membrane lipid microenvironment, direct protein interactions, gene transcription and epigenetics, all of which have been shown to be influenced by alcohol abuse (Pietrzykowski and Treistman 2008).

3.12 Omega-3-Fatty Acids in Neuronal Plasma Membranes

In addition to increases in cholesterol content, chronic alcohol abuse alters the composition of neuronal membranes by reducing unsaturated phospholipids (Chin et al. 1978), particularly the highly unsaturated omega-3 fatty acid, docosahexaenoic (DHA) (Pawlosky et al. 2001). Interestingly, ethanol increases incorporation of the membrane phospholipid, phosphatideylethanol (PE), but decreases its preferential association with DHA. Reduced DHA levels are also found in behavioral disorders and visual impairments associated with alcoholism, such as depression and retinal degenerative disease (Hibbeln and Salem 1995, Opreaunu et al. 2010, Ranjekar et al. 2003). In the healthy brain, DHA comprises approximately 50% of the phospholipid acyl chains with even greater concentrations in the synaptosomes. The hippocampus, critical for its role in learning and memory, is particularly sensitive to these alterations. Hippocampal dysfunction is clearly observed in cases of fetal alcohol syndrome and alcoholism (Cazzaniga et al. 2010, Gil-Mohapel et al. 2010).

3.13 Dietary Therapies

Overwhelming evidence has shown that alcohol abuse promotes chronic neuroinflammation which induces oxidative stress, immune system impairment, and compromised neuronal health. Because continued oxidative stress can ultimately end in neurodegeneration and altered brain function, therapeutic interventions are imperative. Along with behavioral modifications, dietary changes offer the quickest and most affordable means to improve overall health and specifically combat oxidative stress. Antioxidants are naturally enriched in fruits, vegetables, and tea due to their flavonoid content. Many of these compounds have proven to be effective in inhibiting oxidative stress and lipid peroxidation specific to alcohol consumption. One such example is the grape. Grape skins are rich in many polyphenols to include resveratrol, quercetin, catechin, and proanthocanindins. Enrichment of grape extracts into chronic ethanol fed rats protected neurons by inhibiting ROS generation and lipid peroxidation, protecting against excitotoxic insult, restoring dopamine uptake, and by preventing calcium influx and depletion of glutathione. Additionally, this study clearly showed grapes to reverse the up-regulation of cyclooxygenase (COX-2) that ethanol intake had induced in yet another ethanol mediated mechanism yielding oxidative stress in the brain (Sun et al. 2002). Other fruits, such as blueberries, have also exhibited potent neuroprotective qualities that alleviate cognitive decline and even improve cognitive abilities and motor skills in the aging population (Joseph et al. 1999, Youdim et al. 2000, Youdim et al. 2002,

Lau et al. 2007). Moreover, diets rich in fruits and vegetables induce epigenetic changes that further inhibit the expression of inflammatory genes (Szic et al. 2010) that are up-regulated through alcohol abuse.

3.14 Membrane Fluidity and DHA

Along with oxidative stress, alterations in the lipid composition of the plasma membrane pose additional challenges to overall neuronal health. Membrane fluidity is critical to proper synapse function where highly disordered regions rich in DHA allow for optimal vesicular neurotransmitter release (Stillwell et al. 2006). Additionally, DHA is a key factor in proper fetal brain development and continued neural growth as it crosses through the placenta and later into breast milk. To review, alcohol intake increases cholesterol and reduces DHA incorporation into the membranes, causing a stiffening effect. Studies now reveal that dietary DHA supplementation completely reverses this event by lowing cholesterol levels and increasing the concentration of DHA into the membranes (Stillwell et al. 2005). DHA is easily obtained through a diet rich in fish, particularly fatty fish like salmon, or through over-the-counter fish oil supplements. Further research in human endothelial retinal cells (HERC) has demonstrated DHA's capacity to inhibit cytokine induced sphingomeylinase activity and further downstream NF-kB activation. Blunting the up-regulation of inflammatory genes like cellular adhesion molecules (CAMs) prevents inflammation induced by leukocyte migration into the retina through the retinal

blood barrier (Opreanu et al. 2010). A similar response to DHA likely occurs in the brain at the BBB. Taken together, DHA supplementation provides another effective means to alleviate oxidative stress and improve neuronal health and brain function in instances of alcohol abuse.

3.15 Conclusions

In conclusion, alcohol abuse produces devastating effects on the brain through the ramifications of neuroinflammation and oxidative stress on cellular membranes. Oxidative stress is compounded by BBB breakdown, deregulation of the immune system, depression of the innate antioxidant defense system, and a sustained presence of inflammatory stressors in the brain. Neuronal membranes deteriorate in response to lipid peroxidation and impart drastic alterations in lipid composition. These changes suppress synapse function and thus lead to lasting behavioral, cognitive, and motor impairments in alcoholics. Fortunately, natural compounds easily accessible in the diet have been found to counteract the neuroinflammation and oxidative stress induced by alcohol abuse. Easily instituted dietary modifications may break the tragic cycle of inflammation and reverse the long term health impact of alcohol abuse in at risk individuals and developing babies subject to maternal alcohol abuse.

Chapter 4: Materials and Methods

4.1 Materials

BCA Protein assay kit	Pierce Biotech (Rockford, IL)
Cell Proliferation Kit (MTT)	Roche (Mannheim, Germany)
Chicken TNFα assay kit	Cusabio Biotech (Donghu, China)
DMEM powder	Mediatech (Herndon, VA)
F-12 powder	Sigma-Aldrich (St. Louis, MO)
FBS	Gibco (Grand Island, NY)
Fertilized chicken eggs	Holly Halvarson (North Pole, AK)
Fluorescent mounting media	KPL (Gaithersburg, MD)
GFAP Ab-6 (mouse) for astrocytes	Thermo Scientific (Fremont, CA)
GlutaMAX-1	Invitrogen (Carlsbad, CA)
HBSS	Sigma-Aldrich (St. Louis, MO)
Hoechst dye 33258 dye for dsDNA	Invitrogen (Camarillo, CA)
Laminin, murine EHS sarcoma	Trevigen (Gaithersburg, MD)
Lipid Peroxidation assay kit	Oxford Biomed (Oxford, MI)
Monoclonal mouse anti-Calbindin-D-28K ab	Sigma-Aldrich (St. Louis, MO)
Monoclonal mouse anti-SCN8A, Nav1.6 ab	Abnova (Taipei, Taiwan)
Nerve Growth Factor 7S (mouse)	Enzo Life Sci (Plymouth Meeting, PA)
Neurofilament (mouse anti-NF-M)	Invitrogen (Camarillo, CA)
Penicillin/Streptomycin	Mediatech (Herndon, VA)
Rabbit anti-Nav-pan ab	Assay Biotech (Sunnyvale, CA)

Recombinant human TNFα	ProSpec (Ness-Ziona, Israel)
ROS Detection Kit	Molecular Probes (Eugene, OR)
Secondary antibodies	Santa Cruz Biotech (Santa Cruz, CA)
Total Antioxidant Power assay kit	Oxford Biomed (Oxford, MI)
Trypsin/EDTA	Invitrogen (Carlsbad, CA)
Vibrant Lipid Raft labeling kit	Molecular Probes (Eugene, OR)
All other reagants	Sigma-Aldrich (St. Louis, MO)

4.2 Blueberry Extract Preparation

Wild Alaska Bog Blueberries were collected from locations within interior Alaska and stored at -20 C. Berries were lyophilized and crushed to powder. Samples (~20 g) were fractionated over a silica column in 500 ml segments with a mobile phase of 80/20 dichloromethane/methanol. Extracts were filtered, roto-vaporized at 40°C to remove volatile organics, frozen and then lyophilized again. The powder extracts were stored at -20 C until reconstituted immediately prior to use in a 70/30-acetone/water solution, and diluted 1:20 into deionized (18 mega Ω) water to produce non-polar and polar blueberry stock. Fractions were further separated into isolated compounds which produced the ursolic acid used in this thesis work. Blueberry extract preparations and fractionations were performed by Colin McGill of University of Alaska, Fairbanks, during his thesis work, 2010.

4.3 Chick Embryo Incubation

Fertilized *Buff Orpington* chicken eggs were purchased from a local supplier in North Pole, Alaska. Eggs were incubated at 37 degrees Celsius in a humidified egg incubator for 10 days to obtain neuronal samples from the forebrain, cerebellum, spine, DRGs, and olfactory bulb. Eggs were incubated for 15 or 18 days to obtain additional cerebellar glia samples. Eggs were not washed before incubation to prevent disruption of the permeable membrane and transfer of microbes to the chick.

4.4 Chick Embryo Dissection

4.4.1 Brain

Embryonic chick neurological tissue was dissected from chicks at embryonic day-10 (ED10), ED15, and ED18 under a dissection microscope in a laminar flow hood. Chicken eggs were washed with soap and water, dried, and sprayed with 70% ethanol. Using sterilized forceps, the top of the egg shell was removed and the chick was extracted and placed into a sterilized glass dissection dish filled with iced HBSS fortified with 1% penicillin-streptomycin (PS). The neck was quickly and completely severed. The head and bodies were rinsed with hanks buffered saline solution (HBSS) and placed separate dishes filled with HBSS/1% PS. Brains were dissected by carefully removing skin, the skull cap, and all surrounding meninges. Different sections of the brain were then dissected out and placed in new dishes with HBSS/1% PS. All dishes containing

dissected tissue were placed on ice. This process was repeated for additional eggs. Generally, 12 eggs were dissected at a time. The forebrain, cerebellum, olfactory bulb, spine and DRGs were identified utilizing *The Atlas of Chick Development* (Bellairs and Osmond 2005).

4.4.1.1 Forebrain

Forebrains were dissected from ED10 chicks as detailed in section 4.4.1. The two lobes of the forebrain were identified, dissected, and held on ice until all brain sections and spinal/DRG samples were collected from all eggs. The tissues were then collectively triturated by section and dissociated as detailed in 4.5.1.

4.4.1.2 Cerebellum

Dissections of the cerebellum occurred at ED10 (neuronal cultures), ED15 (glial cultures), and ED18 (glial cultures used to produce glial conditioned media). Using the same general dissection procedure, the cerebellum was removed from the hindbrain. Great care was taken to cut through thicker skin and connective tissue covering ED10 cerebella. Later at ED15 and ED18, the formation of the skull was significantly more advanced and was carefully removed to expose the brain.

4.4.1.3 Olfactory Bulbs

The olfactory bulbs (OB) were dissected at ED10. The two OBs were somewhat difficult to identify and are located on the anterior/inferior side of the two lobes of the forebrain. Careful examination revealed the olfactory nerve running from the OB to the nasal cavity of the beak. Using the same dissection techniques, OBs were removed without the connecting nerve.

4.4.2 Spine

After all the brain tissue was dissected from ED10 chicks, the spine and DRGs were dissected from the bodies that were still held on ice. We laid each body supine in a new sterilized dish filled with fresh iced HBSS/1% PS. The chest cavity was opened and organs removed until the spinal column was exposed. The connective tissue surrounding the spinal column was carefully removed to expose the spine and DRGs. The spine was dissected out, meninges removed, and placed on ice in a new dish containing HBSS/1% PS.

4.4.3 DRGs

After the spine was dissected out, DRGs were individually extracted. The nerve connected to each DRG was removed and the meninges were separated off. The cleaned DRG was placed on ice in a separate dish containing HBSS/1% PS.

4.5 Cell Culture

4.5.1 Cell Culture - Neurons

Neurons were dissociated from dissected forebrain, cerebellum, spine, DRG, and olfactory bulb tissue of ED10 chicks. Dissociation began by incubating neurological tissues in 0.025% trypsin/EDTA and 1% penicillin/streptomycin (PS) solutions of HBSS for 20 minutes, followed by 10 minutes of trituration through glass pipets. Suspended tissue was then spun down, pelletized, and re-suspended in plating media. Dissociated neurons were cultured on falcon dishes first coated with 10 ug/ml poly-D-lysine in borate buffer and then 1 mg/ml laminin in F-12. The media contained high glucose DMEM supplemented with 10% fetal bovine serum (FBS), 3.7 g/L sodium bicarbonate, 1% PS, 1% GlutaMax-1 (GM), 1% N3, and 1% 5-fluorodeoxyuridine (FdUr) mitosis inhibitor in F-12. Nerve growth factor, 20 ng/ml, was added to media for DRG and olfactory bulb (OB) cultures. Cerebellar neuron cultures were also supplemented with 5% astrocyte conditioned media. Cultures were incubated in 5% CO2 at 37 C. After 24 hours, cultures were rinsed with HBSS and replenished with fresh media. After one week in culture, media was replaced with serum free media supplemented as detailed above with the exception of 5 mg/ml bovine serum albumin (BSA) in place of FBS. All experiments were run 24-hours after serum depriving the neuron cultures.

4.5.2 Cell Culture – Glia

Glia cells were dissociated from dissected cerebellums of ED-15 and ED-18 chicks by first incubating the cerebellum in 0.025% trypsin/EDTA and 1% penicillin/streptomycin (PS) solutions of HBSS for 20 minutes, followed by 10 minutes of trituration through a glass pipet. Suspended tissue was then spun down, pelletized, and re-suspended in plating media. Glia cultures were grown in DMEM medium supplemented with 10% FBS, 3.7 g/L sodium bicarbonate, 1% PS and1% GM. Every two days, media was removed. Media removed from ED18 glia cultures was further filtered through 0.2 micron polyethersulfone (PES) membrane filters to collect astrocyte conditioned media used to supplement cerebellar neuron cultures. Glia cultures were rinsed with HBSS and replenished with fresh media. After one week in culture, ED15 media was replaced with serum free media supplemented as detailed above with the exception of 5 mg/ml BSA in place of FBS and the addition of FdUr mitosis inhibitor to prevent further cell division. All experiments were run 24-hours after serum depriving the ED15 neuron cultures. ED18 cultures were used for the sole purpose of producing astrocyte conditioned media for cerebellar neuron cultures.

4.6 Cell Viability

4.6.1 Cell Viability - Light Microscopy of Neurons and Glia

After growing cells in culture for one week, neurons and glia cells were observed under the Nikon Eclipse TE 2000U inverted microscope to give a visual

assessment of health. Only cultures free of microbial contamination were used for further experimentation. Cultures free from microbes were held under serum free conditions for 24 hours and then treated with 200ng/ml TNFα, E17, E35, or E100 to evaluate the toxic effects of TNFα and ethanol on neurite outgrowth, membrane blebbing, and cell death. Cells were also supplemented with 5ug/ml blueberry extracts (BBX, NP, and UA) to likewise assess viability. Pre- and post-treatments of these extracts were used to visualize the effects of blueberry supplementation on the neurons and glia cultured with TNFα or ethanol.

4.6.2 Cell Viability – MTT Assay

Neurons were cultured on 96-well clear falcon plates coated with poly-D-lysine and laminin for one week and then serum deprived overnight prior to experimentation. Metabolic cell viability was assessed using an MTT assay as per manufacturer's instructions (Roche). Formazan generation was measured by absorbance (595nm – 620nm) using a Beckman Coulter Multimode DTX 880 multi-plate reader. Protein content was determined for each sample using the BCA protein assay kit (Pierce) and used to calculate absorbance per whole cell protein content.

4.7 ROS Detection

ROS was quantified as DCF-fluorescence produced from the oxidation of H2DCFDA to DCF by peroxide. Neurons were cultured on 6-well clear falcon plates coated with poly-D-lysine and laminin for one week and then serum deprived overnight prior to experimentation. Immediate ROS generation assays determine ROS produced after 45 minutes of pretreatment and 45 additional minutes of post-treatment. Longer term ROS generation was determined by pretreating cultures for 24 hours and post-treating for an additional 24 hours.

4.7.1 Immediate ROS Generation

Pretreatments were applied for 45 minutes in conjunction with 10uM H2DCFDA in SF media. After 45 minutes, cell cultures were washed with HBSS and allowed to rest in SF media for 30 minutes in cell culture incubator. Cells were then lysed with 2% SDS, scraped with a cell scraper, homogenized, and transferred to a 96-well black Falcon plate in 100ul samples. A BCA protein assay was run on each sample to determine whole cell protein content. Formation of ROS was quantified as DCF-fluorescence intensity read by a Beckman-Coulter Multimode DTX 880 microplate reader using 495 nm excitation and 525 nm emission filters. ROS generation was also determined at the completion of pre- and post-treatments. Cells were pretreated for 45 minutes, rinsed with HBSS, and post-treated in conjunction with 10uM H2DCFDA in SF media. Cells were rested, lysed, scraped, and transferred for protein assays and

DCF-fluorescence assays as previously described. Data was compiled in graphs to compare ROS generation after 45 minutes (pretreatments) and after 90 minutes (pre- + post-treatments).

4.7.2 Long Term ROS Generation

Pretreatments were applied for 24 hours and followed by media removal, rinsing with HBSS, and 24 hours of post-treatment. After 24 hours of post-treatments, cultures were rinsed with HBSS and loaded with 10uM H2DCFDA in SF media for 45 minutes. Cell cultures were then washed with HBSS and allowed to rest in SF media for 30 minutes in cell culture incubator. Cells were then lysed with 2% SDS, scraped with a cell scraper, homogenized, and transferred to a 96-well black falcon plate in 100ul samples. A BCA protein assay was run on each sample to determine whole cell protein content. Formation of ROS was quantified as DCF-fluorescence intensity read by a Beckman-Coulter Multimode DTX 880 microplate reader using 495 nm excitation and 525 nm emission filters.

4.8 Total Antioxidant Power Assay

Total antioxidant capacity of both cellular and treatment samples was determined by quantifying their reduction potential to convert Cu+2 to Cu+1. The copper reduction potential is expressed in calibrated Trolox equivalents. Higher levels of Trolox indicate higher total antioxidant power and protection from

oxidation. The colorimetric measurement of optical density was read at 450nm using a Beckman-Coulter Multimode DTX 880 microplate. A BCA protein assay was run on cellular samples to determine Trolox equivalent per ug of whole cell protein. The Oxford Biomedical antioxidant power kit provides procedures for cell culture and liquid food samples. Antioxidant assays were performed for treatments (untreated media, diluents, BBX, NP, P, UA, and E35), cells (C, Cb, S, DRG, OB, and G), and treated cells (Cb, DRG, and G).

4.9 Lipid Peroxidation Assay

Lipid peroxidation is an indicator of cellular injury due to oxidative stress. The lipid peroxidation assay quantifies compounds (malondialdehyde – MDA and 4-hydroxyalkenals – HAE) that are produced from the decomposition of unstable lipid peroxides. The protocol provided by Oxford Biomedical Research was closely followed to quantitatively determine lipid peroxidation products produced in cerebellar neuron cultures due to various treatments specified in the results section. The BCA protein assay was utilized to determine protein content under each treatment condition. A Beckman-Coulter Multimode DTX 880 multi-plate reader generated absorbance measurements at 595nm relative to MDA equivalents. Results of the lipid peroxidation assay were adjusted for protein content and compared to the MDA calibration curve to determine lipid peroxidation end product content.

4.10 TNFα ELISA

The chicken TNFα ELISA measures secreted and cellular TNFα from neurons and glia. By following the kit's published directions (Cusabio), we were able to detect a colorimetric change in the samples corresponding to TNFα abundance. A Beckman-Coulter Multimode DTX 880 multi-plate reader detected the color change at 450nm. The BCA protein assay was utilized to determine protein content under each treatment condition specified in chapter 5. Results of the TNFα ELISA were adjusted for protein content and compared to the TNFα calibration curve to determine TNFα content.

TNFα levels were determined for both secreted and cellular concentrations in cerebellar neurons and glia. Secreted TNFα was a measure of the TNFα present in the media as a result of treatments. After 48 hours of treatments (24-hr pre-/ 24-hr post-), the media was removed, sonicated and utilized in the TNFα ELISA (secretion). The same cultures were rinsed with PBS. Cells were removed through freeze/thaw cycling and scraping in ice cold PBS (the diluent used in the ELISA) and sonicated for 5 seconds. The BCA protein assay was used to determine protein content and appropriate delivery of samples for the ELISA (cellular TNFα).

4.11 Immunostaining and Fluorescent Labeling

Fluorescent labeling techniques were utilized to observe specific proteins present in the neurons and glia studied. Labeled cells were either viewed under

a Nikon Eclipse TE 2000U inverted microscope or utilized in fluorescent density assays read by a Beckman Coulter Multimode DTX 880 multi-plate reader. Cells used in microscopy were grown on coverslips coated with 10 ug/ml poly-D-lysine in borate buffer and then 1 mg/ml laminin in F-12. Cells were fixed for 20 minutes with 4% paraformaldehyde, and permeabilized (cytoplasmic proteins) for 20 minutes with 0.3% TritonX-100 in 1 X PBS prior to immunostaining. Cultures used for fluorescent density assays were not fixed. They were rinsed with HBSS, solubilized and scraped with TBST into eppendorf tubes to be immunolabeled.

Immunolabeling was initiated by blocking cells with 0.1% host serum for one hour, washing once with 1 X HBSS, and adding primary antibody in 0.1% Triton X-100. Cultures were refrigerated overnight at 4 degrees Celsius with agitation. Primary antibodies were then removed and cultures were rinsed twice with HBSS. Secondary antibodies tagged with fluorescent probes (FITC, TRITC, Alexa 555) were added to cultures for 2 hours at 4 degrees Celsius with agitation. Cultures were then rinsed three times with 1 X HBBS.

Cells were sometimes doubly labeled (LR/Nav1.6, LR/Nav-pan, NF/Cal) or counter stained with Hoechst (GFAP/Hoechst, NF/Cal/Hoechst). Double labels were produced by blocking cultures in 1% BSA in PBST for one hour, rinsing three times with 1 X HBSS, and incubating cells in a mixture of two primary antibodies in the refrigerator overnight. Cultures were rinsed three more times and incubated with a mixture of two secondary antibodies that were raised in different species and conjugated to different fluorochromes in 1% BSA for one

hour in the dark. Cultures were washed with 1 X HBSS five times in the dark. When counterstaining with Hoechst was needed, cells were incubated in 0.5ug/ml Hoechst for one minute and rinsed with HBSS one time.

Cells that were destined for fluorescent microscopy were mounted to microscope slides with fluorescent mounting media. The coverslip was sealed with clear fingernail polish around the edges of to prevent drying. Slides were stored in the dark at room temperature. Cells used in fluorescent density assays were assayed for protein content and then pipetted into 96-well black falcon plates.

4.12 Fluorescent Microscopy

Fluorescent microscopy was used to visualize lipid rafts, neuronal neurofilaments (NF), glial fibrillary acidic protein (GFAP), cellular DNA through Hoechst staining, cerebellar Purkinje neurons through Calbindin-D-28K labeling, and voltage-gated sodium ion channels through Nav1.6 and Nav-pan labeling. This technique was used to verify the cellular composition within cultures as well as to determine molecular localization within the cells. Additional fluorescent and ELISA assays were run to quantify what was visualized under a Nikon Eclipse TE 2000U inverted microscope.

4.13 Lipid Raft Labeling

Neurons were labeled with Alexa Fluor 555-lipid raft labeling kit (Invitrogen) as per manufacturer's directions which cross-linked fluorescent dye conjugates to plasma membrane ganglioside (GM1) specifically found in lipid rafts. Lipid raft labeling was often done in conjunction with Nav1.6 and Nav-pan labeling to compare the effects of inflammation and blueberry supplementation on lipid raft/Nav channel localization and density.

4.13.1 Lipid Raft - Microscopy

Neurons were cultured for one week on poly-lysine and laminin coated glass coverslips and then incubated overnight in serum-free media prior to experimentation. Treatments were carried out in serum-free media. After the treatment period concluded, lipid rafts were labeled and cells fixed with paraformaldehyde, mounted with fluorescent media, and viewed under a Nikon Eclipse TE 2000U inverted microscope.

4.13.2 Lipid Raft – Density Assay

Neurons and glia were cultured for one week in 6-well falcon plates coated with poly-D-lysine and laminin and then serum deprived overnight prior to experimentation. Treatments were delivered in serum free (SF) media. After treatment duration, neurons were labeled with Alexa Fluor 555-lipid raft labeling kit. Neurons were rinsed twice with cold HBSS, scraped and solubilized with

TBST, transferred into eppendorf tubes, sonicated for 5 seconds, and transferred into 96-well black falcon plates. Lipid raft density was measured as fluorescent density of Alexa Fluor 555 using the Beckman Coulter Multimode DTX 880 multi-plate reader. Protein content was determined for each sample using the BCA protein assay kit (Pierce) and used to calculate fluorescent intensity per microgram of protein assayed.

4.14 Cell Fractionation

Cell fractionation was performed to separate cytosolic and plasma membrane fractions from cerebellar neurons. Neurons were sonicated in a sucrose buffer (20mM Tris-HCl, 2mM EDTA, 0.5mM EGTA, 2 mM AEBSF, 25 ug/ml leupeptin, 0.33M sucrose, pH 8.0), and then centrifuged at 14000 rpm for 20 minutes (Labnet Spectrafuge 16M). The cytosolic fraction (supernatant) was removed. The remaining membrane fraction (pellet) was re-suspended in a sucrose buffer without leupeptin. The membrane fraction was centrifuged for an additional 20 minutes. The plasma membrane (supernatant) was collected. A BCA protein assay was run on cytosolic and plasma membrane fractions to determine protein content per sample.

4.15 Nav Channel Localization

Cerebellar neuron cultures were treated with 24 hours of pretreatments (TNFα, E35, BBX and UA) and 24 hours of post-treatments. After completion of

the 48 hour treatment phase, neurons were separated into cytosolic and membrane fractions as detailed in section 4.14. Neurons were labeled with Nav-pan as indicated in section 4.11. A BCA protein assay was performed to determine micrograms of protein per test sample. Cytosolic and membrane samples were transferred into 96-well black falcon plates and analyzed with the Beckman Coulter Multimode DTX 880 multi-plate reader to measure Nav density. Density of cytosolic and membrane Nav channels was reported as a percentage of the whole cell Nav density, thus illustrating differences in localization due to treatments.

4.16 Statistical Analysis

The data is presented as mean values ± standard deviations. Significant differences between treatments and within multiple groups ($p<0.05$ or $p<0.001$) were examined using analysis of variance (ANOVA) followed by Tukey's Post hoc analyses. Statistical analyses were conducted utilizing StatsPro 2009 professional software package. Significance is indicated in the results (Chapter 5), and further statistical data (including n-values) is available in Appendix B.

Chapter 5: Results

5.1 Isolation of Embryonic Chick Brain

Embryonic chick brains were cleanly dissected from ED10 chicks and inspected for deformity. Only anatomical normal brains were utilized in this research. Nearly 800 brains were dissected. A typical brain was photographed and labeled in Fig 5.1.

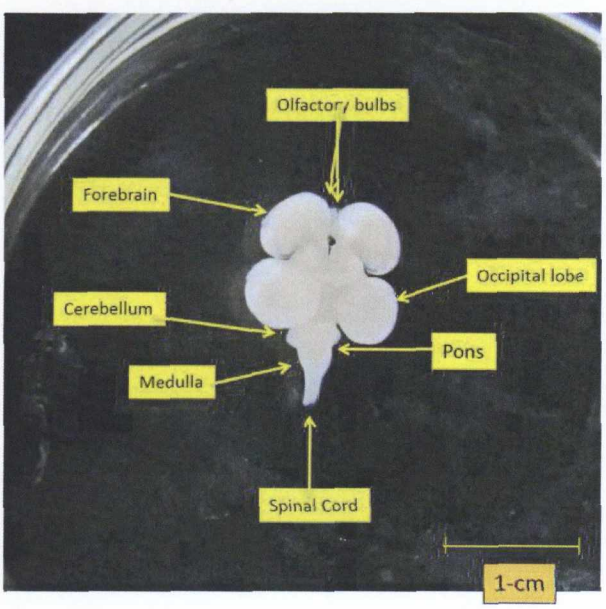

Fig 5.1 Embryonic Chick Brain Photo (ED10)

The brain was further dissected into the forebrain, olfactory bulbs (anterior to the forebrain), and cerebellum. Nervous tissue was triturated to dissociate the neurons utilized in this study. All neurons were obtained from embryonic day ten (ED10) chicks. Spinal and DRG neurons were concurrently obtained from dissections of the spine (not pictured).

5.2 Cell Viability – Microscopy of Neurons and Glia

The embryonic chick model was successfully utilized to culture dissociated neurons from the forebrain, cerebellum, spine, olfactory bulb and dorsal root ganglia, as well as glia from the cerebellum. Photographs of neuron (ED10) and glia (ED15) one-week old cultures are shown in Fig 5.2. These cultures provided the basis for all further experimentation. Visual inspection through a light microscope ensured only cultures free of microbial contamination and displaying good neurite outgrowth were used in this research. Neurons were recognized by their small cell body and long simply branched neurites; whereas, glia cells displayed larger cell bodies, more intricate processes, and often active cell division.

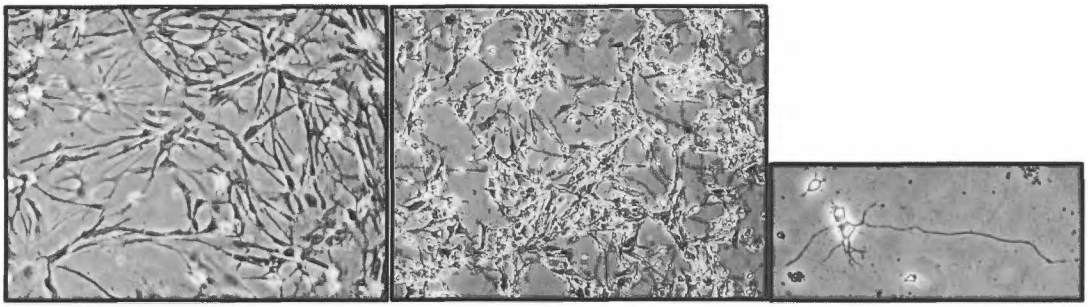

a. Cerebellum b. Forebrain c. Forebrain Neuron

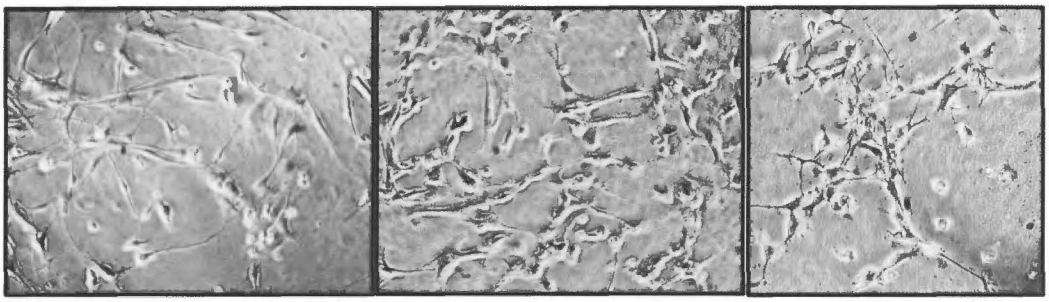

d. DRG e. Spine f. Olfactory Bulb

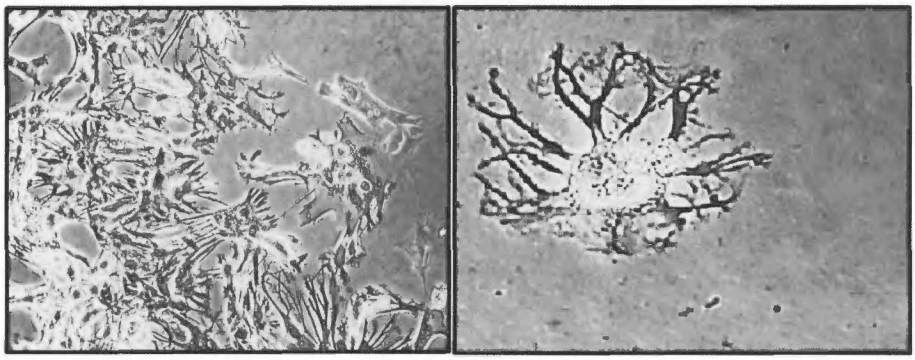

g. Glia h. Glial Cell

Fig 5.2 Microscopy of Cell Cultures

Images of cell cultures taken under the light microscope reveal healthy cultures of each cell type studied in this research. Neuronal cultures (a.-f.) were obtained from ED10 chicks and glia cultures (g.&h.) were derived from ED15 chicks. Photographs were taken at one week in culture.

5.3 Immunochemical Confirmation of Neurons and Glia

To ensure our cultures were predominately composed of the neurons and glia of interest, immunochemical techniques were utilized. All neuron cultures were found to be densely packed with positive neurofilament (NF) fluorescence (Fig 5.3a). Neurofilaments are a neuron specific component of their cytoskeletons. Neuronal cultures contained only minimal numbers of astrocytes (Fig 5.3c), whereas glia cultures contained about 90% astrocytes and were void of neurons.

Astrocytes were positively identified through glial fibrillary acidic protein (GFAP) labeling, (Fig 5.3c). GFAP is an intermediate filament contributing to the shape and structure of astrocytes within the CNS. Any astrocytes present in neuronal cultures were part of the initial dissected tissue but did not multiply due to a mitosis inhibitor in the media. The glia cultures were designed to grow and multiply astrocytes (no mitosis inhibitor), but to preferentially kill neurons through alterations in plating substrate. Glia cultures were supplemented with a mitosis inhibitor 24 hours prior to experimental manipulation to hold the cell count constant.

The contribution of the Purkinje neuron was of particular interest in the unique molecular anatomy of the cerebellum. Cerebellar neuron cultures were labeled with a Purkinje specific marker, Calbindin-D-28K (Cal). Our cerebellar cultures contained an abundance of developing Purkinje neurons (Fig 5.3b) whose architecture was enhanced through astrocyte conditioned media.

Embryonic chicks provided an ideal model to study Purkinje neurons. Unlike mammalian models, early embryonic avian cultures are nearly free from other cerebellar neurons (Baptista et al. 1994, Feirabend 1990, Feirabend et al. 1985).

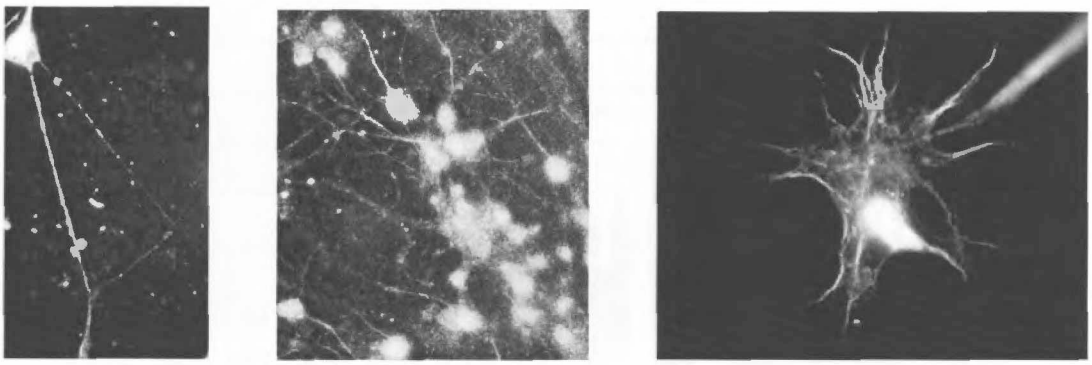

a. NF–Neuron **b. Cal–Purkinje** **c. GFAP–Astrocyte**

Fig 5.3. Immunochemical Identification of Neurons and Glia
Cultures were labeled with primary antibodies and secondary antibodies tagged with FITC or TRITC. Fluorescent microscopy confirms the presence of neurofilaments (marked with mouse NF-M/FITC) in neuronal cultures (a.), Purkinje neurons (marked by mouse Calbindin-D-28K/TRITC) in the cerebellar neuron cultures (b.), and astrocytes (marked by mouse GFAP/TRITC) in the glia cultures (c.).

5.4 Metabolic Cell Viability

Metabolic viability of neurons and glia was assessed utilizing an MTT assay. In metabolically active cells, formazen dye was cleaved from tetrazolium salts and measured in the MTT colorimetric assay. Here we show that over a 24-hour period, pre- and post-treatments of crude blueberry extracts (BBX),

nonpolar BBX fractions (NP), and ursolic acid (UA), increase the metabolic rate of cells even when exposed to TNFα (Fig 5.4). We also see in Fig 5.5, that alcohol did not metabolically kill the cells until significant concentrations above 100 uM ethanol were delivered.

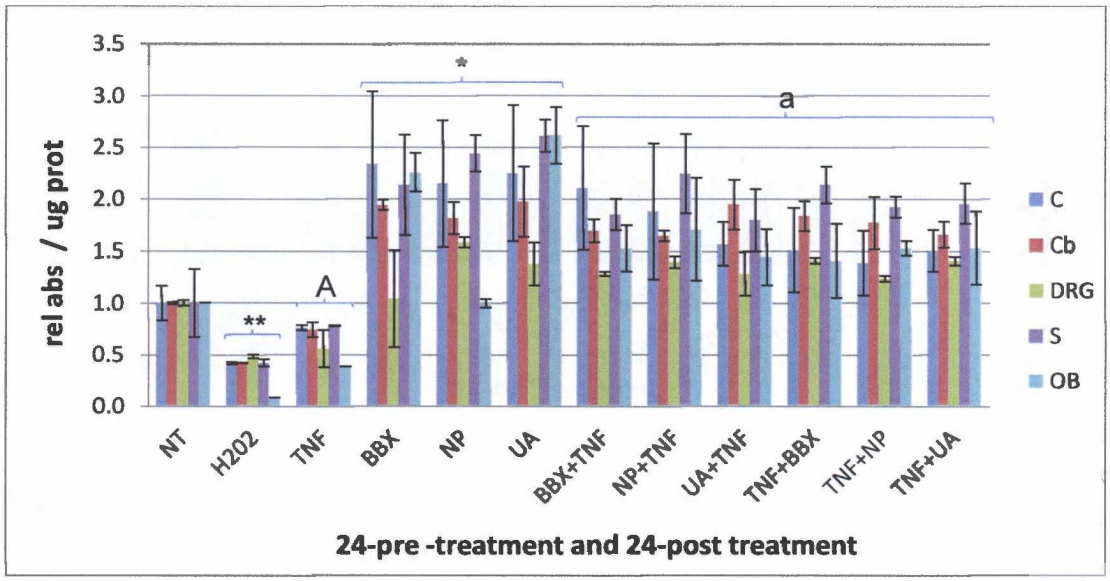

Fig 5.4 Comparative Neuronal Viability

Dissociated neurons from multiple regions (C-Forebrain Cortex, Cb-Cerebellum, DRG, S-Spine, OB-Olfactory Bulb) were assessed for metabolic activity via an MTT assay. Pretreatments were applied for 24 hours, rinsed, and followed by 24 hours of post treatment before the MTT assay was performed. Columns with no pretreatment reflect samples held in fresh SF media for 24 hours followed by the indicated treatments (NT, 10mM H_2O_2, 200ng/ml TNFα, 5ug/ml BBX, 5ug/ml NP, 5ug/ml UA) for 24 hours. All results are reported as absorbance (595nm – 620nm) normalized to the negative control (NT-no treatment) per microgram of protein assayed. Values are reported as $P< 0.05$ where ** indicates reduced viability from NT, (*) indicates increased viability from NT with the exception of DRG(BBX) and OB(NP), and "a" indicates improved viability from "A".

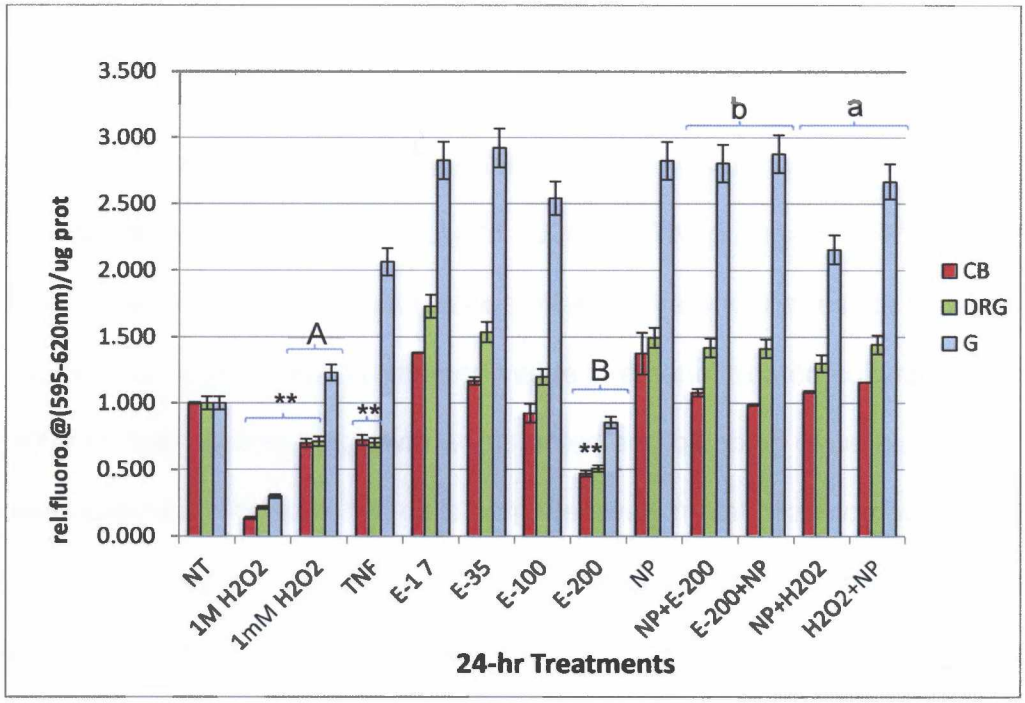

Fig 5.5 Comparative Viability of CNS, PNS, Glial Cells

The CNS is represented by cerebellar neurons (red), the PNS is represented by DRG neurons (green), and the glia cells (blue) were obtained from the cerebellum. Pretreatments were applied for 24 hours, rinsed, and followed by 24 hours of post treatment before the MTT assay was performed. Columns with no pretreatment reflect samples held in fresh SF media for 24 hours followed by the indicated treatments (NT, 1M H_2O_2, 1mM H_2O_2, 200ng/ml TNFα, 17.4 mM ethanol – E17, E35, E100, E200, 5ug/ml NP) for 24 hours. All results are reported as absorbance (595nm – 620nm) normalized to the negative control (NT-no treatment) per microgram of protein assayed. Values are reported as $P< 0.05$ where (**) indicates reduced viability from NT, and "a" and "b" indicate improved viability from "A" and "B" respectfully.

Cellular viability as a result of treatments was determined by the MTT assay (Fig 5.4 and Fig 5.5) and confirmed via light phase microscopy (not shown). Berry fractions were found to increase viability, whereas high doses (greater than 100mM) of ethanol and 200ng/ml TNFα began to kill cells within 24 hrs. Visual inspection of cultures was often contrary to the results of the MTT assay. Although neurons remained viable in ethanol treated cultures less than 100mM, their neurite outgrowth was stunted and blebbing of cellular membranes was observed. Presumably, cells can effectively metabolize compounds while undergoing structural demise. It was evident that cerebellar neurons were more sensitive to ethanol than the other neuronal types studied and glia cells were most resistant to ethanol toxicity. As a result of these findings, we turned to immunolabeling techniques that quantify some of these visually observable changes in cerebellar health.

5.5 Cerebellar Neuron and Glial Health

Neurons were labeled with NF, Cal, and Hoechst to assess changes in the cytoskeletal structure, Purkinje density, and DNA of cerebellar neurons. Glia were comparatively labeled with GFAP and Hoechst to quantify changes in astrocyte density and glial DNA. Fluorescent assays were performed to quantify changes in cellular health as measured by structure, specific cell density, and DNA nuclear stability in ethanol/TNFα treated cells. We also conducted assays to investigate the effectiveness of BBX/UA treatments and to identify proponents

of cellular demise due to increasing levels of ethanol. In general, we observed a progressive decline in cellular morphology that preceded cell death, but that can be both prevented and reversed by BBX/UA treatments.

The results of these assays support our observations from under the light microscope. It is apparent that NF and GFAP, both structural filaments, are quickly bolstered by BBX and UA supplementation as compared to less variable DNA levels (Figs 5.6 and 5.8). Blueberry treatments, whether before or after insult, prevent the ill effects of ethanol and TNFα to neurite outgrowth, Purkinje density, astrocyte density, and DNA stability (Figs 5.6 and 5.8). In cerebellar neurons, we also discover increasing doses of ethanol to most quickly diminish NF density, followed by Purkinje density, and lastly Hoechst labeled DNA (Fig 5.7). In the glia culture we observed a more delayed decline of Hoechst labeling as compared to the neuronal culture while GFAP fluorescence was quickly reduced at physiological levels below100mM ethanol (Fig 5.9).

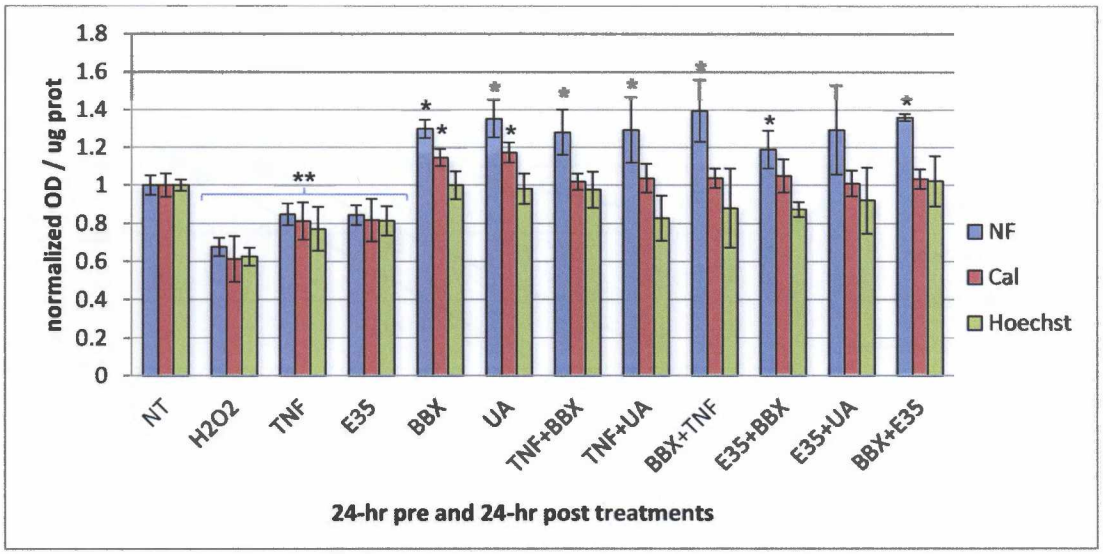

Fig 5.6 Cerebellar Neuronal Health

Cerebellar neuron cultures were dyed with Hoechst and doubly immuno-labeled with NF and Cal. Colormetric assays of Hoechst dyed cellular DNA is compared to fluorescent density assays of NF (marked with mouse NF-M/FITC) and Cal (marked with mouse Cal/TRITC). Pretreatments were applied for 24 hours, rinsed, and followed by 24 hours of post treatment before performing colormetric and fluorescent density assays. Columns with no pretreatment reflect samples held in fresh SF media for 24 hours followed by the indicated treatments (NT, 1mM H202, 200ng/ml TNFα, E35, 5ug/ml BBX, 5ug/ml UA) for 24 hours. Results are normalized to the negative control (NT) and reported as optical density (OD) per microgram of protein assayed. Values are reported as $P < 0.05$ where (**) indicates reduced viability from NT and (*) indicates increased viability from NT.

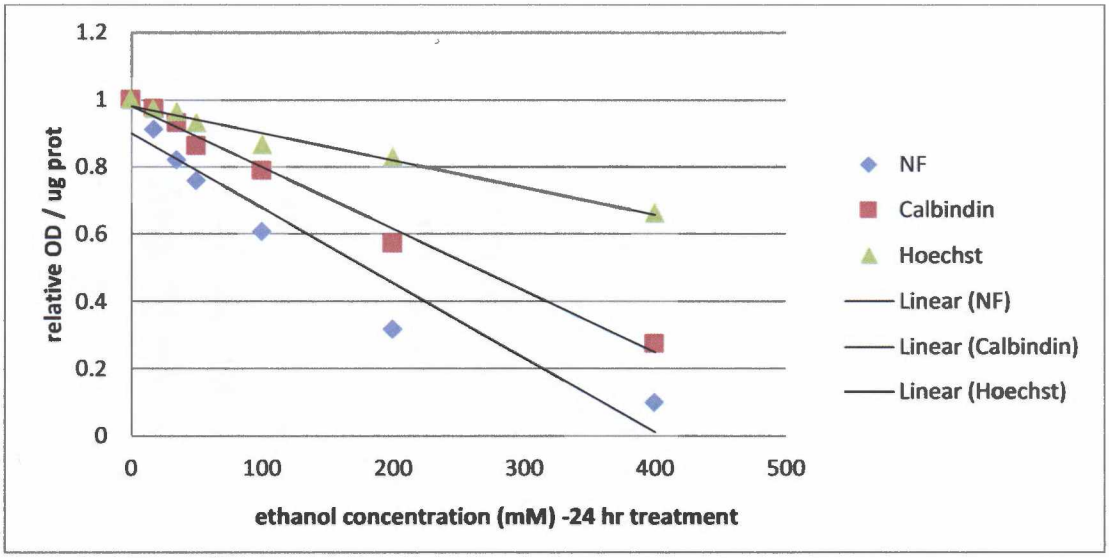

Fig 5.7 Effects of Increasing Ethanol on Cerebellar Neurons

Cerebellar neuron cultures were dyed with Hoechst and doubly immuno-labeled with NF and Cal. Colormetric assays of Hoechst dyed cellular DNA is compared to fluorescent density assays of NF (marked with mouse NF-M/FITC) and Cal (marked with mouse Cal/TRITC). Cultures were held for 24 hours under increasing levels of ethanol (0, 17.4, 35, 50, 100, 200, and 400 mM) in SF media. Results are normalized to the negative control (NT) and reported as optical density (OD) per microgram of protein assayed.

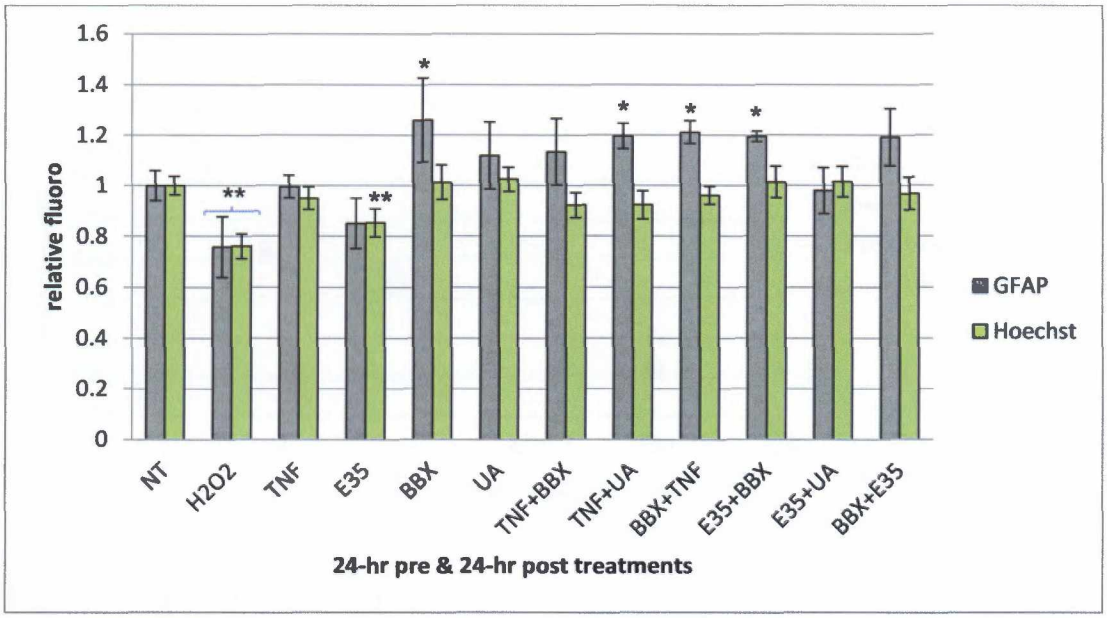

Fig 5.8 Cerebellar Glia Health

Cerebellar glia cultures were dyed with Hoechst and immuno-labeled with GFAP. Colormetric assays of Hoechst dyed cellular DNA is compared to fluorescent density assay of GFAP (marked with mouse GFAP/TRITC). Pretreatments were applied for 24 hours, rinsed, and followed by 24 hours of post treatment before performing colormetric and fluorescent density assays. Columns with no pretreatment reflect samples held in fresh SF media for 24 hours followed by the indicated treatments (NT, 1mM H_2O_2, 200ng/ml TNFα, E35, 5ug/ml BBX, 5ug/ml UA) for 24 hours. Results are normalized to the negative control (NT) and reported as optical density (OD) per microgram of protein assayed. Values are reported as $P< 0.05$ where ** indicates reduced viability from NT and * indicates increased viability from NT.

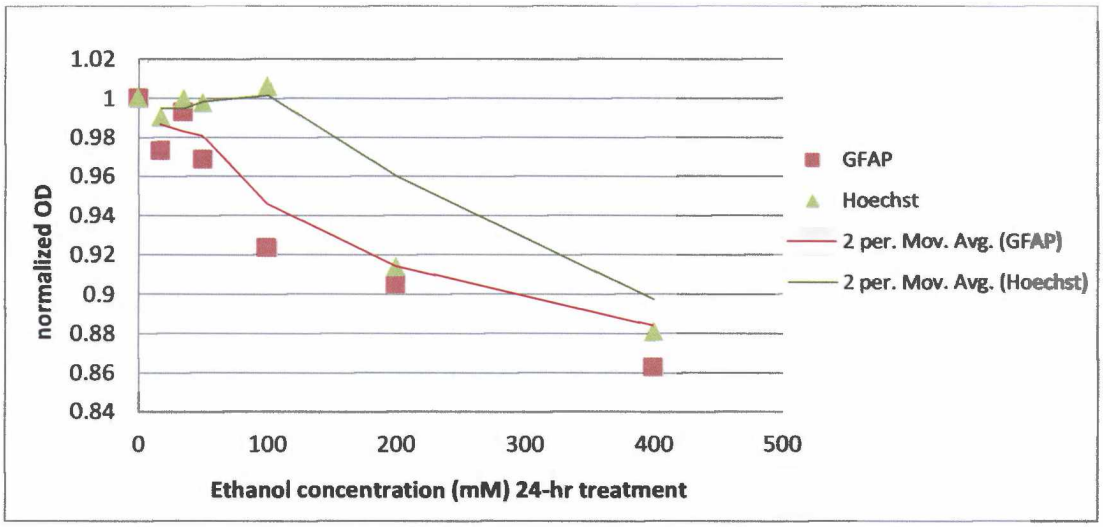

Fig 5.9 Effects of Increasing Ethanol on Cerebellar Glia

Cerebellar glia cultures were dyed with Hoechst and immuno-labeled with GFAP. Colormetric assays of Hoechst dyed cellular DNA is compared to the fluorescent density assay of GFAP (marked with mouse GFAP/TRITC). Cultures were held for 24 hours under increasing levels of ethanol (0, 17.4, 35, 50, 100, 200, and 400 mM) in SF media. Results are normalized to the negative control (NT) and reported as optical density (OD) per microgram of protein assayed.

5.6 ROS Detection

Cellular ROS production is a measure of oxidative stress that can be quantified by indirectly detecting levels of peroxide. The results of the ROS detection assay foretell the oxidative environment that may lead to oxidative damage of lipids, proteins, and DNA. In total, we found ethanol and TNFα treatments to increase neuronal ROS production, and conversely for blueberry extracts to decrease ROS. When applied before or after ethanol /TNFα, blueberry extracts successfully blunted ROS production. The cerebellar neurons

produced the most ROS at rest (Fig 5.10) and were most responsive to stimuli (TNFα and ethanol) as compared to forebrain cortical neurons, spinal neurons, and DRGs (Fig 5.11). This was true in both immediate response tests (45-90 minutes), as well as after 24 hours of ethanol or TNFα treatments (Fig 5.11 and 5.12). Additional ROS assays from chick forebrain cortical, spinal, DRG and human neuroblastoma cells are included in the Appendix with similar reductions in ROS production attributed to blueberry supplementation (Fig A.1 – Fig A.5).

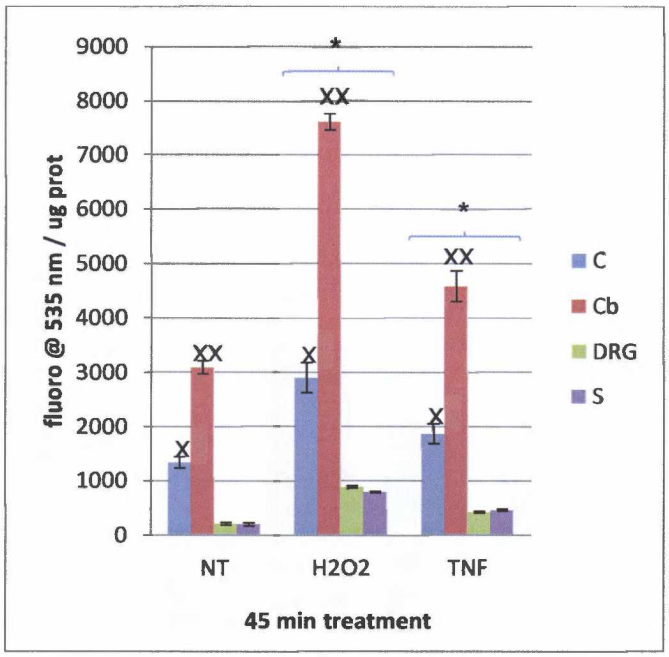

Fig 5.10 Comparison of Total ROS Produced

ROS is detected as a measure of DCF fluorescent output at 535 nm per microgram of protein sampled. Neuronal cultures (C, Cb, DRG, and S) were held for 45 minutes under three conditions (no treatment, 1mM H202, and 200ng/ml TNFα). Values are reported as $P < 0.001$ where (*) indicates increased ROS generation compared to NT. Cerebellar neurons (Cb-xx) and forebrain cortical neurons (C-x) both produced significantly higher ROS than DRG and spinal (S) neurons, with Cb-xx > C-x.

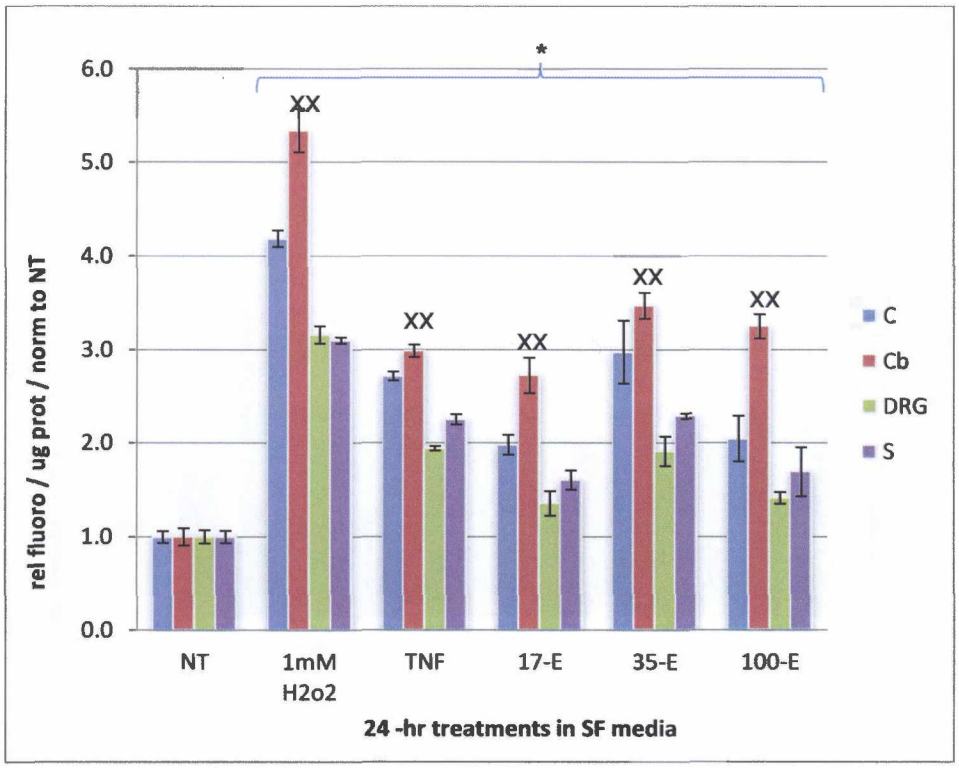

Fig 5.11 Cerebellar Neurons Generate Most ROS due to Ethanol

ROS is reported as a measure of relative fluorescence per microgram of protein sampled. All results are normalized to the negative control (NT). Neuronal cultures (C, Cb, DRG, and S) were held for 24 hours under six conditions (no treatment, 1mM H_2O_2, and 200ng/ml TNFα, 17.4 mM ethanol – 17E, 35E, and 100E). Values are reported as $P< 0.05$ where (*) indicates increased ROS generation compared to NT. Cerebellar neurons (Cb-xx) produced higher ROS than other neuronal types.

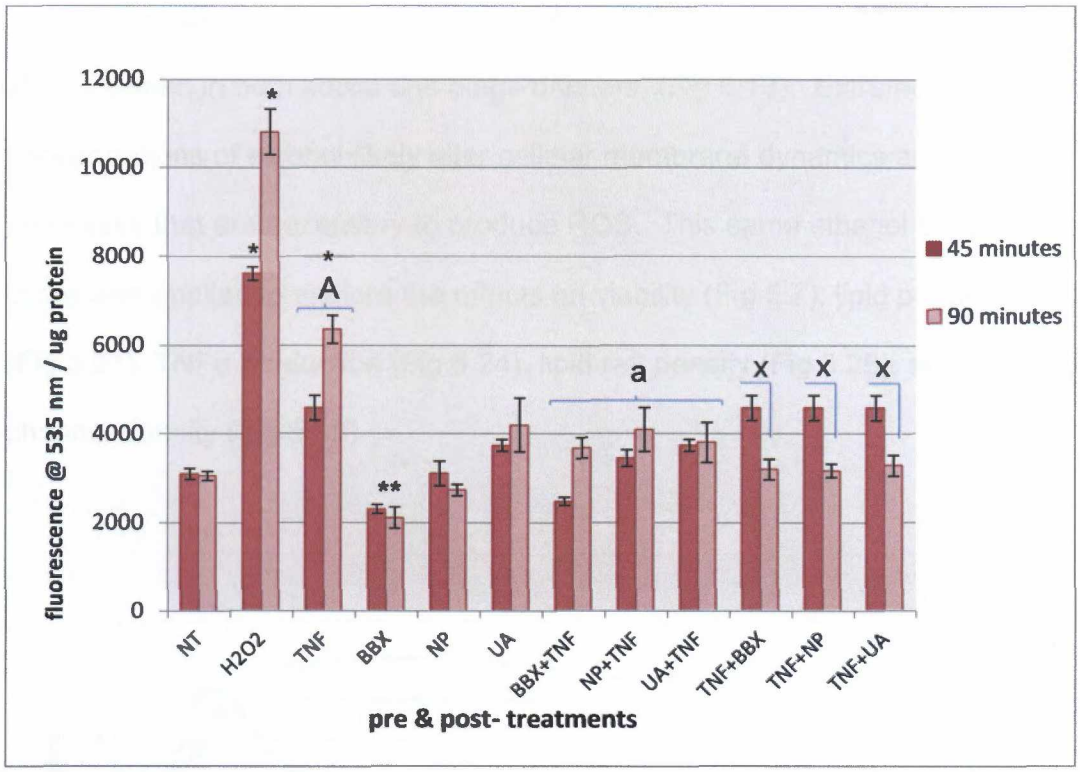

Fig 5.12 Immediate ROS Generation in Cerebellar Neurons

ROS is reported as a measure of fluorescent output at 535 nm per microgram of protein sampled taken at 45 minutes (after pretreatments) and at 90 minutes (after pre- and post-treatments are complete). Cerebellar neuronal cultures were held for 45 minutes under different conditions. Columns NT through UA had the same pre- and post-treatments and the remaining columns were pretreated with 5ug/ml BBX, 5ug/ml NP, 5ug/ml UA, and 200ng/ml TNFα (last three columns). Pretreatments were rinsed and post-treatments were added for another 45 minutes: no treatment (NT), 1mM H_2O_2, 200ng/ml TNFα, 5ug/ml BBX, 5ug/ml NP, 5ug/ml UA, 200ng/ml TNFα, 5ug/ml BBX, 5ug/ml NP, and 5ug/ml UA. Values are reported as $P< 0.05$ where "a" indicates decreased ROS generation compared to "A". BBX** is significantly lower than NT while (*) is higher. ROS was decreased ($P< 0.001$) at 90 minutes (x) by BBX, NP, and UA compared to 45 minutes.

Interestingly, we discovered that the highest levels of ROS are generated at levels seen in both social and binge drinkers, (Fig 5.13). Extreme concentrations of alcohol likely alter cellular membrane dynamics and metabolic processes that are necessary to produce ROS. This same ethanol concentration curve was applied to explore the effects on viability (Fig 5.7), lipid peroxidation (Fig 5.21), TNFα production (Fig 5.24), lipid raft density (Fig 5.28), and Nav channel density (Fig 5.33).

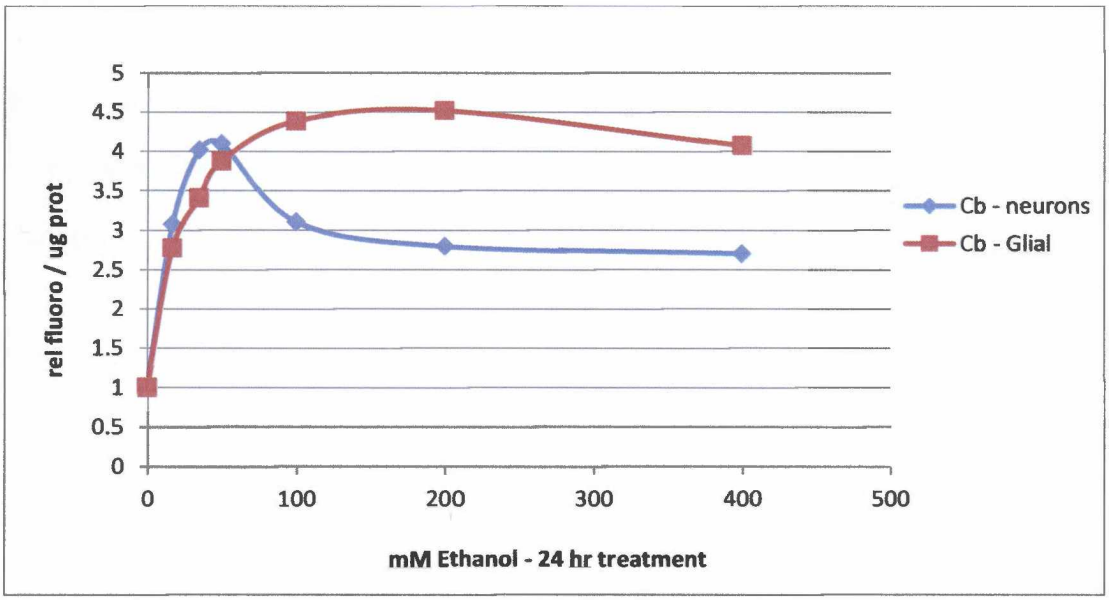

Fig 5.13 ROS Generated by Cerebellar Neurons and Glia with Increasing Ethanol Exposure - ROS is reported as a measure of relative fluorescence normalized to the control per micrograms of protein sampled. Cerebellar neuron and glia cultures were held in increasing concentrations of ethanol (0, 17.4, 35, 50, 100, 200, 400 mM) in serum-free media for 24 hours.

The central nervous system (CNS) is thought to be severely affected by alcohol abuse. Obvious delirious effects are presented by loss of coordination, slurred speech, poor decision making, and loss of inhibitions. We sought to compare representative neurons from the CNS and the peripheral nervous system (PNS) to identify whether the CNS may produce more ROS due to ethanol. At physiological observed levels of blood alcohol content (BAC), the CNS does indeed produce more ROS than both the PNS and glia cells (Fig 5.14). At these concentrations of ethanol (17.4mM ethanol = 0.08 BAC, and 35mM ethanol = 0.16 BAC), the nonpolar (NP) fraction of blueberries blunted ethanol induced ROS generation as both a pre- and post-treatment (Fig 5.14). The ursolic acid used through this study was isolated from the nonpolar (NP) fraction.

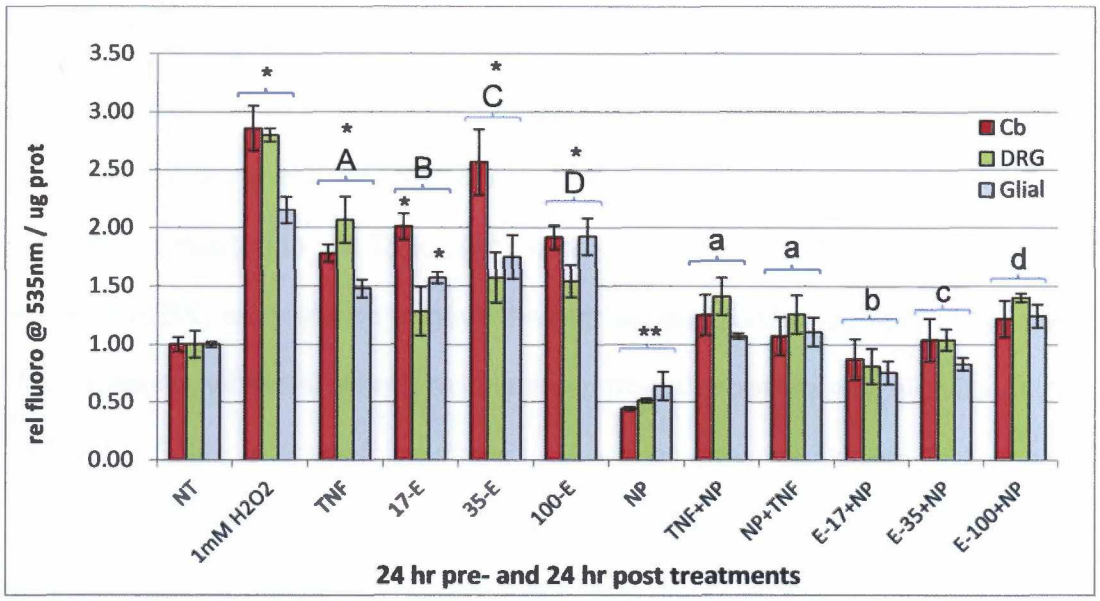

Fig 5.14 Comparative ROS Response: CNS vs. PNS vs. Glia

The CNS is represented by cerebellar neurons (red), the PNS is represented by DRG neurons (green), and the glia cells (blue) were obtained from the cerebellum. ROS is reported as a measure of fluorescent output at 535 nm per microgram of protein sampled taken at 48 hours after pre- and post-treatments are complete. Results are normalized to the negative control (NT). Cultures were held for 24 hours under different conditions. Columns NT through NP had no treatment and the remaining columns were pretreated with 200ng/ml TNFα, 5ug/ml NP, 17.4 mM ethanol, 35mM ethanol, and 100mM ethanol. Pretreatments were rinsed and post-treatments were added for another 24 hours: NT (1), 1mM H_2O_2 (2), 200ng/ml TNFα (3), 17E (4), 35E (5), 100E (6), NP (7&8), TNFα (9), NP (10-12). Values are reported as $P< 0.05$ where "a, b, c & d" indicate decreased ROS generation compared to "A, B, C & D" respectfully. Treatments indicated by (*) increased ROS while (NP **) resulted in significantly lower ROS than NT.

5.7 Antioxidant Capacity

The antioxidant capacity of Alaska wild blueberries stands at up to ten times that of commercially cultivated berries as assessed by copper reduction potential converted to uM Trolox (antioxidant) equivalents. Crude blueberry extracts (BBX) were shown to have the highest antioxidant capacity (1195 uM Trolox equiv), whereas ursolic acid isolated from the berries was significantly lower (Fig 5.15). Interestingly, ursolic acid was as effective as both BBX and NP in reducing ROS (Fig 5.18), therefore avenues other than direct ROS scavenging potential may be relevant to ursolic acid's capacity as an antioxidant.

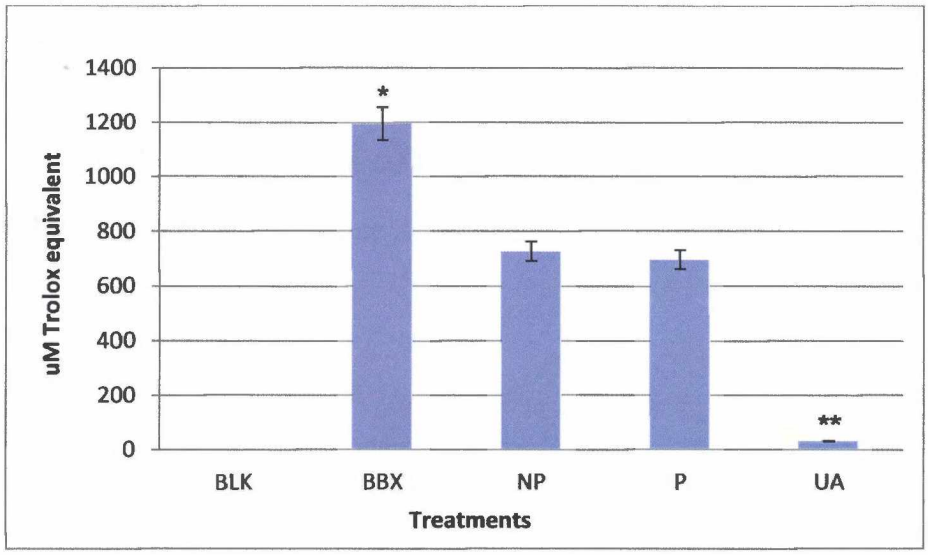

Fig 5.15 Antioxidant Capacity of Wild Alaska Blueberries
Total antioxidant power was determined by the ability of blueberry fractions to reduce copper. Antioxidant capacity is reported in calibrated Trolox equivalents as measured by colormetric analysis. The columns include: 1) blank (dilutent only), 2) crude blueberry extracts, 3) non-polar blueberry fraction, 4) polar blueberry fraction, 5) isolated ursolic acid. Results are calibrated to reflect approximate antioxidant capacity found in one cup of fresh blueberries. Values are reported as $P < 0.05$ where (**) indicates reduced antioxidant capacity from P and NP; (*) indicates increased antioxidant capacity from P and NP.

The total antioxidant capacity of all neurons was similar with the exception of the olfactory bulb neurons which were significantly lower (Fig 5.16). Interestingly, loss of smell is commonly found as a preliminary sign of Parkinson's disease, Alzheimer's disease, some genetically linked cerebellar ataxias, and alcoholism (Haehner et al. 2007, Abele et al. 2003, Connelly et al. 2003, Rupp et al. 2003, Nordin et al. 1995). Cerebellar glia cells displayed a

30% increase in antioxidant capacity compared to neurons (Fig 5.16). Alcohol exposure reduced this capacity in all cells. When berry fractions were applied to neurons and glia cells, the cellular antioxidant capacity increased and prevented depression of cellular antioxidant defenses by alcohol (Fig 5.18).

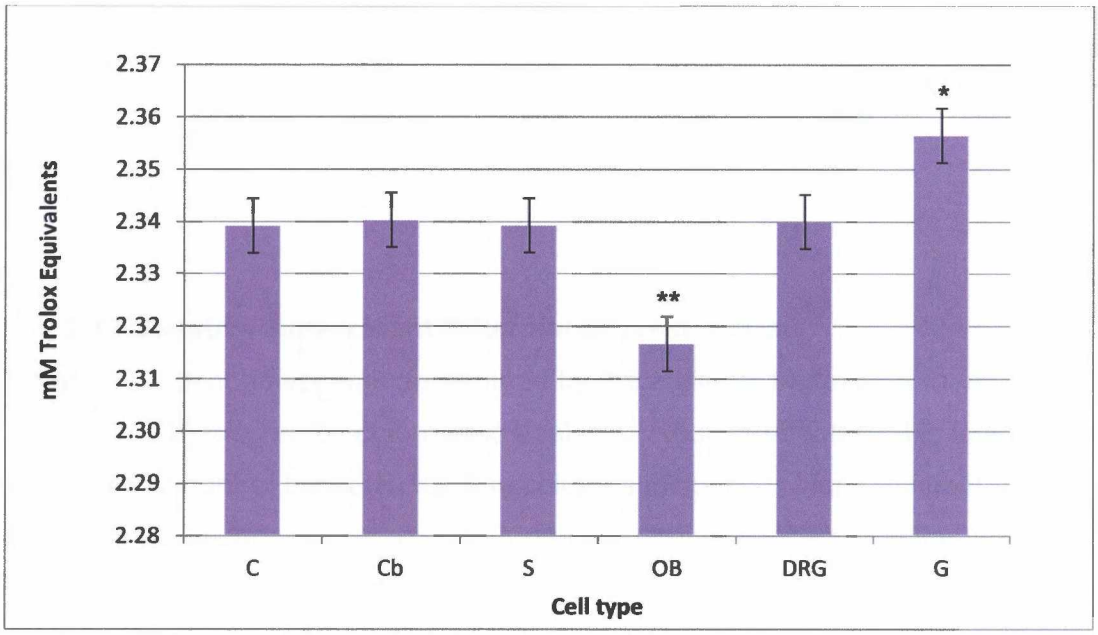

Fig 5.16 Innate Antioxidant Capacity of Neurons and Glia

Total antioxidant power was determined by the ability of different cell types to reduce copper. Antioxidant capacity is reported in calibrated Trolox equivalents as measured by colormetric analysis. The columns include neurons from the forbrain cortex (C), cerebellum (Cb), spine (S), olfactory bulb (OB), and DRGs. Glia cells (G) were obtained from the cerebellum. Values are reported as $P<0.05$ where (**) indicates reduced antioxidant capacity from other neurons while (*) indicates increased antioxidant capacity from other neurons.

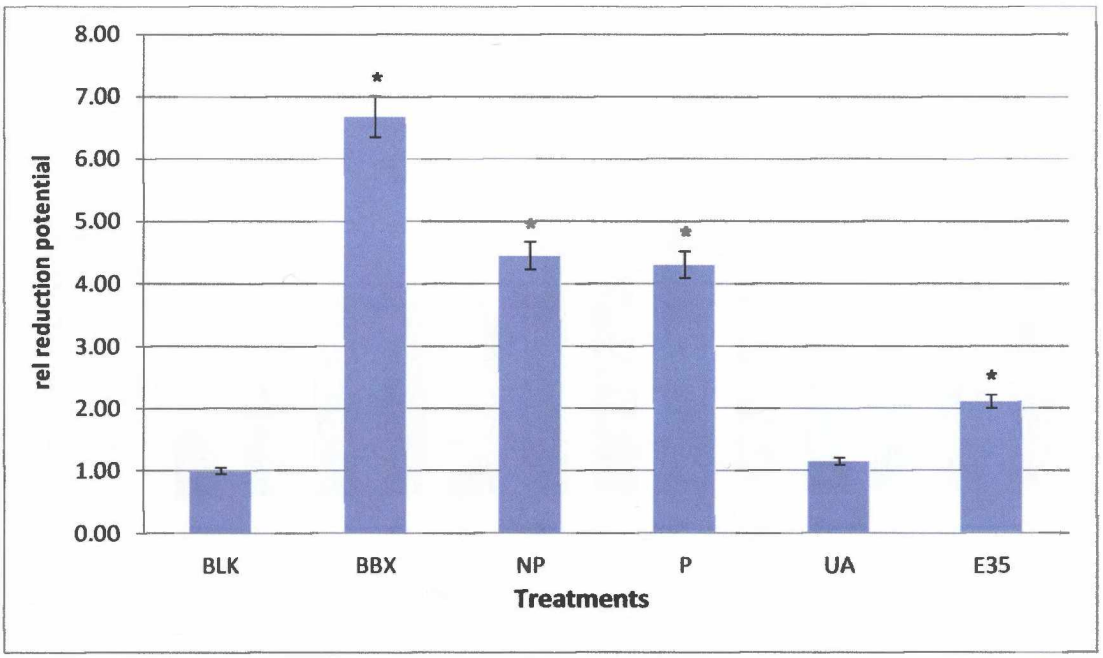

Fig 5.17 Relative Antioxidant Potential of Treatments

Total antioxidant power was determined by the ability of treatments to reduce copper and measured by colormetric analysis. Reduction potential is relative to the negative control blank (BLK). The columns include: 1) blank (dilutent only), 2) 5ug/ml crude blueberry extracts, 3) 5ug/ml non-polar blueberry fraction, 4) 5ug/ml polar blueberry fraction, 5) 5ug/ml isolated ursolic acid, 6) 35mM ethanol. Values are reported as $P < 0.05$ where (*) indicates increased antioxidant capacity from the BLK.

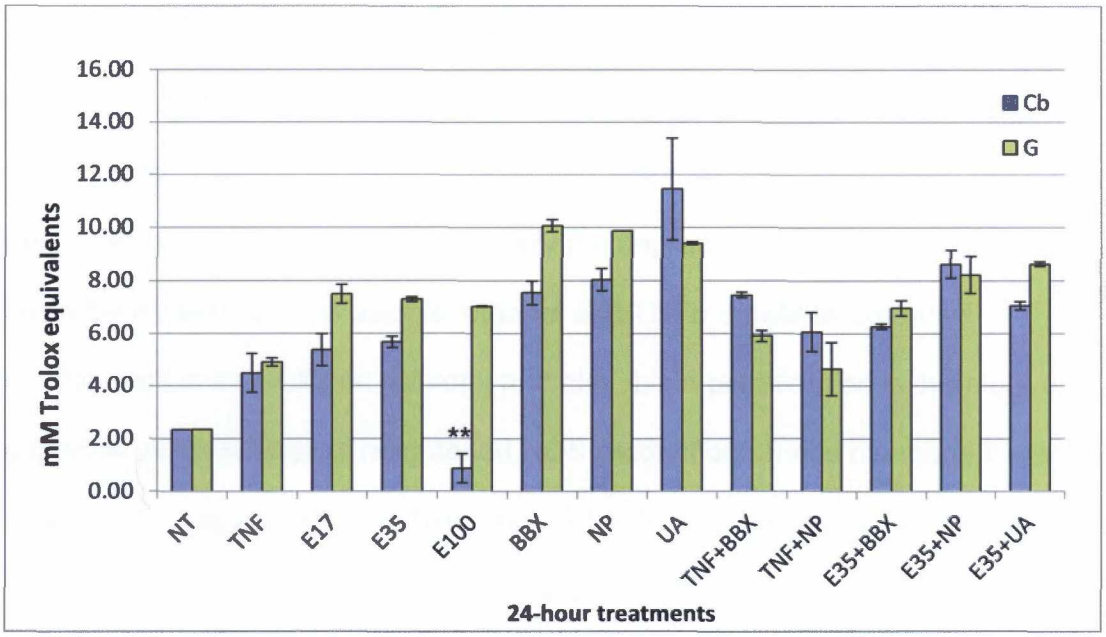

Fig 5.18 Total Antioxidant Capacity of Cerebellar Neurons and Glia

Total antioxidant power was determined by the ability of cerebellar neurons (Cb) and glia (G) to reduce copper after undergoing 48 hours of treatments (24 hour pre- and 24 hour post-treatments). Antioxidant capacity is reported in calibrated Trolox equivalents as measured by colormetric analysis. Cultures were held for 24 hours under different conditions. Columns NT through UA had no treatment and the remaining columns were pretreated with 200ng/ml TNFα (9&10), and 35mM ethanol (11-13). Pretreatments were rinsed and post-treatments were added for another 24 hours: NT, 200ng/ml TNFα, E17, E35, E100, 5ug/ml BBX, 5ug/ml NP, 5ug/ml UA, BBX, NP, UA, NP, UA. Values are reported as $P < 0.05$ where (**) indicates decreased antioxidant capacity from the control (NT). All other treatments resulted in increased antioxidant capacity.

5.8 Lipid Peroxidation

The data presented from the lipid peroxidation assays clearly illustrate that exposure to ethanol and TNFα induced peroxidation of the lipids within cellular membranes. Lipid peroxidation is simply the degradation of lipids via oxidation. As evident from the ROS assays, ethanol and TNFα create an oxidative environment in the cultured neurons and glia. Lipid peroxidation is therefore an expected consequence of heightened ROS production. Since blueberry extracts successfully negated ethanol/TNFα induced ROS, we anticipated similar abatement in lipid peroxidation end products.

Blueberry fractions ably protected the cerebellar membranes from lipid peroxidation (Fig 5.19). Additionally, depletion of membrane cholesterol by methyl-beta-cylcodextrin (MBCD) reduced peroxidation end product (MDA), possibly indicating the role of lipid rafts in oxidative events within the neuron (Fig 5.20). Comparable to results presented in Fig 5.13, ROS production, lipid peroxidation assays revealed a peak in lipid peroxidation end products at physiologically observed BAC levels (Fig 5.21).

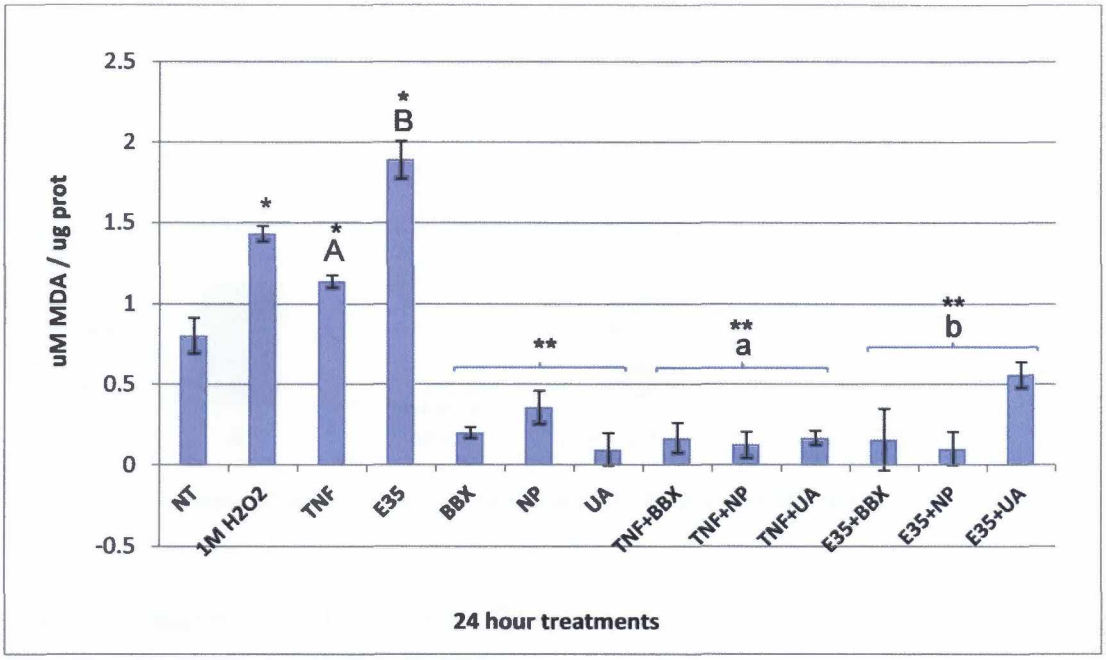

Fig 5.19 Blueberry Fractions Blunt Lipid Peroxidation Induced by TNFα and 35mM Ethanol in Cerebellar Neurons - Lipid peroxidation products were measured through a colorimetric assay and calibrated to equivalents of MDA per microgram of protein per sample. Cerebellar neurons were cultured for 24 hours under pretreatment conditions, rinsed and followed with 24 hours of post-treatments. Concentrations of blueberry fractions (BBX, NP, and UA) were all 5ug/ml and TNFα was 200ng/ml. The first seven columns were held in untreated media as a pretreatment, followed by the indicated post-treatments. Values are reported as $P< 0.05$ where "a" and "b" indicate decreased lipid peroxidation compared to "A" and "B" respectfully. Treatments (**) significantly lowered lipid peroxidation while (*) caused an increase as compared to NT.

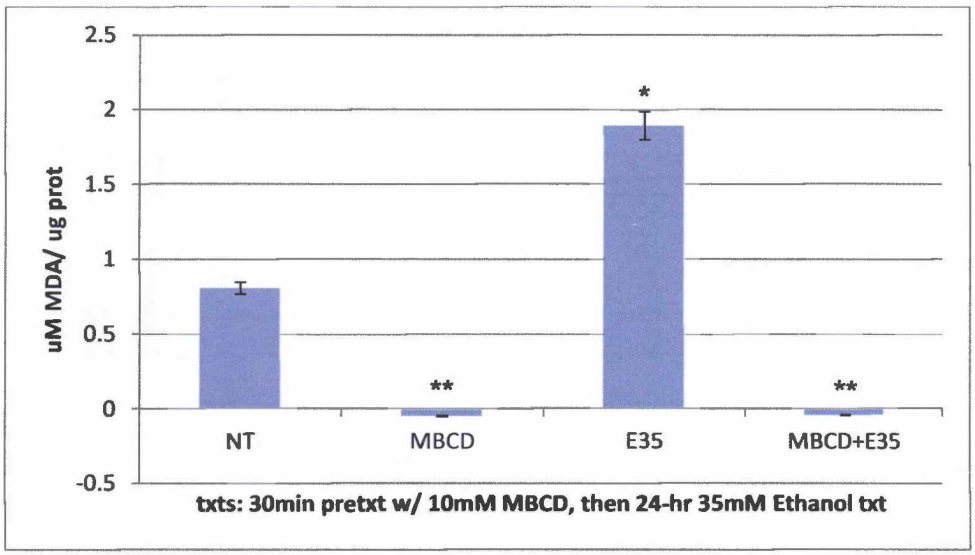

Fig 5.20 Depletion of Lipid Rafts Prevents Lipid Peroxidation of Ethanol Treated Cerebellar Neurons - Lipid Peroxidation end product (MDA) values are negated by the cholesterol depletion drug MBCD. Cerebellar neurons were cultured as follows: 1) 24 hours of serum free media (no treatment), 2) 23.5 hours of NT followed by 30 minutes of 10mM methyl-beta-cyclodextrin (MBCD), 3) 24 hours of 35mM ethanol, 4) 30 minutes of 10mM MBCD pre-treatment, followed by 23.5 hours of 35mM ethanol. Values are reported as $P< 0.05$ where (**) significantly lowered lipid peroxidation while (*) caused an increase as compared to NT.

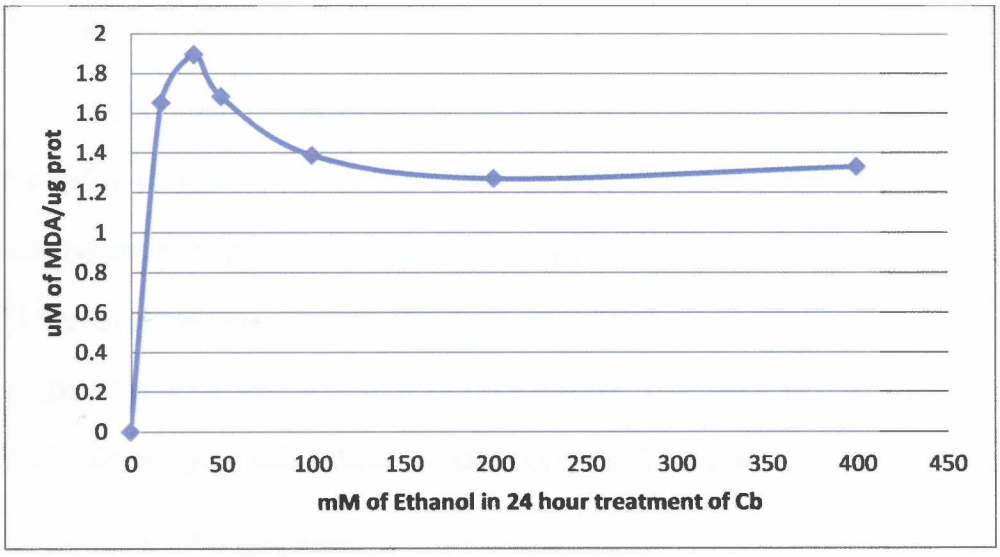

Fig 5.21 Lipid Peroxidation Peaks at Physiologically Relevant Concentrations of Ethanol in Cerebellar Neurons - Results are calibrated to reflect the production of lipid peroxidation end product (MDA) as measured by colorimetric analysis per microgram of protein. Cerebellar neuron cultures were treated with increasing levels of ethanol (0, 17.4, 35, 50, 100, 200, 400 mM) for 24 hours prior to reading absorbance assays.

5.9 TNFα Production

Inflammatory cytokines are secreted from cells all over the body to initiate the acute phase of inflammation. Our study sets out to determine the cerebellum's response to ethanol by measuring both secreted TNFα and cellular TNFα levels in neurons and glia. Secreted TNFα was a measure of TNFα secreted into the media over a 24 hour period. Cellular TNFα was a measure of TNFα expression within the cells and bound to TNFα receptors.

Cerebellar glia cells clearly secreted more TNFα than neurons (Fig 5.22) and do so in an ethanol dose dependent manner (Fig 5.24). Assays performed on cellular TNFα levels did not demonstrate large disparity between glia and neurons (Fig 5.23). Importantly, blueberry fractions return TNFα levels to normal in both neurons and glia within 24 hours of BBX/UA treatments after ethanol exposure (Fig 5.22 and Fig 5.23). Disruption of lipid rafts through MBCD pretreatments likewise reduced TNFα production (Fig 5.25). Once again, a relationship between lipid rafts and inflammatory processes is indicated.

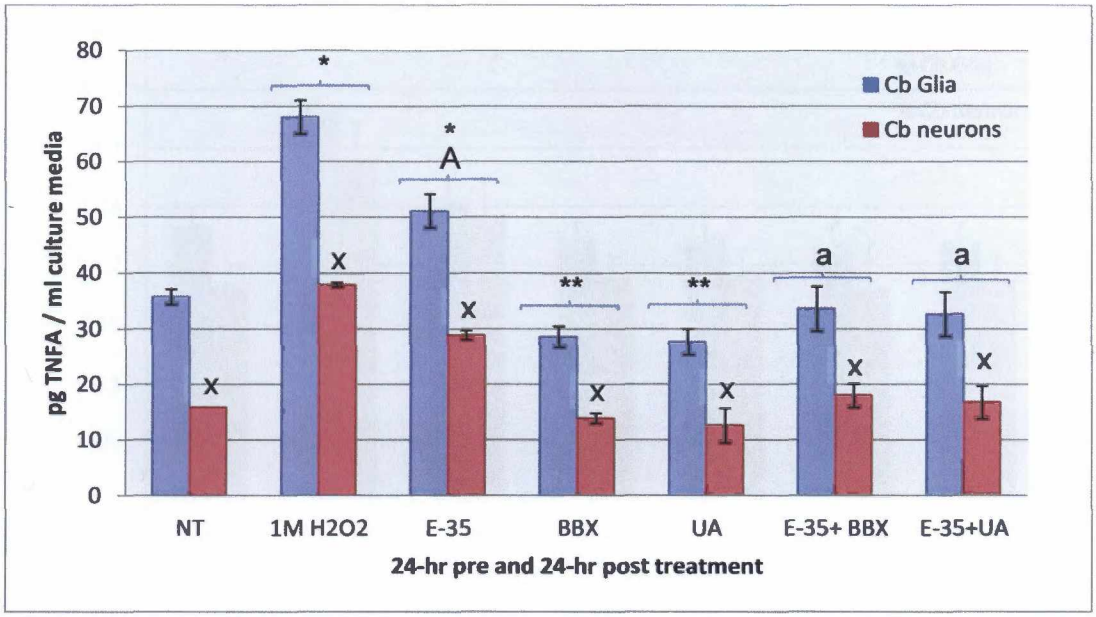

Fig 5.22 Cerebellar Glia vs. Neuronal TNFα Secretion

The media housing cerebellar glia and neurons was analyzed to determine TNFα secretion from the cells into the media. Colormetric assays were used to evaluate changes in TNFα production due to culturing conditions. Cerebellar neurons were cultured for 24 hours under pretreatment conditions, rinsed and followed with 24 hours of post-treatments. The first five columns were held in untreated media as a pretreatment, followed by the indicated post-treatments. Concentrations of blueberry fractions (BBX and UA) were 5ug/ml. Values are reported as $P< 0.05$ where "a" indicates decreased TNFα secretion compared to "A". Treatments (**) significantly lowered TNFα secretion while (*) caused an increase as compared to NT. Cerebellar neurons "x" secrete significantly less TNFα than cerebellar glia, ($P<0.001$).

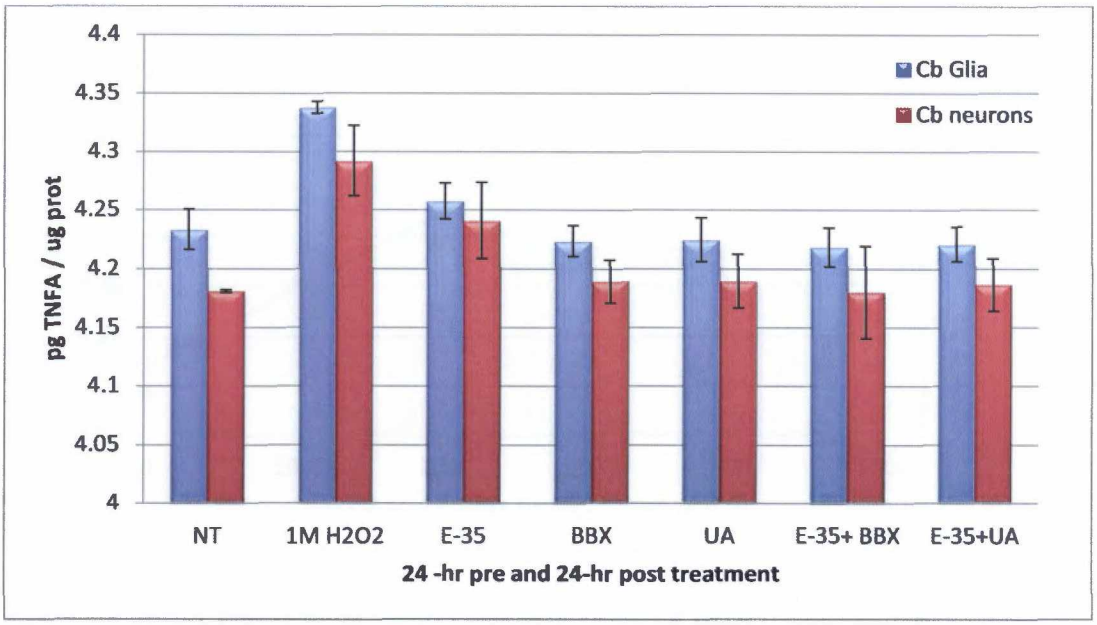

Fig 5.23 Cerebellar Glia vs. Neuronal Cellular TNFα

Cerebellar glia and neurons were analyzed to determine cellular levels of TNFα. Colormetric assays were used to evaluate changes in TNFα within the cells due to culturing conditions. Cerebellar neurons were cultured for 24 hours under pretreatment conditions, rinsed and followed with 24 hours of post-treatments. The first five columns were held in untreated media as a pretreatment, followed by the indicated post-treatments. Concentrations of blueberry fractions (BBX and UA) were 5ug/ml. Variations in cellular TNFα are not statistically significant.

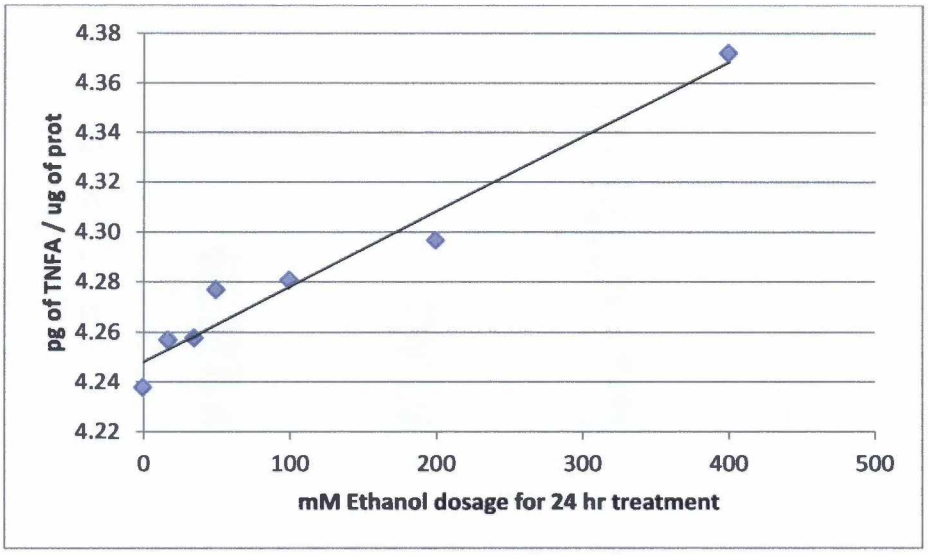

Fig 5.24 Glial TNFα Increases with Increased Ethanol Exposure

Cerebellar glia were analyzed to determine cellular levels of TNFα due to increasing concentrations of ethanol exposure. Colormetric assays were used to evaluate changes in TNFα within the cells due to culturing conditions. Glia were cultured in ethanol concentrations of 0, 17.4, 35, 50, 100, 200, and 400 mM for 24 hours.

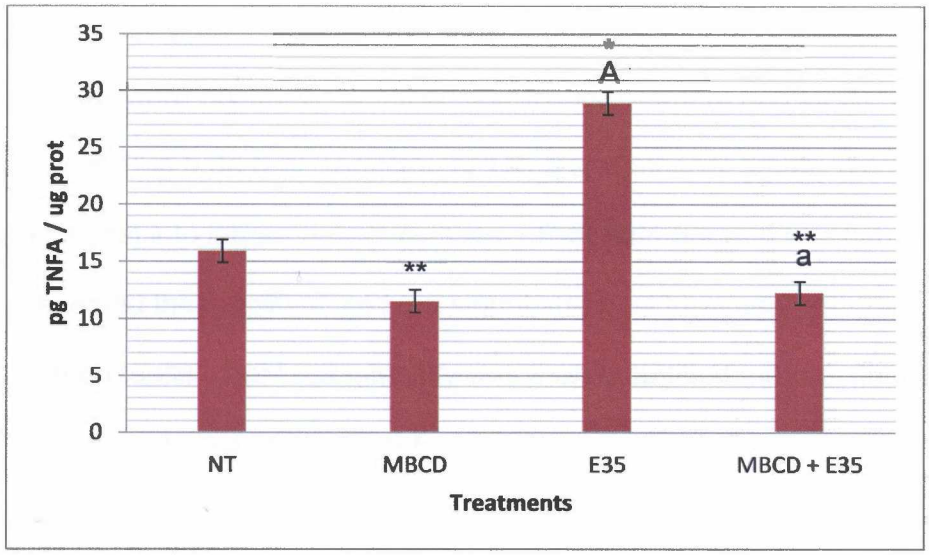

Fig 5.25 Disruption of Lipid Rafts Negates TNFα Secretion in Neurons
The cholesterol depletion drug methyl-beta-cyclodextrin (MBCD) was used to disrupt lipid rafts. Cerebellar neurons were cultured as follows: 1) 24 hours of serum free media (no treatment), 2) 23.5 hours of NT followed by 30 minutes of 10mM MBCD, 3) 24 hours of 35mM ethanol, 4) 30 minutes of 10mM MBCD pre-treatment, followed by 23.5 hours of 35mM ethanol. Values are reported as P< 0.05 where "a" indicates decreased TNFα secretion compared to "A". Treatments (*) caused a significant increase as compared to NT while (**) caused a decrease.

5.10 Lipid Rafts

5.10.1 Lipid Rafts – Cerebellar Neurons

Lipid rafts were visualized in cerebellar and forebrain cortical neurons using Alexa 555 cholera toxin GPI linked fluorescent labeling. Fluorescent microscopy revealed the greatest intensity of lipid rafts localized to the soma with

punctuated presence in the developing neurites (Fig 5.26 & Fig 5.29). Neurons and glia were positively identified using neurofilament and GFAP secondary staining (Fig 5.3a & c). Addition of TNFα and ethanol greatly increased the lipid raft signal into larger distinct masses. Pretreatment with blueberries or MBCD prevented the amplified lipid raft signal and post treatment with berries produced similar results. Lipid raft intensity was then quantified through fluorescent intensity readings (Fig 5.27 & Fig 5.30).

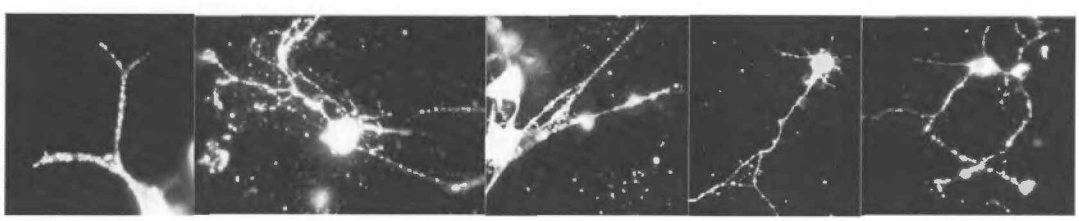

a. NT **b. TNFα** **c. E35** **d. E35 + BBX** **e. TNFα + BBX**

Fig 5.26 Fluorescent Microscopy of Lipid Rafts in Cerebellar Neurons
Lipid rafts were visualized under a Nikon Eclipse TE 2000U inverted microscope utilizing Alexa 555 cholera toxin GPI linked fluorescent labeling. Cerebellar neurons were cultured for 24 hours under pretreatment conditions, rinsed and followed with 24 hours of post-treatments. The photographs (a-c) were held in untreated media as a pretreatments and followed by the indicated post-treatments (NT-no treatment, 200ng/ml TNFα, and E35 - 35mM ethanol). Image (d) was pretreated with E35 followed by 5ug/ml BBX and image (e) was pretreated with 200ng/ml TNFα followed by 5ug/ml BBX.

Lipid rafts were visualized in cerebellar neurons using Alexa 555 cholera toxin GPI linked fluorescent labeling (Fig 5.26). Fluorescent microscopy reveals the greatest intensity of lipid rafts localized to the soma with punctuated presence in the developing neurites. Neurons and glia were positively identified using neurofilament and GFAP secondary staining (not shown). Addition of TNFα and ethanol greatly increased the lipid raft signal into larger distinct masses (Fig 5.26b and c) and is quantified in Fig 5.27. Pretreatments and post-treatments with BBX and UA prevent the amplified lipid raft signal (Fig 5.27).

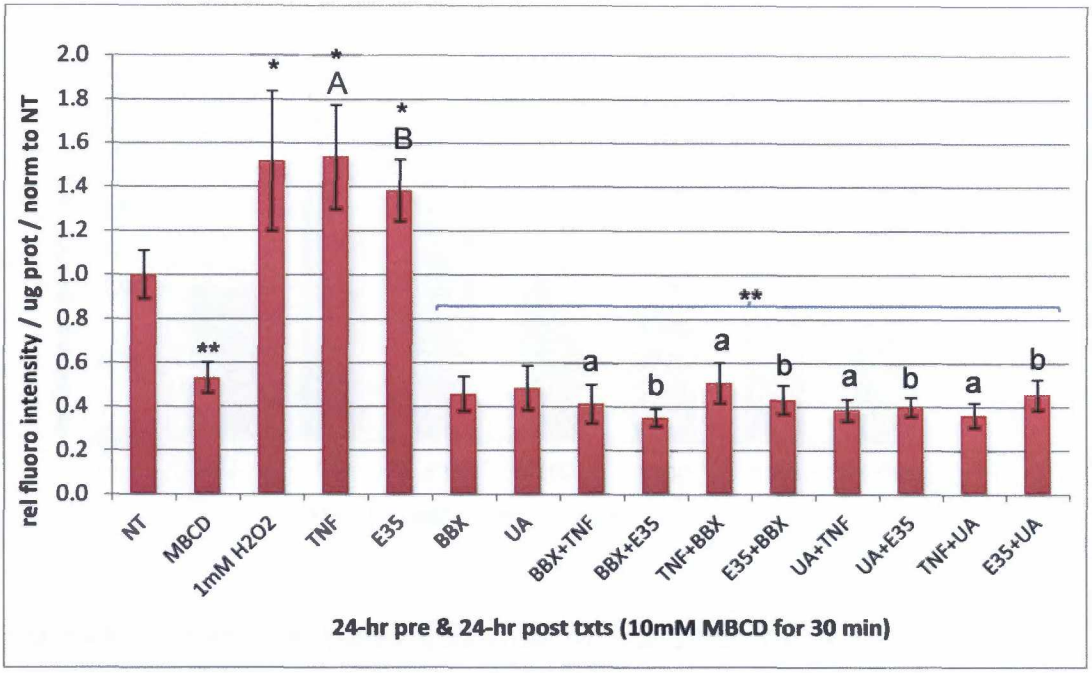

Fig 5.27 Density of Lipid Rafts in Cerebellar Neurons

Lipid rafts were quantified through fluorescent density assays with Alexa 555 cholera toxin GPI linked fluorescent labeled cultures. Cerebellar neurons were cultured for 24 hours under pretreatment conditions, rinsed and followed with 24 hours of post-treatments. A 30-minute treatment of methyl-beta-cyclodextrin (MBCD) was used as a negative control. All columns indicating a single treatment were held in untreated media prior to post-treatments. The following concentrations were used in treated medias: 200ng/ml TNFα, 35mM ethanol, 5ug/ml BBX, 5ug/ml UA. Fluorescent density is quantified per microgram of protein and normalized to the untreated control (NT). Values are reported as $P < 0.05$ where "a" and "b" indicate decreased lipid raft densities compared to "A" and "B" respectfully. Treatments (*) caused a significant increase as compared to NT while (**) caused a decrease.

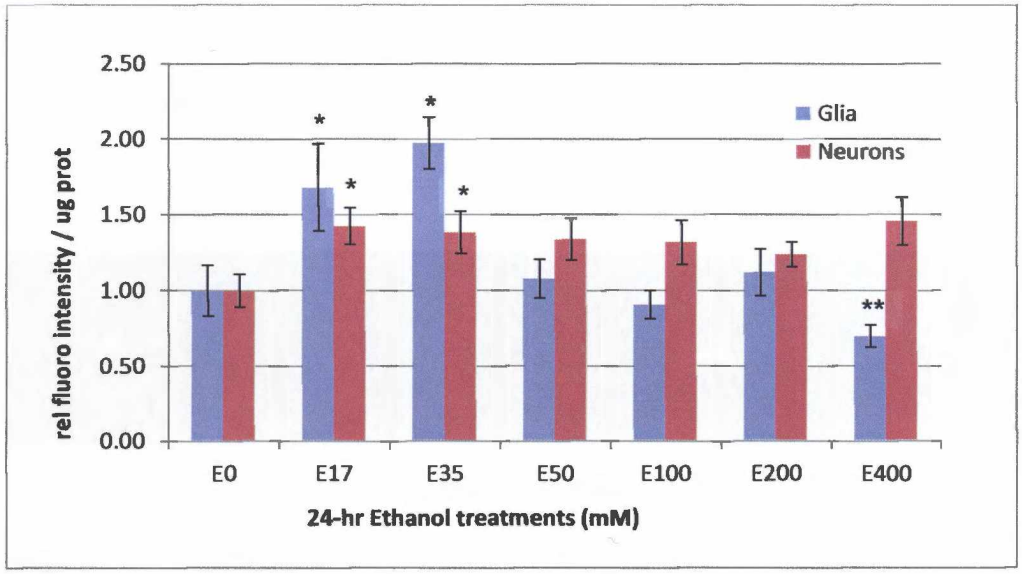

Fig 5.28 Effects of Increasing Ethanol on Lipid Raft Density

Lipid rafts were labeled with Alexa 555 cholera toxin GPI linked fluorescence. Cerebellar glia (blue) and neurons (red) were cultured for 24 hours under increasing concentrations of ethanol (0, 17.4, 35, 50, 100, 200, 400mM). Fluorescent density is quantified per microgram of protein and normalized to 0 mM ethanol. Values are reported as $P< 0.05$ where treatments (*) caused a significant increase in lipid raft density as compared to E0 while (**) caused a decrease.

5.10.2 Lipid Rafts – Forebrain Cortical Neurons

Lipid rafts were visualized in forebrain cortical neurons using Alexa 555 cholera toxin GPI linked fluorescent labeling as described in section 5.10.1. Addition of TNFα greatly increased the lipid rafts into larger distinct masses (Fig 5.29). Pretreatment with UA or MBCD prevented the amplified lipid raft signal

and post- treatment with UA produced similar results. Lipid raft intensity was then quantified through fluorescent intensity readings (Fig 5.10.2.2).

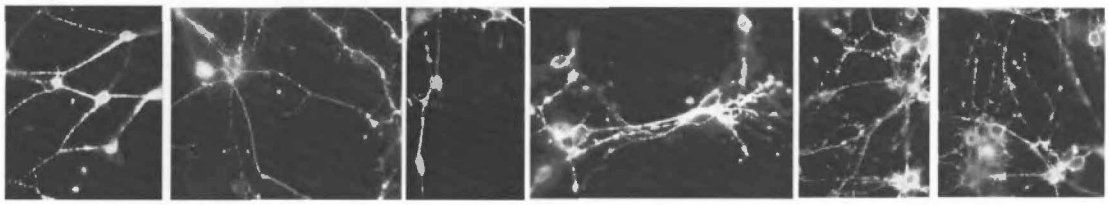

a. NT **b. MBCD** **c. UA** **d. TNFα** **e. UA+TNFα** **f. TNFα+UA**

Fig 5.29 Fluorescent Microscopy of Lipid Rafts in Forebrain Cortical Neurons Neurons were labeled with Alexa fluor 555-lipid raft labeling kit, fixed, mounted and viewed under a Nikon Eclipse TE 2000U inverted microscope. Cultures were photographed after the following conditions: a) 48-hrs no treatment (NT), b) 30-minutes, 10 mM methyl-B-cyclodextrin (MBCD), followed by 48-hrs NT, c) 24-hrs NT followed by 24-hrs UA (5 ug/ml), d) 24-hrs NT followed by 24-hrs TNFα (200 ng/ml), e) 24-hrs UA (5 ug/ml), followed by 24-hrs TNFα (200 ng/ml), f) 24-hrs TNFα (200 ng/ml) followed by 24-hrs UA (5ug/ml). Cholesterol depletion via MBCD reduced lipid raft formation comparable to that of UA whereas TNFα increased lipid raft formation. Pretreatment and post-treatment with UA blunted the TNFα induced lipid raft increase.

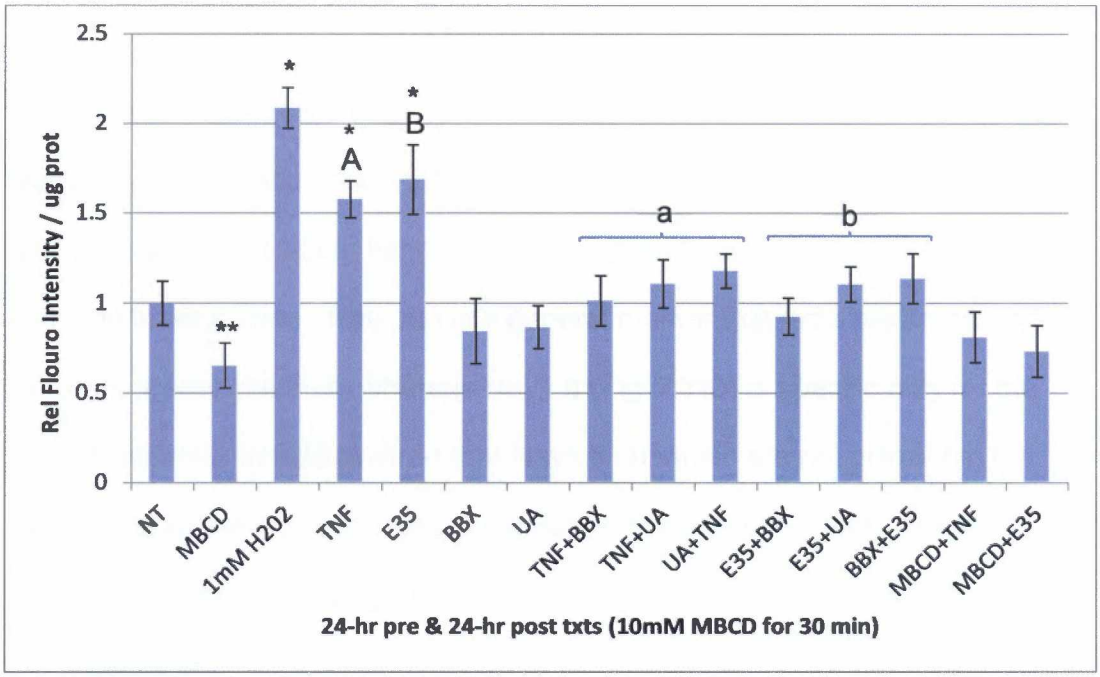

Fig 5.30 Density of Lipid Rafts in Forebrain Cortical Neurons

Lipid rafts were quantified with optical density assays. Forebrain cortical neurons were cultured for 24 hours under pretreatment conditions, rinsed and followed with 24 hours of post-treatments. A 30-minute treatment of methyl-beta-cyclodextrin (MBCD) was used to deplete cholesterol and disrupt lipid rafts. All columns indicating single treatments were held in untreated media prior to post-treatments. The following concentrations were used in treated medias: 10mM MBCD, 1mM H202, 200ng/ml TNFα, 35mM ethanol, 5ug/ml BBX, and 5ug/ml UA. Neurons were labeled with Alexa 555 cholera toxin GPI linked fluorescence after treatments. Fluorescent density was quantified per microgram of protein and normalized to the untreated control (NT). Values are reported as $P< 0.05$ where "a" and "b" indicate decreased lipid raft densities compared to "A" and "B". Treatments (*) caused a significant increase as compared to NT while (**) caused a decrease.

5.10.3 Colocalization of Lipid Rafts and Nav Channels

Encouraging data suggests the dependence of Nav channels on lipid raft platforms. Immunofluorescent microscopy indicates collocalization of lipid rafts and voltage gated sodium ion channels in the soma and neurites (Fig 5.32) of Nav-pan labeled cells. Nav-pan is a general marker that tests positive for all isoforms of Nav channels whereas Nav1.6 (Fig 5.31b) is specific only for the Nav1.6 isoform. We discovered that Nav1.6 channels are not present in the developing axons and dendrites at this stage of maturity but were present in the soma (Fig 5.31). According to literature, Nav1.6 will replace Nav1.2 channels in the neurites after oligodendrite (CNS) or Schwann cell (PNS) dependent meylenation occurs (Afshari et al. 2004, Schaller and Caldwell 2000, Schaller and Caldwell 2003, Raman et al. 1997). Nav1.6 channels are integral to resurgent current and the firing patterns of neurons. Because Nav1.6 expression is limited to the soma in our samples, we chose to use Nav-pan measurements for the rest of this study. Our initial findings indicate that alterations in the lipid rafts will most likely affect sodium ion channel placement in the membrane and thus function. This has great implications for the neuron as sodium ion channels are responsible for action potential. Immediate and lasting changes to neuronal membranes due to alcohol toxicity is medically relevant to alcoholics.

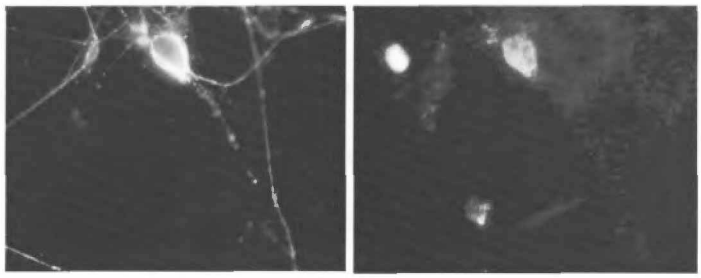

a. Lipid Raft **b. Nav1.6**

Fig 5.31 Lipid Rafts and Nav1.6 Channels in DRG Neurons

DRG cultures were doubly labeled with Alexa Fluor 555 (Lipid Raft) and mouse SCN8A (Nav1.6) antibody. Fluorescent microscopy indicates the presence of Nav1.6 channels (with secondary labeling of FITC) only in the soma (b.), whereas lipid rafts are also present in neurites (a.).

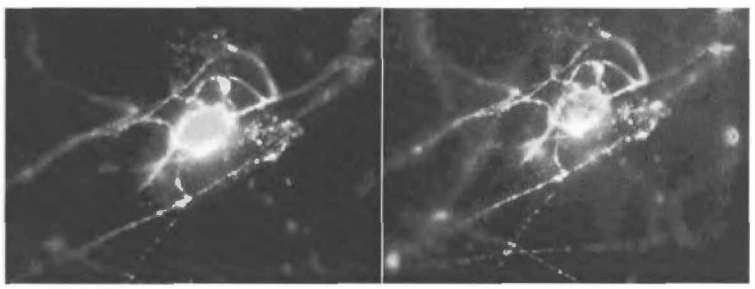

a. Lipid Raft **b. Nav-pan**

Fig 5.32 Lipid Rafts and Nav-pan Channels in DRG Neurons

DRG cultures were doubly labeled with Alexa Fluor 555 (Lipid Raft) and rabbit Nav-pan antibody/FITC. Nav-pan positively identifies all sodium ion channel isoforms. Fluorescent microscopy indicates the colocalization of lipid rafts with Nav-pan in both soma and neurites.

Increasing concentrations of alcohol once again reveal a similar pattern of response between lipid rafts and Nav channels. The increase in lipid rafts at physiological levels is consistant with ROS (Fig 5.13) and lipid peroxidation (Fig 5.21) assays. It is clear that Nav channel densities also dramatically intensify at this range (35-50mM ethanol).

Sodium ion channel expression was also found to positively correlate to lipid raft density in response to treatments specified in Fig 5.34. Both densities were heightened due to the inflammatory effects of ethanol and TNFα, reduced due to BBX and UA, and normalized due to intervening blueberry treatments. When lipid rafts were intentionally disrupted by the cholesterol depleting agent, MBCD, membrane Nav channel expression was also abated.

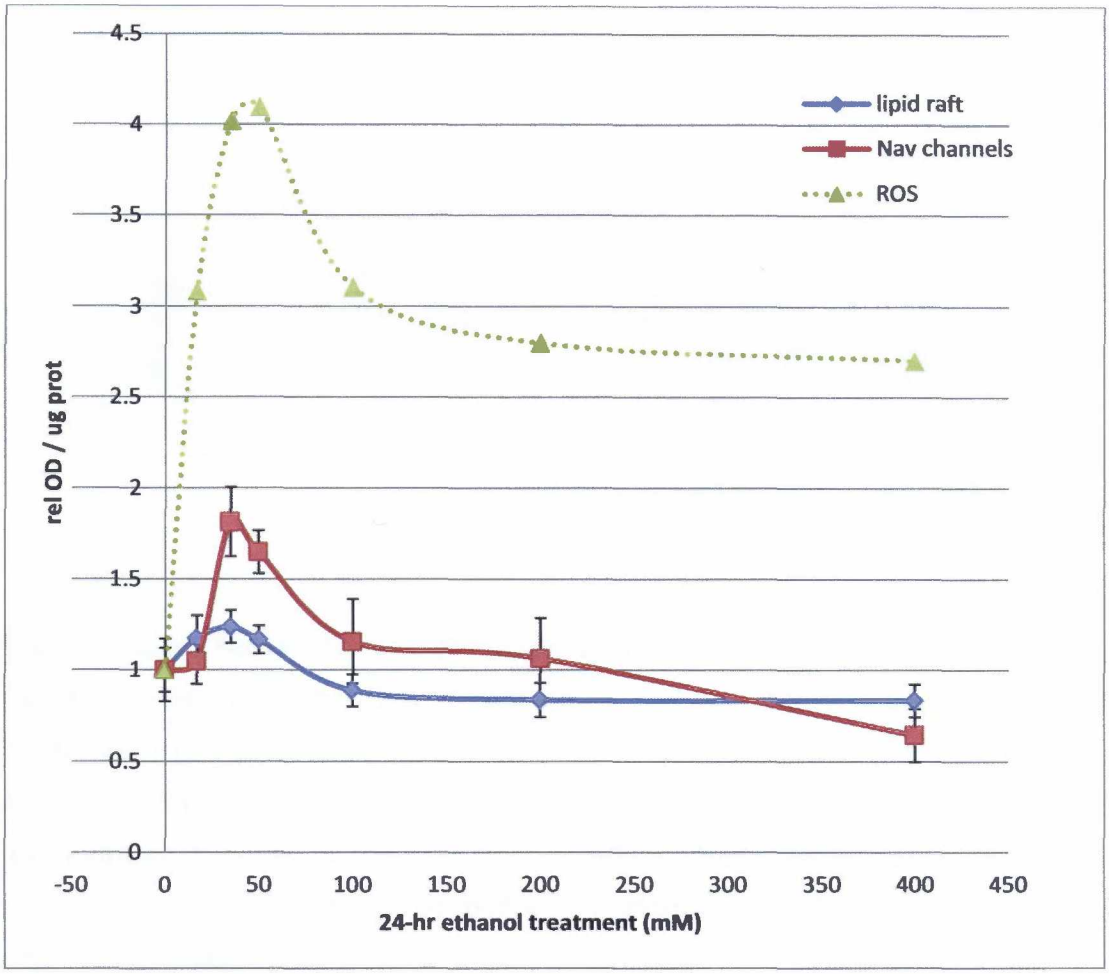

Fig 5.33 Lipid Raft and Nav Channel Density in Cerebellar Neurons with Increasing Ethanol Concentration - Cerebellar neurons were cultured in increasing concentrations of ethanol (0, 17.4, 35, 50, 100, 200, 400 mM) for 24 hours. Neurons were doubly labeled with Alexa Fluor 555 (Lipid Raft) and rabbit Nav-pan antibody/FITC. Fluorescent density (optical density – OD), is quantified per microgram of protein and normalized to 0 mM ethanol. Lipid rafts (blue) and Nav channel (red) densities reveal similar plot patterns and both display peak intensities at 35 mM ethanol (twice the legal blood alcohol content for driving). The ROS generation plot (green dots) was transferred from Fig 5.13.

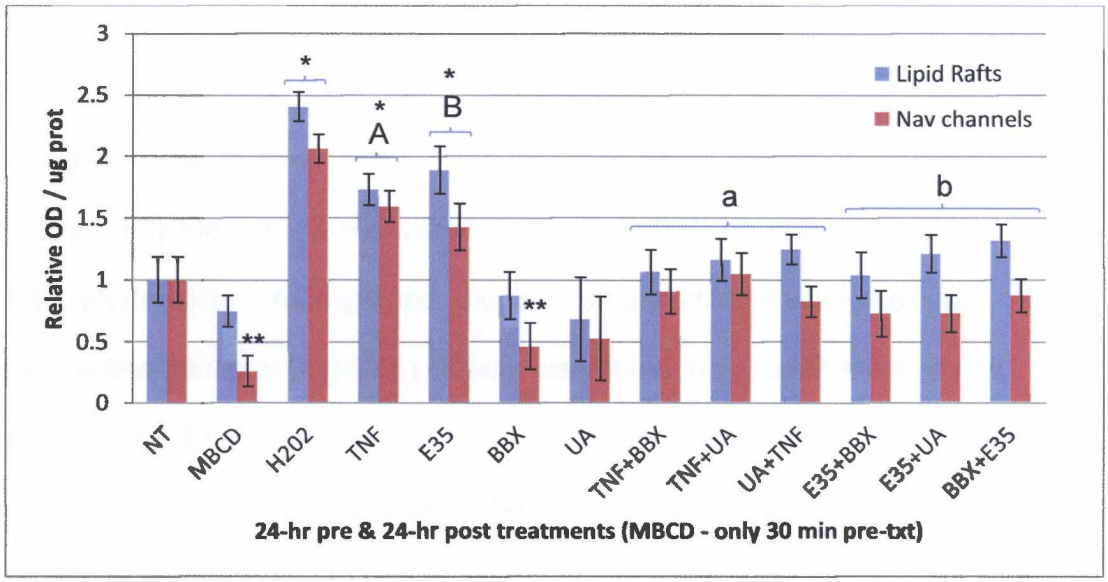

Fig 5.34 Lipid Rafts and Nav Channels Display Common Expression in Cerebellar Neuron Membrane Fractions - Cerebellar neurons were cultured for 24 hours under pretreatment conditions, rinsed and followed with 24 hours of post-treatments. The first seven columns were held in untreated media as a pretreatment, followed by the indicated post-treatments. Methyl-beta-cyclodextrin (MBCD) was utilized to disrupt lipid rafts through cholesterol depletion in a 30 minute treatment. At the completion of treatments, neurons were doubly labeled with Alexa Fluor 555 (Lipid Raft) and rabbit Nav-pan antibody/FITC. Fluorescent density (optical density – OD), is quantified per microgram of protein and normalized to cultures given no treatments (NT). **Values are reported as P< 0.05 where "a" and "b" indicate decreased expression compared to "A" and "B" respectfully. Treatments (*) caused a significant** increase as compared to NT while (**) caused a decrease.

5.11 Cellular Fractionation and Nav Channel Localization

In preparation for specific localization of Nav channels, we first needed to confirm our cell fractionation techniques. Cerebellar neurons were treated as indicated by Fig 5.35. Cells were fractionated and then assayed to determine lipid raft densities. As expected, the lipid raft densities of whole cell and membrane fractions (Fig 5.35) closely resembled the experimental results presented in Fig 5.34. The cytosolic fraction (Fig 5.35) was essentially void of lipid rafts and confirms the fractionation procedures were effective. The next phase of the study was to repeat this particular experiment for Nav channels.

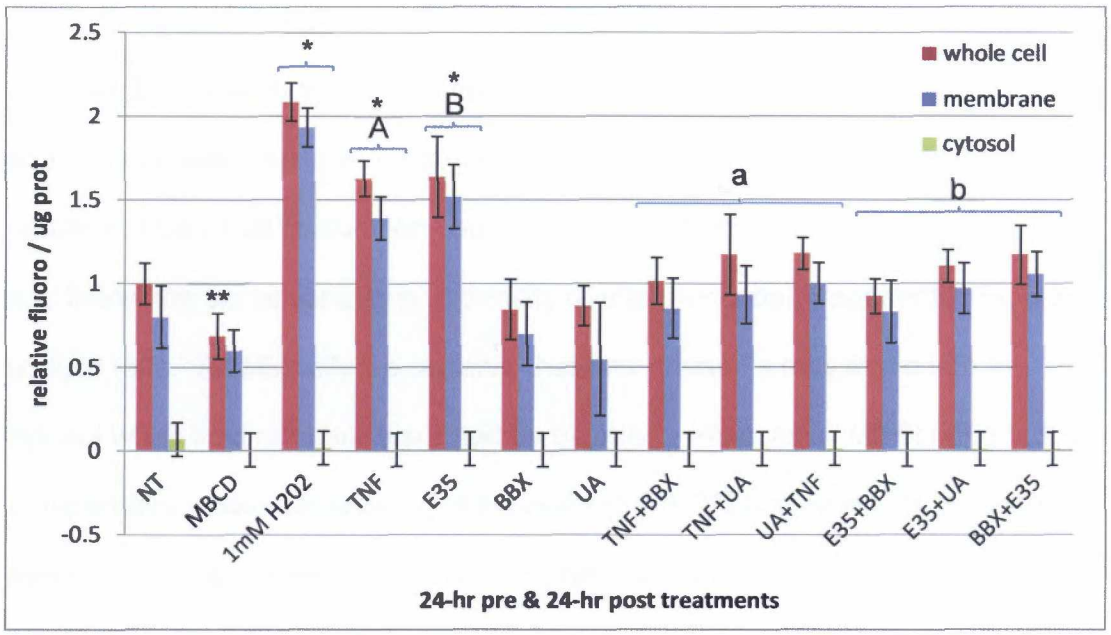

Fig 5.35 Lipid Raft Density in Cerebellar Fractions

Cerebellar neurons were split into membrane/cytosol fractions and tested for lipid raft fluorescence to ensure proper cellular fractionation. Successful fractionation techniques should not reveal GMI tagged lipid rafts in the cytosol. Pre- and post-treatment protocols match those identified in Fig 5.34. Relative fluorescence was compared to whole cell untreated cells (NT). Values are reported as $P < 0.05$ where "a" and "b" indicate decreased densities compared to "A" and "B" respectfully. Treatments (*) caused a significant increase as compared to NT while (**) caused a decrease.

Cells were treated as indicated in Fig 5.36 and then separated into cytosol and membrane fractions. We then determined the localization of sodium ion channels in response to ethanol, TNFα, and blueberry fractions. Preliminary results indicate that sodium ion channels are localized within lipid rafts (Fig 5.32) and follow the same variations in density due to prescribed treatments (Fig 5.34) as lipid rafts. Additionally we observe that Nav channels may move into the cytosol when lipid rafts are disrupted by blueberry fractions or MBCD (Fig 5.36). Independent whole-cell labeling of Nav-pan (Fig 5.37) confirmed the combined expression of Nav channels in the membrane and cytosolic fractions. Nav channels are known to tightly associate with cytoskeleton proteins such as ankyrin, and may be quickly relocated into the cytosol (Caldwell et al. 2000). More research needs to be conducted to elucidate the mechanism underlying this pathway and the relevance of sodium ion channels in neuroinflammation and alcohol abuse.

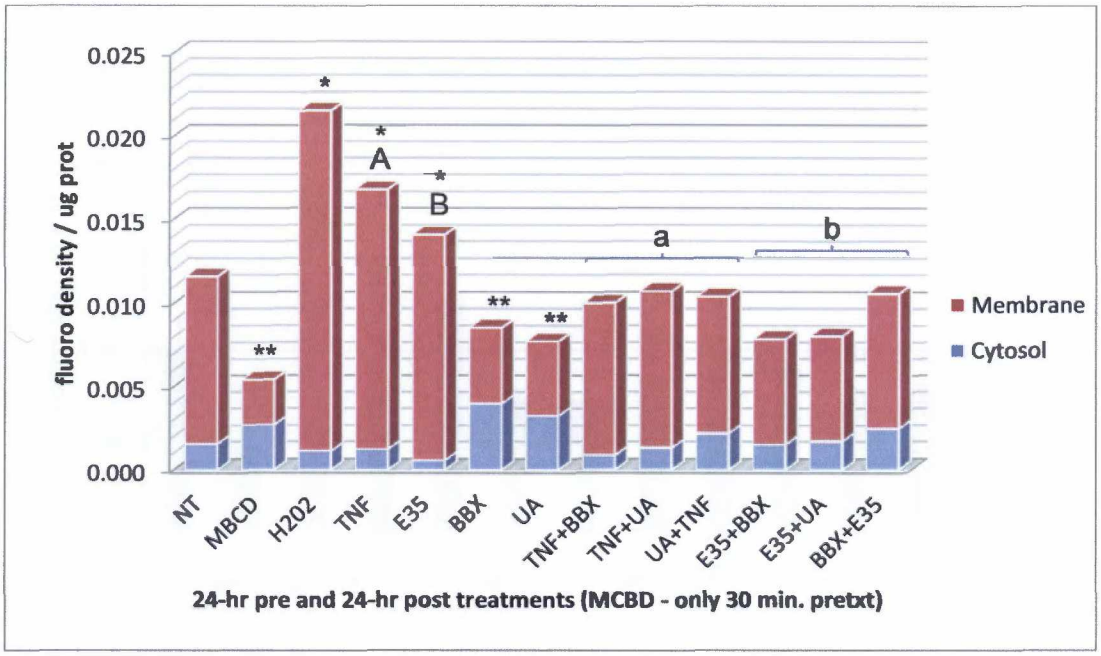

Fig 5.36 Localization of Nav Channels in Cerebellar Neurons

Cerebellar neurons were cultured for 24 hours under pretreatment conditions, rinsed and followed with 24 hours of post-treatments. The first seven columns were held in untreated media (NT) as a pretreatment, followed by the indicated post-treatments. Methyl-beta-cyclodextrin (MBCD) was utilized to disrupt lipid rafts through cholesterol depletion in a 30 minute treatment. Reagent concentrations were as follows: 10mM MBCD, 200ng/ml TNFα, 35mM ethanol, and 5ug/ml of BBX and UA. At the completion of treatments, neurons were fractioned into membrane and cytosol samples and labeled with rabbit Nav-pan antibody/FITC. Fluorescent density is reported per microgram of protein. This style of graph did not support use of error bars to indicate the standard deviation of the 7 samples analyzed. Values are reported as $P < 0.05$ where "a" and "b" indicate decreased densities compared to "A" and "B" respectfully. Treatments (*) caused a significant increase as compared to NT while (**) caused a decrease.

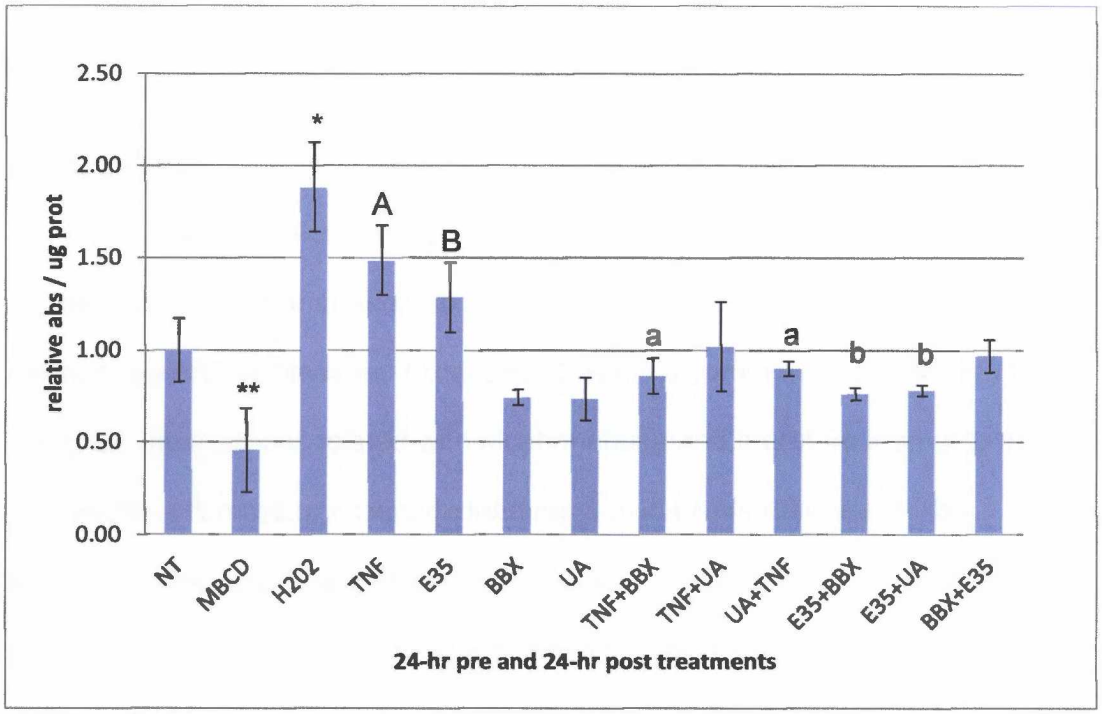

Fig 5.37 Nav Channel Expression in Whole-cell Cerebellar Neurons

Cerebellar neurons were cultured for 24 hours under pretreatment conditions, rinsed and followed with 24 hours of post-treatments. The first seven columns were held in untreated media (NT) as a pretreatment, followed by the indicated post-treatments. Methyl-beta-cyclodextrin (MBCD) was utilized to disrupt lipid rafts through cholesterol depletion in a 30 minute treatment. Reagent concentrations were as follows: 10mM MBCD, 200ng/ml TNFα, 35mM ethanol, and 5ug/ml of BBX and UA. At the completion of treatments, neurons were solubilized and labeled with rabbit Nav-pan antibody/FITC to indicate total expression of Nav channels in membranes and cytosol. Fluorescent density is normalized to the control and reported per microgram of protein. Values are reported as $P < 0.05$ where "a" and "b" indicate decreased expression compared to "A" and "B" respectfully. Treatments (*) caused a significant increase as compared to NT while (**) caused a decrease.

Chapter 6: Discussion

6.1 Overview

High rates of alcohol abuse coupled with inadequate nutrition may increase chronic inflammation and predispose individuals to future neurodegenerative disease. Oxidative stress is a common thread among the complex diseases associated with alcohol abuse and therefore interventions that disrupt the inflammatory cascade leading to oxidative stress are critical. Blueberries represent an inexpensive and accessible means to mitigate this process. Blueberries and ursolic acid have shown great promise in abutting alcohol induced oxidative stress in the liver and cardiovascular system, but very little is known about their ability to confer protection to the brain and nervous system in cases of alcohol abuse (Saravanan et al. 2006, Saravanan and Pugalendi 2006, Saraswat et al. 2000).

This study aimed to determine whether blueberry extracts could effectively combat oxidative stress and neuroinflammation invoked by alcohol abuse. Utilizing the embryonic chick model, neurons and supporting glia cells were dissociated from different regions of the brain and peripheral nervous system. These cells were grown in culture and stimulated with increasing levels of ethanol over time to produce physiologically relevant models. Blueberry extracts (BBX) and the isolated compound, ursolic acid (UA), were applied before (prevention) or after (intervention) alcohol exposure. Convincingly, both

preventive and therapeutic blueberry treatments yielded similar beneficial outcomes.

6.2 BBX and UA Blunt Ethanol Induced Oxidative Stress

The results of this study clearly indicate that Wild Alaska Bog Blueberries exhibit potent anti-inflammatory properties that protect neurons and glia from the toxic inflammatory effects of alcohol. At physiologically relevant doses of alcohol, equivalent to blood alcohol content of 0.08 (17.4 mM) and above, oxidative stress was greatly amplified at the cellular level (Fig 5.11). Supplementation with blueberry extracts and ursolic acid was found to improve cellular viability (Figs 5.4, 5.6, and 5.8), prevent alcohol toxicity (Figs 5.5, 5.6, and 5.8), and reverse alcohol induced neuroinflammation by drastically reducing oxidative stress. Blueberry biomolecules up-regulated cellular antioxidant defenses (Fig 5.18), reduced oxygen radicals (Figs 5.12, 5.14, A.1-A.4), prevented cellular membrane degradation (Fig 5.19), disrupted inflammatory signaling via lipid rafts (Figs 5.22, 5.25, and 5.27), and improved cellular architecture and morphology (Figs 5.6 and 5.8). While crude blueberry extracts are known to contain antioxidants that impart protection from oxidative stress, ursolic acid is not.

6.3 Ursolic Acid Modulates Lipid Rafts

Ursolic acid does not demonstrate a strong reducing power of free radicals (Fig 5.15); however, it was clearly effective in reducing overall ROS production in

both neurons and glia (Fig 5.18). Therefore, ursolic acid must exert its antioxidant power through an indirect means. Labeling of lipid rafts clearly indicates ursolic acid's ability to block the coalescence and increased density of lipid rafts within cellular membranes (Figs 5.29, Fig 5.30, and Fig 5.27).

Ursolic acid may interrupt subunit assembly of pro-inflammatory enzymes that are dependent on lipid raft platforms to become functional. Two such membrane bound enzymes, NOX and nSMase, generate a cycle of up-regulated ROS production when neurons are subject to inflammatory cytokine TNFα. If functional assembly/activation of these enzymes is prohibited, ROS production should be tempered even when subject to TNFα or the inflammatory effects of ethanol. We propose that ursolic acid negates the inflammatory signal that leads to heightened ROS production in this manner. Because ursolic acid is lipophilic and structurally resembles cholesterol naturally imbedded in lipid rafts, it may replace some of the cholesterol in rafts. This substitution would impose structural changes to the cellular membranes and lipid rafts that may prevent nSMase activation and interrupt functional assembly of NOX. Throughout the study we found that the depletion of cholesterol by MBCD caused changes in lipid raft densities comparable to ursolic acid. Further research will determine the occurrence of cholesterol displacement and density when cells are exposed to ursolic acid.

6.4 Cerebellar Neurons Generate High Levels of ROS

In contrast to other neurons, cerebellar neurons were found to generate the highest levels of ROS at rest and in response to ethanol and TNFα (Fig 5.10 and Fig 5.11). The cerebellum may be more metabolically active than the other areas tested and therefore require more oxygen for biological processes, hence more oxygen radical byproducts. The health of the surrounding glia, particularly the astrocytes, is paramount to protecting the cerebellum from oxidative damage.

6.5 Astrocytes Protect Neurons from Oxidative Stress

The glia culture, positively marked for astrocytes, was found to display markedly increased antioxidant capacity (Fig 5.16) and a significantly lower ROS generation in response to physiological levels of ethanol (Fig 5.13). We also found that both architecture (GFAP labeling) and DNA (Hoechst labeling) of the glia culture were less impacted by ethanol and TNFα than that of cerebellar neurons (NF and Hoechst labeling), Fig 5.7 and Fig 5.9. The importance of glia, often ignored in neurological studies, should not be understated.

6.6 Cerebellar Neurons are Particular Sensitive to Alcohol

The results presented in this study point to a particular susceptibility of the cerebellar Purkinje neurons to alcohol during embryonic development. Since Purkinje neurons were grown in a heterogenous cerebellar cell culture, we were able to investigate the structural demise of Purkinje neurons (Cal labeling) as

well as generic cerebellar neurons (NF labeling) in culture. It is clear that neurofilament and Purkinje specific cytoskeleton densities declined prior to DNA damage (Hoechst labeling, Fig 5.7) and metabolic decline (MTT viability assays, Fig 5.4). Consequently, it is no surprise that neuronal dysfunction precedes the cellular death and anatomical changes observed in clinical studies (Sullivan 2000, Sullivan et al. 2000a, Sullivan et al. 2000b, Sullivan et al. 2006). It is imperative to improve therapies for individuals suffering from neuroinflammatory disease and alcoholism before they suffer irreparable brain damage.

Alcohol abuse leads to a sustained elevation of inflammatory TNFα in the brain comparable to levels found in end-stage neurodegenerative disease. Our research confirms that alcohol increases inflammation in part through stimulating TNFα secretion. Therefore, interventions that prevent heightened TNFα may ameliorate neurological symptoms caused by a myriad of neuroinflammatory and neurodegenerative diseases. In this study we tested the effectiveness of blueberry treatments against inflammatory insult by both ethanol and TNFα. We discovered that 35mM ethanol (0.16 BAC) and 200ng/ml TNFα (end-stage neurodegenerative disease) inflict similar damage to neurons as measured by cellular viability, ROS production, antioxidant capacity, lipid raft density, and lipid peroxidation. We report complete reversal of this damage through blueberry supplementation.

6.7 Blueberry Biomolecules may Reverse Neuroinflammation

Most commonly individuals seek medical treatment after a problem has developed rather than initiating preventive measures. Encouraging data from this study not only supports the idea of blueberry supplementation in preventive medicine, but also the more realistic therapeutic supplementation of BBX and UA. If blueberry extracts are taken after neuroinflammatory insult (ethanol or TNFα) has occurred, they may rescue neurons and glia from death and prevent permanent damage to the brain. Within the time-frame applied to this study, we believe blueberry extracts and ursolic acid accomplished this very thing. Our data provides a thorough picture of the devastating effects of ethanol and TNFα on metabolic viability, cellular morphology, ROS generation, lipid peroxidation, TNFα secretion, lipid rafts, and sodium ion channels. In all cases, it was found that the initial detrimental effects of oxidative stress could be reversed through blueberry supplementation.

6.8 BBX and UA Enhance Cell Viability

Not only did blueberries protect neurons from oxidative stress, but BBX and UA also increased cellular viability. Immunofluorescent assays indicated a significant increase in neuronal neurofilaments (Fig 5.6) and glial GFAP (Fig 5.8) as a result of supplementation. This enhanced architecture is observed in conjunction with increased metabolic viability (Fig 5.4 and Fig 5.5). Therefore, our *in vitro* study is consistent with popular *in vivo* studies supporting

enhancement of brain health via blueberry supplementation (Youdim et al. 2000, Joseph et al. 1999). We believe wild Alaskan blueberries will provide even stronger therapies than berries grown at lower latitudes due to their significantly increased antioxidant composition (Flint and Robinson 2011). Our research found the total antioxidant power of wild Alaskan berries (grown in the Interior), to be three times more powerful than the average cultivated berry of the continental United States (Haytowitz and Bhagwat 2010).

6.9 Sodium Ion Channel Localization is Altered by Alcohol

For the first time, the relevance of sodium ion channel localization to lipid rafts and possible modifications due to alcohol exposure was investigated. Our findings lead us to conclude that inflammation has a drastic impact on the density of sodium ion channels found in the membranes collocated with lipid rafts. Blueberry supplementation may minimize this effect by preventing large coalescence of lipid rafts. As we have previously discussed, large lipid raft signaling platforms host assembly of ROS generating enzymes that create an oxidative environment. When left unchecked, densities of these enzymes, lipid rafts, and Nav channels remain high and lead to a chronic inflammatory state. It is unknown how this increase in Nav channels manifests clinically, however the high occurrence of epileptic seizures (Nav disorder) observed in alcoholics yields important clues (Frucht et al. 2000).

6.10 Future Directions

The embryonic chick proved to be an excellent and economical means to establish comparative cellular research between different regions of the brain and peripheral nervous system. It could likewise be utilized to examine morphological and electrophysiological changes in the brain during embryonic development. The results presented in this study will advance our understanding of the neuroinflammatory effects of alcohol and provide a novel nutritional approach to improve the overall health of alcoholics and unborn babies subject to maternal alcohol abuse.

Blueberries and ursolic acid present raw materials for further medical research and therapies targeted at inflammatory and neurodegenerative disease. Studies addressing the bioavailability of blueberry metabolites in the bloodstream and their ability to cross the BBB are logical steps to pursue in animal models as well as in humans. Strong efforts will be made to communicate our findings with health care professionals and medical researchers to bridge the gap between scientific discovery, education and patient care.

Chapter 7: References

Abele M, Riet A, Hummel T, Klockgether T, Wullner U (2003). Olfactory dysfunction in cerebellar ataxia and multiple system atrophy. *J Neurol* 250: 1453-1455.

Afshari FS, Ptak K, Khaliq ZM, Grieco TM, Slater NT, McCrimmon DR & Raman IM (2004). Resurgent Na currents in four classes of neurons of the cerebellum. *J Neurophysiol* 92: 2831-2843.

Andres-Lacueva C, Shukitt-Hale B, Galli R, Jauregui O, Lamuela-Raventos R, Joseph J (2005). Anthocyanins in aged blueberry-fed rats are found centrally and may enhance memory. *Nutr Neurosci* 10: 111-120.

Baker K, Harding A, Halliday G, Kril J, Harper C (1999). Neuronal loss in functional zones of the cerebellum of chronic alcoholics with and without Wernicke's encephalopathy. *J Neurosci* 91: 429-438.

Baptista CA, Hatten ME, Blazeski R, Mason CA (1994). Cell-cell interactions influence survival and differentiation of purified Purkinje cells in vitro. *Neuron* 12: 243–260.

Bar KJ, Franke S, Wenda B, Muller S, Kientsch-Engel R, Stein G, Sauer H (2003). Pentosidine and N(epsilon)-(carboxymethyl)-lysine in Alzheimer's disease and vascular dementia. *Neurobiol Aging* 24: 333-338.

Beal (1995). Aging, Energy, and Oxidative Stress in Neurodegenerative Diseases. Ann Neurol 38: 357-366.

Bean BP (2005). The Molecular Machinery of Resurgent Sodium Current Revealed. Neuron 45(2): 185-187.

Bellairs R, Osmond M (2005). The Atlas of Chick Development. Elsevier Academic Press, San Deigo, CA.

Black JA, Renganathan M & Waxman SG (2002). Sodium channel Nav1.6 is expressed along nonmyelinated axons and it contributes to conduction. *Mol Brain Res* 105: 19-28.

Blanco A, Valles S, Pascual M, Guerri C (2006). Involvement of TLR4/Type I IL-1 Receptor Signaling in the Induction of Inflammatory Mediators and Cell Death Induced by Ethanol in Cultured Astrocytes. *The Journal of Immunology* 175: 6893–6899.

Brieskorn CHZ, Klinger H (1961). Über das gemeinsame Vorkommen von Triterpenen und Sterinen im Blatt von Salvia triloba und Pirus malus: Mitteilung zur Kenntnis der Biochemie der Triterpene. *Archiv der Pharmazie* 294(7): 389-391.

Caldwell JH, Schaller L, Lasher RS, Peles E, Levinson SR (2000). Sodium channel Nav1.6 is localized at nodes of Ranvier, dendrites, and synapsis. *PNAS* 97: 5616-5620.

Cazzaniga E, Bulbarelli A, Masserini M (2010). Alcohol and Neural Lipids. Eds: Lajtha A, Tettamanti G, Goracci G. *Handbook of Neurochemistry and Molecular Neurobiology.* 503-515.

Chin JH, Parsons LM, Goldstein DB (1978). Increased cholesterol content of erythrocyte and brain membranes in ethanol-tolerant mice. *Biochim Biophys Acta* 513(3): 358-63.

Chung HJ, Steinberg JP, Huganir RL, Linden, DJ (2003). Requirement of AMPA receptor GluR2 phosphorylation for cerebellar long-term depression. *Science* 300: 1751–1755.

Clark BA, Monsivais P, Branco T, London M, Hausser M (2005). The site of action potential initiation in cerebellar Purkinje neurons. Nat Neurosci 8: 137–139.

Connelly T, Farmer JM, Lynch DR, Doty RL (2003). Olfactory dysfunction in degenerative ataxias. *J Neurol Neurosurg Psychiatry* 74: 1435-1437.

Crews FT, Bechara R, Brown LA, Guidot DM, Mandrekar P, Oak S, Qin L, Szabo G, Wheeler M, Zou J (2006). Cytokines and Alcohol. *Alcoholism: Clin and Exp Res* 30: 720–730.

Crews FT, Nixon K (2009). Mechanisms of neurodegeneration and regeneration in alcoholism. *Alcohol Alcohol.* 44(2): 115-27.

Cummins TR, Dib-Hajj SD, Herzog RI and Waxman SG (2005). Nav1.6 channels generate resurgent sodium currents in spinal sensory neurons. *FEBS Lett* 579: 2166–2170.

Dai Q, Zhang J, Pruett SB (2005). Ethanol alters cellular activation and CD14 partitioning in lipid rafts. *Biochem Biophys Res Commun* 33: 37–42.

de Queiroz GM, de Souza MM, de Carvalho TC, Casemiro LA, Cunha WR, Martins CH (2011). Absence of the antibacterial activity of the crude extracts and compounds isolated from M. rubiginosa against extended-spectrum β-lactamase producing enterobacteria. *J Pharm Negative Results* 2: 1-7.

Dick DJ, Boakes RJ, Harris JB (1985). A cerebellar abnormality in the mouse with motor end-plate disease. *Neuropathol Appl Neurobiol* 11: 141–147.

Dowlati Y, Herrmann N, Swardfager W, Liu H, Sham L, Reim EK, Lanctôt KL (2010). A meta-analysis of cytokines in major depression. *Biol Psychiatry* 67(5): 446–457.

Dringen R, Gutterer R, and Hirrlinger J (2000). Glutathione metabolism in brain - Metabolic interaction between astrocytes and neurons in the defense against reactive oxygen species. *Eur J Biochem* 267: 4912-4916.

Ehrlander M (2010). The Historical Roots of a Frontier Alcohol Culture: Alaska and Northern Canada. *The Northern Review* 32: 63–103.

Erlanger J, Blair EA (1938). Comparative observations on motor and sensory fibers with special reference to repetitiousness. *Amer J Physiol* 121: 431-453.

Feirabend HKP (1990). Development of longitudinal patterns in cerebellum of the chick *Gallus domesticus*: A cytoarchitectural study on the genesis of cerebellar modules. *Eur J Morphol* 28: 169-223.

Feirabend HKP, Van Luxemburg EA, Van Dnederen- Van Dorp H, Voogd J (1985). A 3H-thymidime autoradiographic study of the development of the cerebellum of the white leghorn (*Gallus domesticus*): Evidence for longitudinal neuroblast generation patterns. *Acta Morphol Neerl Scand* 23: 115-126.

Fenaughty A, Fink K, Peck D, Wells R, Utermohle C, Peterson E (2009). The Burden of Overweight and Obesity in Alaska, Summary Report. *Anchorage, AK: Section of Chronic Disease Prevention and Health Promotion, Division of Public Health, Alaska Department of Health and Social Services.*

Fernandez-Lizarbe S, Pascual M, Soledad Gascon M, Blanco A, Guerri C (2007). Lipid rafts regulate ethanol-induced activation of TLR4 signaling in murine macrophages. *Molecular Immunology* 45: 2007–2016.

Flint C, Robinson E (2011). Promoting Wellness in Alaskan Villages: Integrating Traditional Knowledge and Science of Wild Berries. *Eco Health* 8(2): 199-209.

Frank-Cannon T, Alto L, McAlpine F, Tansey M (2009). Does neuroinflammation fan the flame in neurodegenerative diseases? *Mol Neurodegener* 4: 47.

Frucht M, Quigg M, Schwaner C, Fountain N (2000). Distribution of Seizure Precipitants Among Epilepsy Syndromes. *Epilepsia* 41: 1534–1539.

Ghez C, Fahn S, and edited by Kandel ER and Schwartz JH (1985). The cerebellum. *Principles of Neural Science, 2nd edition*, New York, Elsevier 502–522.

Gil-Mohapel J, Boehmea F, Kainera L, Christiea B (2010). Hippocampal cell loss and neurogenesis after fetal alcohol exposure: Insights from different rodent models. *Brain Research Reviews* 64: 283-303.

Goetz R, Dover K, Laezza F, Shtraizent N, Huang X, Tchetchik D, Eliseenkova A, Xu C, Neubert T, Ornitz D, Goldfarb M, Mohammadi M (2009). Crystal Structure of a Fibroblast Growth Factor Homologous Factor (FHF) Defines a Conserved Surface on FHFs for Binding and Modulation of Voltage-gated Sodium Channels. *J Biol Chem* 284: 17883-17896.

Goldin AL (2001). Resurgence of sodium channel research. *Annu Rev Physiol* 63:871-894.

Gustafson S, Dunlap K, McGill C, Kuhn T. A nonpolar blueberry fraction blunts NADPH oxidase activation in neuronal cells exposed to tumor necrosis factor alpha. *Oxidative Medicine and Cellular Longevity*. (2012), In Press.

Haehner A, Hummel T, Hummel C, Sommer U, Junghanns S, Reichmann H (2007). Olfactory Loss May Be a First Sign of Idiopathic Parkinson's Disease. *Movement Disorders*: 22(6): 839-842.

Han W, Li H, Villar VA, Pascua AM, Dajani MI, Wang X, Natarajan A, Quinn MT, Felder RA, Jose PA, Yu P (2008). Lipid rafts keep NADPH oxidase in the inactive state in human renal proximal tubule cells. *Hypertension* 51: 481-487.

Haorah J, Heilman D, Knipe B, Chrastil J, Leibhart J, Ghorpade A, Miller DW, Persidsky Y (2005a). Ethanol-induced activation of myosin light chain kinase leads to dysfunction of tight junctions and blood–brain barrier compromise. *Alcohol Clin Exp Res* 29: 999–1009.

Haorah J, Knipe B, Leibhart J, Ghorpade A, Persidsky Y (2005b). Alcohol-induced oxidative stress in brain endothelial cells causes blood–brain barrier dysfunction. *J Leukoc Biol* 78: 1223–1232.

Haorah J, Knipe B, Gorantla S, Zheng J, Persidsky Y (2007). Alcohol-induced blood–brain barrier dysfunction is mediated via inositol 1,4,5-triphosphate receptor (IP3R)-gated intracellular calcium release. *Journal of Neurochemistry* 100: 324–336.

Harder T, Engelhardt K (2004). Membrane Domains in Lymphocytes – From Lipid Rafts to Protein Scaffolds. *Traffic* 5: 265-275.

Haytowitz D, Bhagwat S (2010). USDA Database for the Oxygen Radical Absorbance Capacity (ORAC) of Selected Foods, Release 2. *Nutrient Data Laboratory, BHNRC, ARS, USDA.*

Hibbeln JR, Salem Jr N (1995). Dietary polyunsaturated fatty acids and depression: when cholesterol does not satisfy. *Am J Clin Nutr* 62(1): 1-9.

Hong S, Wiley JW (2006). Altered expression and function of sodium channels in large DRG neurons and myelinated A-fibers in early diabetic neuropathy in the rat. *Biochem and Biophys Res Comm* 339(2): 652-660.

Jenkins SM, Bennett V (2001). Ankyrin-G coordinates assembly of the spectrin-based membrane skeleton, voltage-gated sodium channels, and L1 CAMs at Purkinje neuron initial segments. *J Cell Biol* 155: 739–746.

Joseph JA, Shukitt-Hale B, Denisova NA, Bielinski D, Martin A, McEwen JJ, Bickford PC (1999). Reversal of age-related declines in neuronal signal transduction, cognitive, and motor behavioral deficits with blueberry, spinach, or strawberry dietary supplementation. *J Neurosci* 19(18): 8114-21.

Kaplan M, Cho M, Ullian E, Isom L, Levinson S, Barres B (2001). Differential Control of Clustering of the Sodium Channels Nav1.2 and Nav1.6 at Developing CNS Nodes of Ranvier. *Neuron* 30: 105-119.

Kearney JA, Buchner DA, De Haan G, Adamska M, Levin SI, Furay AR, Albin RL, Jones JM, Montal M, Stevens MJ, Sprunger LK, Meisler MH (2002). Molecular and pathological effects of a modifier gene on deficiency of the sodium channel Scn8a (Na(v)1. 6). *Hum Mol Genet* 11: 2765–2775.

Klopfenstein DR, Tomishige M, Stuurman N and Vale RD (2002). Role ofphosphatidylinositol(4,5)bisphosphate organization in membrane transport by the Unc104 kinesin motor. *Cell* 109: 347-58.

Kohrman DC, Smith MR, Goldin AL, Harris J, Meisler MH (1996). A Missense Mutation in the Sodium Channel Scn8a Is Responsible for Cerebellar Ataxia in the Mouse Mutant *jolting*. *J Neurosci* 16(19): 5993–5999.

Lau F, Shukitt-Hale B, Joseph J (2007). Nutritional Intervention in Brain Aging. *Inflammation in the Pathogenesis of Chronic Diseases* 14: 299-318.

Le Bel CP, Odunze IN, Adams JD, Bondy SC (1989). Brain formation and membrane order following vitamin E deficiency. *Biochem Biophys Res Commun* 163: 860-6.

Li Q, Spencer NY, Oakley FD, Buettner JR, Engelhardt JF (2009). Endosomal Nox2 Facilitates Redox-Dependent Induction of NF-κB by TNFα. *Antioxidants & Redox Signaling* 11(6): 1249-1263.

Liu B, Gao H-M, Hong J-A (2003). Parkinson's disease and exposure to infectious agents and pesticides and the occurrence of brain injuries: role of neuroinflammation. *Enviro Health Perspec* 111(8): 1065-1073.

Liu, J (1995). Pharmacology of oleanolic acid and ursolic acid. J Ethnopharm 49(2): 57-68.

Locksley RM, Killeen N, Lenardo MJ (2001). The TNFα and TNFα receptor superfamilies: integrating mammalian biology. *Cell* 104 (4): 487–501.

Lou JY, Laezza F, Gerber BR, Xiao M, Yamada KA, Hartmann H, Craig AM, Nerbonne JM, Ornitz DM (2005). Fibroblast growth factor 14 is an intracellular modulator of voltage-gated sodium channels. *J Physiol (Lond)* 569: 179-193.

Lu J, Zheng Y-L (2007). Ursolic acid ameliorates cognition deficits and attenuates oxidative damage in the brain of senescent mice induced by d-galactose. *Biochem Pharm* 74(7): 1078-1090.

Mahadik S, Evans D, Lal H (2001). Oxidative Stress and Role of Antioxidant and omega-3 essential fatty acid supplementation in schizophrenia. *Pro Neuro-Psychoparmacol & Bio Psychiat* 25: 463-493.

Meisler MH, Kearney JA (2005). Sodium channel mutations in epilepsy and other neurological disorders. *J Clin Invest* 115(8): 2010-2017.

Mera K, Anraku M, Kitamura K, Nakajou K, Maruyama T, Tomita K, Otagiri M (2005). Oxidation and carboxyl methyl lysine modification of albumin: possible involvement in the progression of oxidative stress in hemodialysis patients. *Hypertens Res* 28: 973-980.

Meydani M, Macauley JB, Blumberg JB (1986). Influence of dietary vitamin E, selenium and age on regional distribution of alpha-tocopherol in the rat brain. *Lipids* 21(12): 786-91.

Monnier VM, Mustata GT, Biemel KL, Reihl O, Lederer MO, Zhenyu D, Sell DR (2005). Cross-linking of the extracellular matrix by the maillard reaction in aging and diabetes: an update on "a puzzle nearing resolution". *Ann NY Acad Sci* 1043: 533-544.

Nimmerjahn A, Kirchohoff F, Helmchen F (2005). Resting Microglial Cells are Highly Dynamic Surveillants of Brain Parenchyma in Vivo. *Science* 27: 1314-1318.

Nordin S, **Monsch** AU, **Murphy** C (1995). Unawareness of smell loss in normal and Alzheimer's disease: discrepancy between self-reported and diagnosed smell sensitivity. *Journal of Gerontology* 50(4): 187-92.

Nordmann R, Ribiere C, Rouach H (1990a). Ethanol-Induced Lipid Peroxidation and Oxidative Stress in Extrahepatic Tissues. *Alcohol and Alcoholism* 25(2-3): 231-237.

Nordmann R, Rouach H, Houze P (1990b). Alcohol, iron and oxidative stress. *Bull Acad Natl Med* 174 (1): 95-102.

Opreanu M, Lydic T, Reid G, McSorley K, Esselman W, and Busik J (2010). Inhibition of Cytokine Signaling in Human Retinal Endothelial Cells through Downregulation of Sphingomyelinases by Docosahexaenoic Acid. *Retinal Cell Bio* 51: 3253-63.

Orbán N, Kozák IO (2009). LC-MS method development to evaluate major triterpenes in skins and cuticular waxes of grape berries. *Internat J Food Sci & Tech* 44(4): 869-873.

Pan F, Beam KG (1999). The absence of resurgent sodium current in mouse spinal neurons. *Brain Res* 849: 162-168.

Pawlosky R, Bacher R, Salem Jr R (2001). Ethanol Consumption Alters Electroretinograms and Depletes Neural Tissues of Docosahexaenoic Acid in Rhesus Monkeys: Nutritional Consequences of a Low Omega-3 Fatty Acid Diet. *Alcohol Clin Exp Res* 25(12): 1758–1765.

Peles E, Salzer JL (2000). Molecular domains of myelinated axons. *Curr Opin Neurobiol* 10: 558–565.

Peoples RW, Weight FF (1997). Anesthetic actions on excitatory amino acid receptors. *Anesthesia: Biologic Foundations* (Biebuyck JF, Lynch C, Maze M, Saidman LJ, Yaksh TI, Zapol WM, eds.) Lippincott-Raven, NY 239-258.

Pietrzykowski A, Treistman S (2008). The Molecular Basis of Tolerance. *Alcohol Research and Health* 31: 298-309.

Qin L, He J, Hanes R, Pluzarev O, Hong JS, Crews FT (2008). Increased systemic and brain cytokine production and neuroinflammation by endotoxin following ethanol treatment. *J Neuroinflam* 5: 10.

Raivich G (2005). Like cops on the beat: the active role of resting microglia. *Trends in Neurosci* 28: 571-573.

Raman IM, Bean BP (1997). Resurgent sodium current and action potential formation in dissociated cerebellar Purkinje neurons. *J Neurosci* 17: 4517–4526.

Raman IM, Sprunger LK, Meisler MH, Bean BP (1997). Altered subthreshold sodium currents and disrupted firing patterns in Purkinje neurons of SCN8a mutant mice. *Neuron* 19: 881-891.

Ranjekar PK, Hinge A, Hegde MV, Ghate M, Kale A, Sitasawad S, Wagh UV, Debsikdar VB, Mahadik SP (2003). Decreased antioxidant enzymes and membrane essential polyunsaturated fatty acids in schizophrenic and bipolar mood disorder patients. *Psychiatry Res* 121: 109–122.

Rapoport M, van Reekum R, Mayberg H (2000). The Role of the Cerebellum in Cognition and Behavior: A Selective Review. *J Neuropsyc & Clin Neurosci* 12: 193-198.

Reddy VP, Beyaz A (2006). Inhibitors of the Maillard reaction and AGE breakers as therapeutics for multiple diseases. *Drug DiscoVery Today* 11: 646-654.

Riikonen J, Jaatinen P, Rintala J, Porsti I, Karjala K, Hervonen A (2002). Intermittent ethanol exposure increases the number of cerebellar microglia. *Alcohol* 37(5): 421-6.

Rivest S (2009). Regulation of innate immune reponses in the brain. *Nature Rev Immun* 9: 429-439.

Rupp C, Kurz M, Kemmler G, Mair D, Hausmann A, Hinterhuber H, Fleischhacker WW (2003). Reduced Olfactory Sensitivity, Discrimination, and Identification in Patients with Alcohol Dependence. *Alcohol Clin Exp Res* 27(3): 432-439.

Saraswat B, Visen PKS, Agarwal DP (2000). Ursolic acid isolated from *Eucalyptus tereticornis* protects against ethanol toxicity in isolated rat hepatocytes. *Phytother Res* 14: 163–166.

Saravanan R, Pugalendi V (2006). Impact of ursolic acid on chronic ethanol-induced oxidative stress in the rat heart. *Pharmalogical Reports* 58: 41-47.

Saravanan R, Viswanathan B, Pugalendi, KV (2006). Protective effect of ursolic acid on ethanol-mediated experimental liver damage in rats. *Life Sciences* 78: 713 –718.

Schaller KL, Caldwell JH (2000). Developmental and regional expression of sodium channel isoform NaCh6 in the rat central nervous system. *J Comp Neurol* 420: 84 –97.

Schaller KL, Caldwell JH (2003). Expression and distribution of voltage-gated sodium channels in the cerebellum. *Cerebellum* 2: 2-9.

Schmahmann JD (2004). Disorders of the cerebellum: ataxia, dysmetria of thought, and the cerebellar cognitive affective syndrome. *J Neuropsych Clin Neurosci* 16: 367-78.

Schmahmann JD, Caplan D (2006). Cognition, emotion and the cerebellum. *Commentary on Brain* 129: 306-320 and *Brain* 129: 290-2.

Schmidt K, Martinez-Gamboa L, Meier S, Witt C, Meisel C, Hanitsch LG, Becker MO, Huscher D, Burmester GR, Riemekasten G (2009). Bronchoalveoloar lavage fluid cytokines and chemokines as markers and predictors for the outcome of interstitial lung disease in systemic sclerosis patients. *Arth Res & Ther* 11: 111.

Schneider P, Hosseiny SS, Szczotka M, Jordan M, Schlitter K (2009). Rapid solubility determination of the triterpenes oleanolic acid and ursolic acid by UV-spectroscopy in different solvents. *Phytochem Let* 2(2): 85-87.

Seis H (1991). Oxidative stress: from basic research to clinical application. *Am J Med* 91: 31-38.

Shih Y, Chein Y, Wang J, Fu Y (2004). Ursolic Acid protects hippocampal neurons against kainite induced excitotoxicity in rats. *Neurosci Lett* 362(2): 136-140.

Simons K, Toomre E (2000). Lipid rafts and signal transduction. *Nat Rev Mol Cell Biol* 1: 31-39.

Stamatovic S, Keep R, Andjelkovic A (2008) Brain endothelial cell-cell junctions: how to "open" the blood brain barrier. *Curr Neuropharmacol* 6(3): 179-92.

Stillwell W, Shaikh SR, Zeoruga M, Siddiqui R, Wassail SR (2005). Docosahexaenoic acid affects cell signaling by altering lipid rafts. *Reprod Nutr Dev* 45: 559-579.

Stillwell W, Shaikh SR, Zerouga M, Siddiqui R, Wassail SR (2006). Docosahexaenoic acid affects cell signaling by altering lipid rafts. *Reprod Nutr Dev* 45(5): 559-79.

Sullivan EV (2000). Human brain vulnerability to alcoholism: evidence from neuroimaging studies. In: Noronha A, Eckardt M, Warren K (eds). *Review of NIAAA's Neuroscience and Behavioral Research Portfolio* NIAAA Research Monograph No. 34. National Institutes of Health: Bethesda, MD. pp 473–508.

Sullivan EV, Adalsteinsson E, Sood R, Mayer D, Bell RL, McBride WJ et al (2006). Part I: longitudinal brain MRI brain study of the alcohol-preferring (P) rat: adult brain growth. *Alcohol Clin Exp Res* 30: 1234–1247.

Sullivan EV, Deshmukh A, Desmond JE, Lim KO, Pfefferbaum A (2000a). Cerebellar volume decline in normal aging, alcoholism, and Korsakoff's syndrome: relation to ataxia. *Neuropsych* 14: 341–352.

Sullivan EV, Deshmukh A, Desmond JE, Mathalon DH, Rosenbloom MJ, Lim KO *et al* (2000b). Contribution of alcohol abuse to cerebellar volume deficits in men with schizophrenia. *Arch Gen Psych* 57: 894–902.

Sun GY, Sun AY (1985). Ethanol and membrane lipids. *Alcohol Clin Exp Res* 9(2): 164-80.

Sun A, Simonyi A, Sun G (2002). The "French Paradox" and beyond: neuroprotective effects of polyphenols. *Free Rad Bio & Med* 32(4): 314-318.

Swardfager W, Lanctôt K, Rothenburg L, Wong A, Cappell J, Herrmann N (2010). A meta-analysis of cytokines in Alzheimer's disease. *Biol Psychiatry* 68 (10): 930–941.

Szabo G (1997). Alcohol's Contribution to Comprised Immunity. *Alcohol Health and Res World* 21: 30-41.

Szabo G, Dolganiuc A, Dai Q, Pruett SB (2007). TLR4, ethanol, and lipid rafts: a new mechanism of ethanol action with implications for other receptor mediated effects. *J Immunol* 178 (3): 1243–1249.

Szic KS, Ndlovu MN, Haegeman G, Vanden Berghe W (2010). Nature or nurture: let food be your epigenetic medicine in chronic inflammatory disorders. *Epigenetics* 15;80(12): 1816-32.

Tansey MG, Wyss-Coray T (2008). Cytokines in CNS inflammation and disease. In: Lane TE, Carson M, Bergmann C, Wyss-Coray T (eds). Central nervous system diseases and inflammation, 1st edn. Springer, New York, pp 59-106.

Tansey MG, McCoy MK, Frank-Cannon TC (2007). Neuroinflammatory mechanisms in Parkinson's disease: potential environmental triggers, pathways, and targets for early therapeutic intervention. *Exp Neurol* 208: 1-25.

Thakur V, Pritchard MT, McMullen MR, Wang Q, Nagy LE (2006). Chronic ethanol feeding increases activation of NADPH oxidase by lipopolysaccharide in rat Kupffer cells: role of increased reactive oxygen in LPS-stimulated ERK1/2 activation and TNFα production. *J Leukoc Biol* 79(6): 1348-56.

Trudeau M, Dalton J, Day J, Ranum L, Meisler M (2006). Heterozygosity for a protein truncation mutation of sodium channel SCN8A in a patient with cerebellar atrophy, ataxia, and mental retardation. *J Med Genet* 43: 527-530.

Tyrrell T and Willshaw D (1992). Cerebellar cortex: its simulation and the relevance of Marr's theory. *Philosophical transactions of the Royal Society of London, Series B, Biological sciences* 336(1277): 239–57.

Valles S, Blanco A, Pascual M, Guerri C (2004). Chronic ethanol treatment enhances inflammatory mediators and cell death in the brain and in astrocytes. *Brain Pathol* 14: 365–371.

Vasdev S, Gill V, Singal P (2006). Beneficial effect of low ethanol intake on the cardiovascular system: possible biochemical mechanisms. *Vascular Health and Risk Management* 2(3): 263–276.

Vilhardt F, Van Deurs B (2004). The phagocyte NADPH oxidase depends on cholesterol-enriched membrane microdomains for assembly. *EMBO J* 23: 739-48.

Wadiche JI, Jahr CE (2001). Multivesicular release at climbing fiber-Purkinje cell synapses. *Neuron* 32(2): 301–13.

Weiss N, Miller F, Cazaubon S, Couraud PO (2009). The blood-brain barrier in brain homeostasis and neurological diseases. *Biochem Biophys Acta* 1788(4): 842-57.

Wheeler D, Knapp E, Bandaru VVR, Wang Y, Knorr D, Poirier C, Mattson MP, Geiger JD, Haughey NJ (2009). Tumor necrosis factor-alpha-induced neutral sphingomyelinase-2 modulates synaptic plasticity by controlling the membrane insertion of NMDA receptors. *J Neurochem* 109(5): 1237-1249.

Wilson JX (1997). Antioxidant defense of the brain: a role for astrocytes. *Can J Physiol Pharmacol* 75(10-11): 1149-63.

Wittmack EK, Rush AM, Craner MJ, Goldfarb M, Waxman SG, Dib-Hajj SD (2004). Fibroblast growth factor homologous factor 2B: association with Nav1.6 and selective colocalization at nodes of Ranvier of dorsal root axons. *J Neurosci* 24: 6765– 6775.

Yang B, Rizzo V (2007). TNFα potentiates protein-tyrosine nitration through activation of NADPH oxidase and eNOS localized in membrane rafts and caveolae of bovine aortic endothelial cells. *Am J Physiol Heart Circ Physiol* 292: H954-62.

Yin MC, Chan KC (2007). Nonenzymatic Antioxidative and Antiglycative Effects of Oleanolic Acid and Ursolic Acid. *J Agric Food Chem* 55: 7177-7181.

Youdim KA, Shukitt-Hale B, MacKinnon S, Kalt W, Joseph JA (2000). Polyphenolics enhance red blood cell reistance to oxidative stress: in vitro and in vivo. *Biochem Biophys Acta* 1523(1): 117-22.

Youdim K, Spencer J, Schroeter H, Rice-Evans C (2002). Dietary flavonoids as potential neuroprotectants. *Biol Chem* 383: 205-231.

Zaleska M, Nagy K, Floyd RA (1989). Iron-induced lipid peroxidation and inhibition of dopamine synthesis in striatum synaptosomes. *Neurochem Res* 14(7): 597-605.

Zhou DS, Lambert PL, Malen S, Carpenter LM, Boland, Bennett V (1998). AnkyrinG is required for clustering of voltage-gated Na channels at axon initial segments and for normal action potential firing. *J Cell Biol* 143: 1295–1304.

Appendix A: Additional Figures

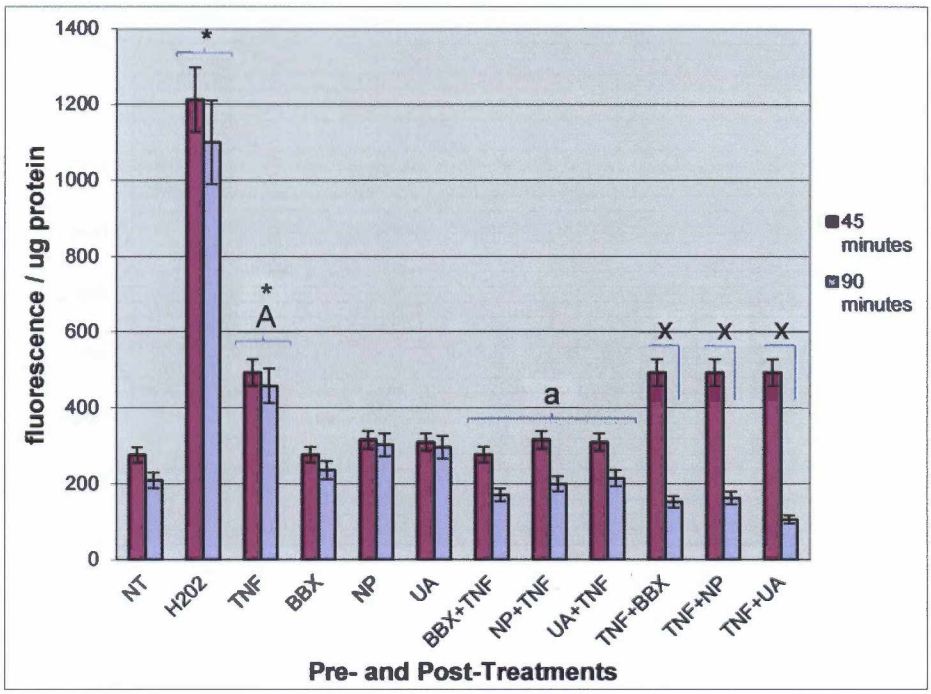

Fig A.1 Immediate ROS Generation in Human SH-SY5Y Neuroblastoma Cells - ROS is reported as a measure of fluorescent output at 535 nm per microgram of protein sampled taken at 45 minutes (after pretreatments) and at 90 minutes (after pre- and post-treatments are complete). Cerebellar neuronal cultures were held for 45 minutes under different conditions. Columns NT through UA had the same pre- and post-treatments and the remaining columns were pretreated with 5ug/ml BBX, 5ug/ml NP, 5ug/ml UA, 200ng/ml TNFα (10-12). Pretreatments were rinsed and post-treatments were added for another 45 minutes: no treatment (NT), 1mM H_2O_2, 200ng/ml TNFα, 5ug/ml BBX, 5ug/ml NP, 5ug/ml UA, 200ng/ml TNFα (7-9), 5ug/ml BBX, 5ug/ml NP, and 5ug/ml UA. Values are reported as $P< 0.05$ where "a" indicates decreased ROS generation compared to "A". ROS was decreased at 90 minutes (x) by BBX, NP, and UA compared to 45 minutes. Treatments identified with (*) increased ROS compared to NT.

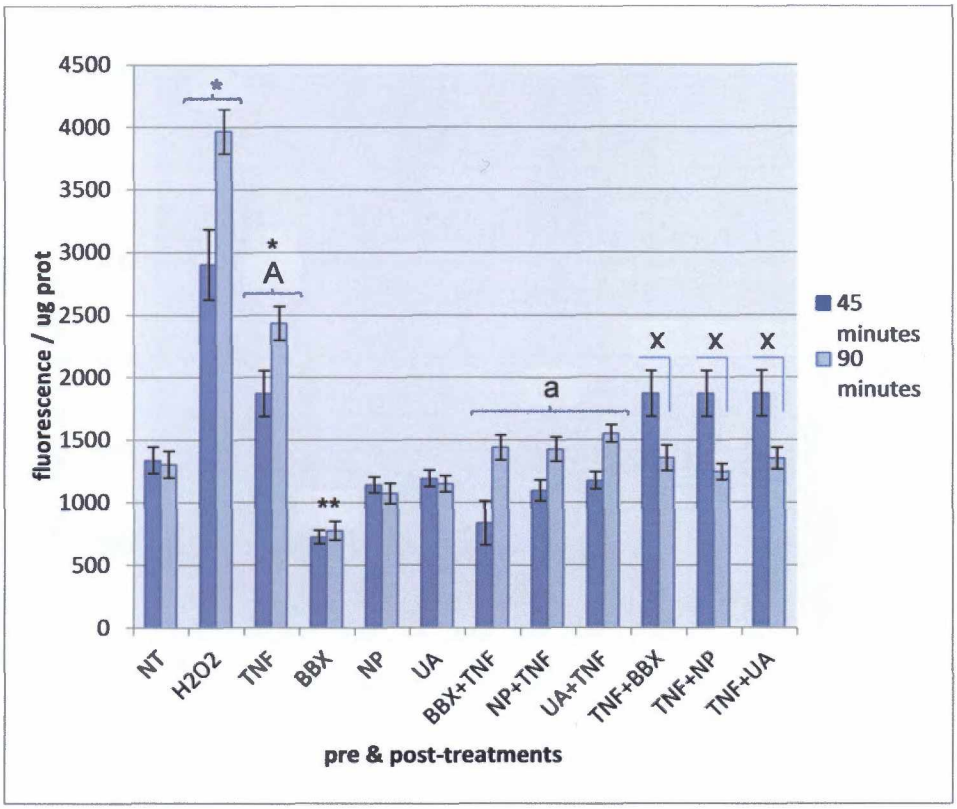

Fig A.2 Immediate ROS Generation in Forebrain Cortical Neurons

ROS is reported as a measure of fluorescent output at 535 nm per microgram of protein sampled taken at 45 minutes (after pretreatments) and at 90 minutes (after pre- and post-treatments are complete). Forebrain cortical neuron cultures were held for 45 minutes under different conditions. The first six columns had the same pre- and post-treatments and the remaining columns were pretreated with 5uq/ml BBX. 5uq/ml NP. 5uq/ml UA. 200nq/ml TNFα (10-12). Pretreatments were rinsed and post-treatments were added for another 45 minutes: no treatment (NT), 1mM H_2O_2, 200ng/ml TNFα, 5ug/ml BBX, 5ug/ml NP, 5ug/ml UA, 200ng/ml TNFα (7-9), 5ug/ml BBX, 5ug/ml NP, and 5ug/ml UA. Values are reported as $P< 0.05$ where "a" indicates decreased ROS generation compared to "A". ROS was decreased at 90 minutes (x) by BBX, NP, and UA compared to 45 minutes. BBX** is significantly lower than NT while (*) is higher.

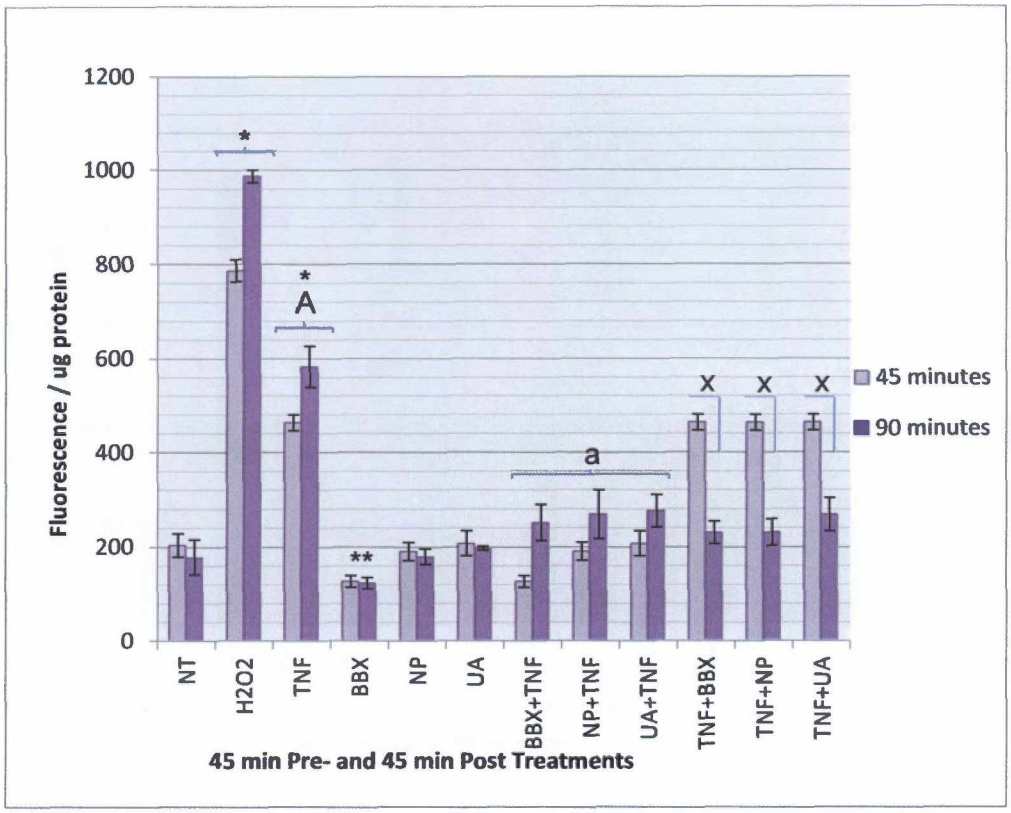

Fig A.3 Immediate ROS Generation in Spinal Neurons

ROS is reported as a measure of fluorescent output at 535 nm per microgram of protein sampled taken at 45 minutes (after pretreatments) and at 90 minutes (after pre- and post-treatments are complete). Spinal cultures were held for 45 minutes under different conditions. Columns 1-6 had the same pre- and post-treatments and the remaining columns were pretreated with 5ug/ml BBX, 5ug/ml NP, 5ug/ml UA, 200ng/ml TNFα (10-12). Pretreatments were rinsed and post-treatments were added for another 45 minutes: no treatment (NT), 1mM H_2O_2, 200ng/ml TNFα, 5ug/ml BBX, 5ug/ml NP, 5ug/ml UA, 200ng/ml TNFα (7-9), 5ug/ml BBX, 5ug/ml NP, and 5ug/ml UA. Values are reported as $P< 0.05$ where "a" indicates decreased ROS generation compared to "A". ROS was decreased at 90 minutes (x) by BBX, NP, and UA compared to 45 minutes. BBX** is significantly lower than NT while (*) is higher.

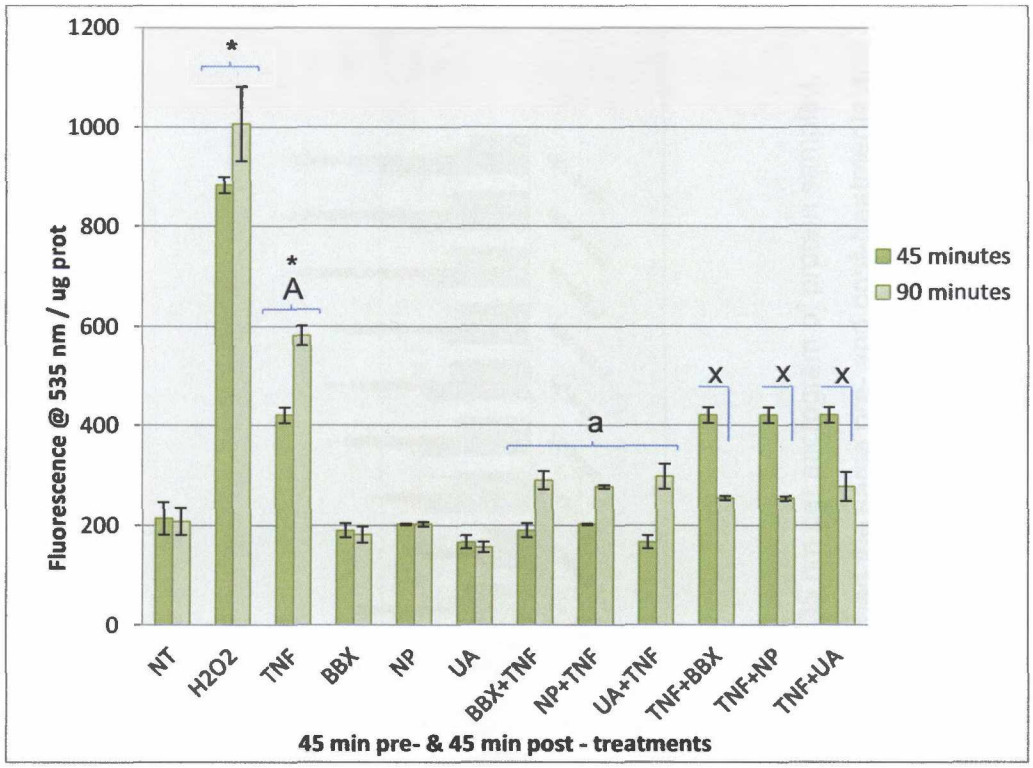

Fig A.4 Immediate ROS Generation in DRG Neurons

ROS is reported as a measure of fluorescent output at 535 nm per microgram of protein sampled taken at 45 minutes (after pretreatments) and at 90 minutes (after pre- and post-treatments are complete). DRG neuronal cultures were held for 45 minutes under different conditions. Columns 1-6 had the same pre- and post-treatments and the remaining lanes were pretreated with 5ug/ml BBX, 5ug/ml NP, 5ug/ml UA, 200ng/ml TNFα (10-12). Pretreatments were rinsed and post-treatments were added for another 45 minutes: no treatment (NT), 1mM H_2O_2, 200ng/ml TNFα, 5ug/ml BBX, 5ug/ml NP, 5ug/ml UA, 200ng/ml TNFα (7-9), 5ug/ml BBX, 5ug/ml NP, and 5ug/ml UA. Values are reported as $P< 0.05$ where "a" indicates decreased ROS generation compared to "A". ROS was decreased at 90 minutes (x) by BBX, NP, and UA compared to 45 minutes. Treatments identified with (*) increased ROS compared to NT.

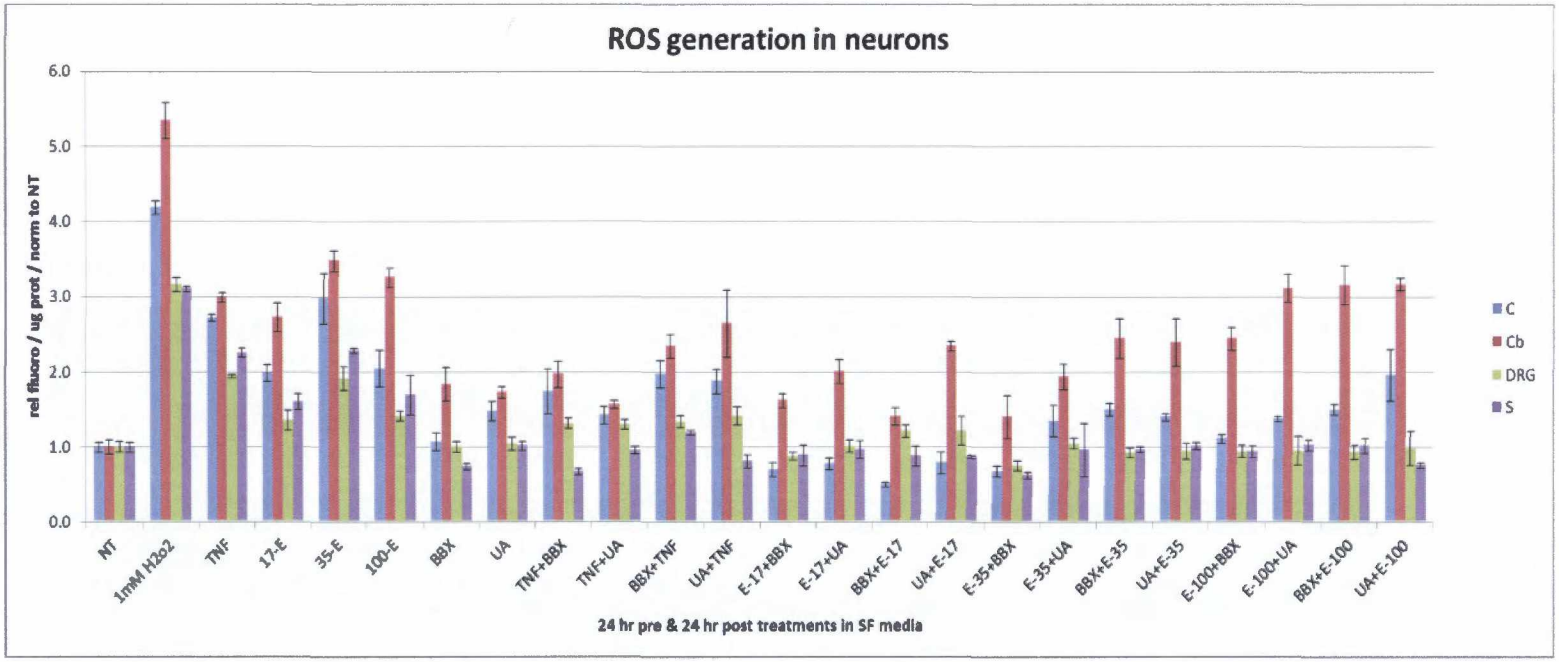

Fig A.5 Comparative ROS Response of Neurons

ROS is reported at 48 hours as a measure of fluorescent output at 535 nm per microgram of protein sampled. Results were normalized to the negative control (NT). Columns 1-8 had the same pre- and post-treatments and were held in serum free media while the remaining columns were pretreated as indicated by the first treatment listed in each column. Pretreatments were rinsed after 24 hours and post-treatments were added for an additional 24 hours. Results for different neurons are presented as C-cortical forebrain (blue), Cb-cerebellum (red), DRG (green), S-spine (purple).

Appendix B

Additional Statistical Data

Table B.1: Corresponds to Fig 5.4

C (n= 6)	NT	H202	TNF	BBX	NP	UA	BBX+TNF	NP+TNF	UA+TNF	TNF+BBX	TNF+NP	TNF+UA
AVG (normalized)	1.0000	0.4204	0.7593	2.3390	2.1499	2.2511	2.1114	1.8825	1.5730	1.5103	1.3855	1.5063
SD (+/-)	0.1646	0.0125	0.0246	0.7073	0.6122	0.6553	0.5929	0.6521	0.2068	0.4043	0.3118	0.2019
Cb (n=5)	**NT**	**H202**	**TNF**	**BBX**	**NP**	**UA**	**BBX+TNF**	**NP+TNF**	**UA+TNF**	**TNF+BBX**	**TNF+NP**	**TNF+UA**
AVG (normalized)	1.0000	0.4232	0.7395	1.9415	1.8164	1.9754	1.6966	1.6487	1.9461	1.8377	1.7718	1.6607
SD (+/-)	0.0085	0.0028	0.0720	0.0497	0.1530	0.3399	0.1095	0.0502	0.2392	0.1427	0.2501	0.1239
DRG (n=4)	**NT**	**H202**	**TNF**	**BBX**	**NP**	**UA**	**BBX+TNF**	**NP+TNF**	**UA+TNF**	**TNF+BBX**	**TNF+NP**	**TNF+UA**
AVG (normalized)	1.0000	0.4863	0.5577	1.0444	1.5842	1.3772	1.2827	1.3959	1.2842	1.4076	1.2350	1.4076
SD (+/-)	0.0266	0.0182	0.1790	0.4683	0.0492	0.2077	0.0182	0.0563	0.2086	0.0286	0.0294	0.0403
S (n=4)	**NT**	**H202**	**TNF**	**BBX**	**NP**	**UA**	**BBX+TNF**	**NP+TNF**	**UA+TNF**	**TNF+BBX**	**TNF+NP**	**TNF+UA**
AVG (normalized)	1.0000	0.4244	0.7797	2.1358	2.4418	2.6117	1.8521	2.2446	1.7954	2.1384	1.9246	1.9570
SD (+/-)	0.3270	0.0351	0.0040	0.4850	0.1757	0.1534	0.1497	0.3818	0.2998	0.1767	0.1002	0.1903
OB (n=3)	**NT**	**H202**	**TNF**	**BBX**	**NP**	**UA**	**BBX+TNF**	**NP+TNF**	**UA+TNF**	**TNF+BBX**	**TNF+NP**	**TNF+UA**
AVG (normalized)	1.0000	0.0861	0.3859	2.2584	0.9983	2.6147	1.5280	1.7131	1.4435	1.4049	1.5291	1.5324
SD (+/-)	0.0000	0.0000	0.0000	0.1848	0.0419	0.2709	0.2227	0.4935	0.2693	0.3585	0.0695	0.3522

Table B.2: Corresponds to Fig 5.5

CB (n=4)	NT	1M H2O2	1mM H2O2	TNF	E17	E35	E100	E200	NP	NP+E200	E200+NP	NP+H202	H2O2+NP
AVG (norm)	1.000	0.134	0.699	0.719	1.382	1.167	0.923	0.468	1.375	1.078	0.986	1.085	1.158
SD (+/-)	0.007	0.008	0.032	0.039	0.001	0.003	0.030	0.068	0.023	0.159	0.027	0.005	0.006
DRG (n=4)	NT	1M H2O2	1mM H2O2	TNF	E17	E35	E100	E200	NP	NP+E200	E200+NP	NP+H202	H2O2+NP
AVG (norm)	1.000	0.212	0.711	0.701	1.730	1.536	1.198	0.506	1.494	1.419	1.413	1.300	1.443
SD (+/-)	0.018	0.040	0.045	0.059	0.028	0.025	0.026	0.062	0.021	0.056	0.062	0.021	0.018
GLIA (n=4)	NT	1M H2O2	1mM H2O2	TNF	E17	E35	E100	E200	NP	NP+E200	E200+NP	NP+H202	H2O2+NP
AVG (norm)	1.000	0.297	1.230	2.064	2.826	2.921	2.541	0.855	2.824	2.804	2.876	2.155	2.667
SD (+/-)	0.219	0.062	0.253	0.124	0.065	0.113	0.449	0.082	0.059	0.106	0.373	0.282	0.074

Table B.3: Corresponds to Fig 5.6

NF (n=6)	NT	H2O2	TNF	E35	BBX	UA	TNF+BBX	TNF+UA	BBX+TNF	E35+BBX	E35+UA	BBX+E35
AVG (norm)	1.0000	0.6766	0.8479	0.8434	1.2985	1.3518	1.2809	1.2933	1.3940	1.1903	1.2936	1.3602
SD (+/-)	0.0520	0.0482	0.0567	0.0511	0.0486	0.0992	0.1197	0.1737	0.1637	0.0999	0.2352	0.0180
CAL (n=6)	**NT**	**H2O2**	**TNF**	**E35**	**BBX**	**UA**	**TNF+BBX**	**TNF+UA**	**BBX+TNF**	**E35+BBX**	**E35+UA**	**BBX+E35**
AVG (norm)	1.0000	0.6130	0.8124	0.8181	1.1471	1.1731	1.0192	1.0380	1.0388	1.0503	1.0109	1.0342
SD (+/-)	0.0611	0.1202	0.0976	0.1119	0.0444	0.0525	0.0436	0.0760	0.0500	0.0867	0.0670	0.0507
Hoechst (n=6)	**NT**	**H2O2**	**TNF**	**E35**	**BBX**	**UA**	**TNF+BBX**	**TNF+UA**	**BBX+TNF**	**E35+BBX**	**E35+UA**	**BBX+E35**
AVG (norm)	1.0000	0.6254	0.7711	0.8133	1.0000	0.9814	0.9770	0.8275	0.8809	0.8730	0.9208	1.0222
SD (+/-)	0.0300	0.0473	0.1155	0.0768	0.0741	0.0789	0.0953	0.1184	0.2071	0.0386	0.1738	0.1325

Table B.4: Corresponds to Fig 5.7

NF (n=6)	0	17.4	35	50	100	200	400
AVG (norm)	1.0000	0.9117	0.8197	0.7584	0.6080	0.3190	0.0991
SD (+/-)	0.0140	0.0455	0.0842	0.0728	0.0362	0.0432	0.0130
CAL (n=6)	0	17.4	35	50	100	200	400
AVG (norm)	1.0000	0.9741	0.9298	0.8623	0.7891	0.5725	0.2749
SD (+/-)	0.0140	0.0598	0.0366	0.0554	0.0609	0.0392	0.1095
Hoechst (n=6)	0	17.4	35	50	100	200	400
AVG (norm)	1.0000	0.9731	0.9638	0.9307	0.8646	0.8280	0.6616
SD (+/-)	0.0096	0.0360	0.1125	0.0784	0.0752	0.0548	0.0574

Table B.5: Corresponds to Fig 5.8

GFAP (n=4)	NT	H2O2	TNF	E35	BBX	UA	TNF+BBX	TNF+UA	BBX+TNF	E35+BBX	E35+UA	BBX+E35
AVG (norm)	1.0000	0.7584	0.9953	0.8515	1.2597	1.1188	1.1337	1.1960	1.2117	1.1935	0.9799	1.1916
SD (+/-)	0.0596	0.1194	0.0447	0.0984	0.1668	0.1337	0.1319	0.0514	0.0452	0.0216	0.0908	0.1129
Hoechst (n=4)	NT	H2O2	TNF	E35	BBX	UA	TNF+BBX	TNF+UA	BBX+TNF	E35+BBX	E35+UA	BBX+E35
AVG (norm)	1.0000	0.7629	0.9501	0.8537	1.0121	1.0246	0.9233	0.9236	0.9610	1.0134	1.0153	0.9684
SD (+/-)	0.0364	0.0486	0.0454	0.0551	0.0685	0.0478	0.0495	0.0555	0.0357	0.0625	0.0606	0.0643

Table B.6: Corresponds to Fig 5.9

GFAP (n=6)	0E	17.4E	35E	50E	100E	200E	400E
AVG (norm)	1.0000	0.9683	1.0795	0.9968	0.9703	0.8684	0.7856
SD (+/-)	0.0978	0.0429	0.0617	0.0244	0.0650	0.0660	0.1356
Hoechst (n=6)	0E	17.4E	35E	50E	100E	200E	400E
AVG (norm)	1.0000	0.9902	0.9996	0.9976	1.0060	0.9140	0.8809
SD (+/-)	0.0162	0.0388	0.0256	0.0451	0.0155	0.0471	0.0088

Table B.7: Corresponds to Fig 5.10

C (n=6)	NT	H2O2	TNF
AVG	1338	2903	1869
SD (+/-)	106	280	184
Cb (n=6)	NT	H2O2	TNF
AVG	3091	7621	4582
SD (+/-)	123	151	280
Spinal (n=6)	NT	H2O2	TNF
AVG	204	787	464
SD (+/-)	25	23	17
DRG (n=6)	NT	H2O2	TNF
AVG	208	1006	394
SD (+/-)	27	76	23

Table B.8: Corresponds to Fig 5.11

C (n=5)	NT	1mM H2o2	TNF	17-E	35-E	100-E
AVG (norm)	1.000	4.182	2.716	1.980	2.975	2.043
SD (+/-)	0.063	0.087	0.048	0.106	0.337	0.243
Cb (n=5)	NT	1mM H2o2	TNF	17-E	35-E	100-E
AVG (norm)	1.000	5.341	2.989	2.724	3.471	3.250
SD (+/-)	0.091	0.233	0.066	0.191	0.138	0.127
DRG (n=5)	NT	1mM H2o2	TNF	17-E	35-E	100-E
AVG (norm)	1.000	3.160	1.942	1.355	1.909	1.410
SD (+/-)	0.070	0.093	0.024	0.131	0.158	0.062
S (n=5)	NT	1mM H2o2	TNF	17-E	35-E	100-E
AVG (norm)	1.000	3.100	2.253	1.603	2.287	1.690
SD (+/-)	0.063	0.033	0.055	0.105	0.029	0.262

Table B.9: Corresponds to Fig 5.12

Cb -45 min	NT	H2O2	TNF	BBX	NP	UA	BBX+TNF	NP+TNF	UA+TNF	TNF+BBX	TNF+NP	TNF+UA
AVG	3090.8	7620.8	4582.4	2305.0	3104.1	3734.8	2479.2	3445.1	3734.8	4582.4	4582.4	4582.4
SD (+/-)	123.0	151.2	279.5	99.2	278.1	136.1	91.4	193.1	136.1	279.5	279.5	279.5
Cb-90 min	**NT**	**H2O2**	**TNF**	**BBX**	**NP**	**UA**	**BBX+TNF**	**NP+TNF**	**UA+TNF**	**TNF+BBX**	**TNF+NP**	**TNF+UA**
AVG	3050.0	10811.1	6360.9	2110.6	2729.7	4194.4	3676.8	4091.7	3802.1	3191.5	3162.4	3287.9
SD (+/-)	101.4	517.7	313.3	238.3	124.6	607.0	234.6	493.9	449.3	230.9	154.0	234.8

Table B.10: Corresponds to Fig 5.13

Cb (n=4)	0E	17.4E	35E	50E	100E	200E	400E
AVG (norm)	1.000	3.08285555	4.018	4.098	3.107	2.799	2.704
SD (+/-)	0.178	0.11465568	0.285	0.082	0.043	0.184	0.224
G (n=4)	**0E**	**17.4E**	**35E**	**50E**	**100E**	**200E**	**400E**
AVG (norm)	1	2.77625637	3.405	3.876	4.386	4.516	4.065
SD (+/-)	0.13413216	0.30674905	0.128	0.298	0.188	0.213	0.357

Table B.11: Corresponds to Fig 5.14

Cb (n=6)	NT	H2O2	TNF	17-E	35-E	100-E	NP	TNF+NP	NP+TNF	E-17+NP	E-35+NP	E-100+NP
AVG (norm)	1.0000	2.8582	1.7807	2.0105	2.5643	1.9181	0.4422	1.2533	1.0719	0.8724	1.0378	1.2202
SD (+/-)	0.0621	0.1934	0.0738	0.1102	0.2812	0.1003	0.0141	0.1722	0.1603	0.1710	0.1804	0.1540
DRG (n=6)	NT	H2O2	TNF	17-E	35-E	100-E	NP	TNF+NP	NP+TNF	E-17+NP	E-35+NP	E-100+NP
AVG (norm)	1.0000	2.7990	2.0681	1.2822	1.5697	1.5415	0.5127	1.4089	1.2546	0.8087	1.0356	1.4009
SD (+/-)	0.1148	0.0583	0.1984	0.2092	0.2162	0.1364	0.0184	0.1598	0.1646	0.1531	0.0922	0.0355
Glial (n=6)	NT	H2O2	TNF	17-E	35-E	100-E	NP	TNF+NP	NP+TNF	E-17+NP	E-35+NP	E-100+NP
AVG (norm)	1.0000	2.1503	1.4783	1.5687	1.7473	1.9218	0.6382	1.0694	1.1057	0.7546	0.8287	1.2402
SD (+/-)	0.0233	0.1125	0.0766	0.0504	0.1875	0.1571	0.1257	0.0264	0.1250	0.0998	0.0548	0.0990

Table B.12: Corresponds to Fig 5.15

Berry fractions (n=3)	BLK	BBX	NP	P	UA
AVG (uM Trolox equiv)	0.0000	1195.3125	726.5625	695.3125	31.2500
SD (+/-)	0.0001	117.6942	69.5648	71.0025	1.9982

Table B.13: Corresponds to Fig 5.16

Cell type (n=3)	C	Cb	S	OB	DRG	G
AVG (uM Trolox equiv)	2.3392	2.3403	2.3393	2.3167	2.3400	2.3565
SD (+/-)	0.0012	0.0023	0.0021	0.0000	0.0006	0.0001

Table B.14: Corresponds to Fig 5.17

Treatment (n=3)	BLK	BBX	NP	P	UA	E35
AVG (uM Trolox equiv)	1.0000	6.6784	4.4516	4.3031	1.1485	2.1134
SD (+/-)	0.0992	0.5850	0.4242	0.4409	0.0740	0.1999

Table B.15: Corresponds to Fig 5.18

Cb (n=3)	NT	TNF	E17	E35	E100	BBX	NP	UA	TNF+BBX	TNF+NP	E35+BBX	E35+NP	E35+UA
AVG	2.3403	4.4935	5.3772	5.6717	0.8605	7.5373	8.0283	11.4649	7.4391	6.0645	6.2609	8.6174	7.0464
SD (+/-)	0.0003	0.7423	0.6098	0.2121	0.5567	0.4507	0.4242	1.9353	0.1060	0.7423	0.1060	0.5302	0.1591
G (n=3)	NT	TNF	E17	E35	E100	BBX	NP	UA	TNF+BBX	TNF+NP	E35+BBX	E35+NP	E35+UA
AVG	2.3565	4.9108	7.4883	7.2901	7.0257	10.0659	9.8676	9.4050	5.9022	4.6465	6.9596	8.2153	8.6119
SD (+/-)	0.0000	0.1606	0.3569	0.0892	0.0178	0.2320	0.0000	0.0535	0.2141	1.0171	0.2855	0.6959	0.0892

Table B.16: Corresponds to Fig 5.19

Cb (n=4)	NT	H2O2	TNF	E35	BBX	NP	UA	TNF+BBX	TNF+NP	TNF+UA	E35+BBX	E35+NP	E35+UA
AVG	0.8059	1.4346	1.1393	1.8924	0.2026	0.3587	0.0971	0.1688	0.1266	0.1688	0.1561	0.1013	0.5612
SD (+/-)	0.1088	0.0459	0.0382	0.1168	0.0333	0.1005	0.1018	0.0929	0.0795	0.0419	0.1912	0.1044	0.0801

Table B.17: Corresponds to Fig 5.20

Cb (n=3)	NT	MBCD	E35	MBCD+E35
AVG	0.8059	-0.0500	1.8924	-0.0422
SD (+/-)	0.1088	0.0038	0.1907	0.001401

Table B.18: Corresponds to Fig 5.21

Cb (n=3)	0E	17.4E	35E	50E	100E	200E	400E
AVG	0.0000	1.6519	1.8924	1.6836	1.3861	1.2696	1.3285
SD (+/-)	0.0004	0.0850	0.0650	0.0700	0.0225	0.0130	0.0195

Table B.19: Corresponds to Fig 5.22

G (n=3)	NT	1M H2O2	E-35	BBX	UA	E-35+ BBX	E-35+UA
AVG	37.4601	69.7921	52.0563	27.7768	27.9714	33.5254	32.5937
SD (+/-)	1.4867	2.1229	2.7926	0.8673	2.1363	2.5005	1.3092
Cb (n=3)	NT	1M H2O2	E-35	BBX	UA	E-35+ BBX	E-35+UA
AVG	17.2763	38.6469	29.9956	13.0754	11.4381	18.7361	18.2926
SD (+/-)	1.2070	0.6470	1.0319	0.6855	1.0289	0.6541	1.3512

Table B.20: Corresponds to Fig 5.23

G (n=3)	NT	1M H2O2	E-35	BBX	UA	E-35+ BBX	E-35+UA
AVG	4.2377	4.3381	4.2577	4.2236	4.2248	4.2185	4.2209
SD (+/-)	0.0221	0.0019	0.0221	0.0211	0.0222	0.0380	0.0231
Cb (n=3)	NT	1M H2O2	E-35	BBX	UA	E35+BBX	E35+UA
AVG	4.1809	4.2921	4.2411	4.1893	4.1897	4.1802	4.1864
SD (+/-)	0.0013	0.0302	0.0325	0.0228	0.0390	0.0223	0.0082

Table B.21: Corresponds to Fig 5.24

G (n=3)	E-0	E-17.4	E-35	E-50	E-100	E-200	E-400
AVG	4.2377	4.2569	4.2577	4.2768	4.2807	4.2966	4.3719
SD (+/-)	0.0682	0.0921	0.1235	0.4023	0.4294	0.1547	0.3965

Table B.22: Corresponds to Fig 5.25

Cb (n=3)	NT	MBCD	E35	MBCD + E35
AVG	15.9043	11.5425	28.9291	12.2669
SD (+/-)	1.1322	1.0346	1.2055	1.0075

Table B.23: Corresponds to Fig 5.27

Cb (n=8)	NT	MBCD	H2O2	TNF	E35	BBX	UA	BBX+TNF	BBX+E35	TNF+BBX	E35+BBX	UA+TNF	UA+E35	TNF+UA	E35+UA
AVG	1.0000	0.5321	1.5179	1.5380	1.3834	0.4590	0.4858	0.4127	0.3493	0.5095	0.4328	0.3852	0.3997	0.3613	0.4557
SD (+/-)	0.1090	0.0701	0.3186	0.2377	0.1395	0.0795	0.1019	0.0873	0.0408	0.0922	0.0652	0.0501	0.0423	0.0554	0.0687

Table B.24: Corresponds to Fig 5.28

G (n=8)	E0	E17.4	E35	E50	E100	E200	E400
AVG (norm)	1.0000	1.6802	1.9752	1.0790	0.9054	1.1206	0.6985
SD (+/-)	0.1674	0.2881	0.1740	0.1283	0.0929	0.1528	0.0734
Cb (n=6)	**E0**	**E17**	**E35**	**E50**	**E100**	**E200**	**E400**
AVG (norm)	1.0000	1.4250	1.3834	1.3370	1.3183	1.2374	1.4554
SD (+/-)	0.1090	0.1208	0.1395	0.1345	0.1441	0.0815	0.1579

Table B.25: Corresponds to Fig 5.30

Cb (n=6)	NT	MBCD	H202	TNF	E35	BBX	UA	TNF+ BBX	TNF+ UA	UA+ TNF	E35+ BBX	E35+ UA	BBX+ E35	MBCD+ TNF	MBCD+ E35
AVG (norm)	1.0000	0.6883	2.0861	1.6252	1.6345	0.8453	0.8675	1.0148	1.1734	1.1782	0.9263	1.1032	1.1714	0.8157	0.7168
SD (+/-)	0.1217	0.1357	0.1142	0.1055	0.2409	0.1798	0.1194	0.1383	0.2389	0.0948	0.1014	0.0972	0.1758	0.0871	0.0478

Table B.26: Corresponds to Fig 5.33

LR (n=6)	0E	17.4E	35E	50E	100E	200E	400E
AVG (norm)	1.0000	1.1747	1.2388	1.1680	0.8875	0.8365	0.8324
SD (+/-)	0.1217	0.1260	0.0897	0.0764	0.0886	0.0926	0.0900
Nav (n=6)	**0E**	**17.4E**	**35E**	**50E**	**100E**	**200E**	**400E**
AVG (norm)	1.0000	1.0480	1.8150	1.6505	1.1575	1.0647	0.6426
SD (+/-)	0.1722	0.1256	0.1905	0.1181	0.2322	0.2232	0.1454
ROS (n=4)	**0E**	**17.4E**	**35E**	**50E**	**100E**	**200E**	**400E**
AVG (norm)	1.0000	3.0829	4.0183	4.0981	3.1067	2.7993	2.7039
SD (+/-)	0.1782	0.1147	0.2847	0.0821	0.0430	0.1838	0.2245

Table B.27: Corresponds to 5.34

LR (n=4)	NT	MBCD	H202	TNF	E35	BBX	UA	TNF+ BBX	TNF+ UA	UA+ TNF	E35+ BBX	E35+ UA	BBX+ E35
AVG (norm)	1.0000	0.7483	2.4084	1.7315	1.8891	0.8737	0.6821	1.0635	1.1619	1.2476	1.0392	1.2115	1.3153
SD (+/-)	0.1856	0.1272	0.1180	0.1273	0.1906	0.1905	0.3406	0.1780	0.1707	0.1213	0.1864	0.1493	0.1323
Nav (n=6)	**NT**	**MBCD**	**H202**	**TNF**	**E35**	**BBX**	**UA**	**TNF+ BBX**	**TNF+ UA**	**UA+ TNF**	**E35+ BBX**	**E35+ UA**	**BBX+ E35**
AVG (norm)	1.0000	0.2586	2.0630	1.5934	1.4279	0.4617	0.5252	0.9076	1.0467	0.8239	0.7286	0.7315	0.8735
SD (+/-)	0.0995	0.0464	0.1243	0.2052	0.1574	0.0959	0.0763	0.1464	0.1654	0.1204	0.1169	0.0694	0.2495

Table B.28: Corresponds to Fig 5.35

Whole (n=6)	NT	MBCD	H202	TNF	E35	BBX	UA	TNF+ BBX	TNF+ UA	UA+ TNF	E35+ BBX	E35+ UA	BBX+ E35
AVG (norm)	1.0000	0.6883	2.0861	1.6252	1.6345	0.8453	0.8675	1.0148	1.1734	1.1782	0.9263	1.1032	1.1714
SD (+/-)	0.1217	0.1357	0.1142	0.1055	0.2409	0.1798	0.1194	0.1383	0.2389	0.0948	0.1014	0.0972	0.1758
Membrane (n=6)	**NT**	**MBCD**	**H202**	**TNF**	**E35**	**BBX**	**UA**	**TNF+ BBX**	**TNF+ UA**	**UA+ TNF**	**E35+ BBX**	**E35+ UA**	**BBX+ E35**
AVG (norm)	0.8026	0.6006	1.9331	1.3898	1.5163	0.7013	0.5475	0.8536	0.9326	1.0013	0.8341	0.9724	1.0557
SD (+/-)	0.1856	0.1272	0.1180	0.1273	0.1906	0.1905	0.3406	0.1780	0.1707	0.1213	0.1864	0.1493	0.1323
Cytosol (n=6)	**NT**	**MBCD**	**H202**	**TNF**	**E35**	**BBX**	**UA**	**TNF+ BBX**	**TNF+ UA**	**UA+ TNF**	**E35+ BBX**	**E35+ UA**	**BBX+ E35**
AVG (norm)	0.0691	0.0046	0.0162	0.0066	0.0105	0.0064	0.0064	0.0076	0.0094	0.0125	0.0064	0.0111	0.0097
SD (+/-)	0.5310	0.5301	0.4061	0.4287	0.3460	0.6813	0.6039	0.5076	0.4797	0.1680	0.6749	0.3975	0.1929

Table B.29: Corresponds to Fig 5.36

Membrane (n=3)	NT	MBCD	H202	TNF	E35	BBX	UA	TNF+ BBX	TNF+ UA	UA+ TNF	E35+ BBX	E35+ UA	BBX+ E35
AVG	0.0100	0.0027	0.0204	0.0155	0.0135	0.0046	0.0045	0.0091	0.0094	0.0082	0.0063	0.0063	0.0081
SD (+/-)	0.0010	0.0015	0.0006	0.0012	0.0009	0.0010	0.0009	0.0014	0.0017	0.0010	0.0012	0.0007	0.0020
Cytosol (n=3)	**NT**	**MBCD**	**H202**	**TNF**	**E35**	**BBX**	**UA**	**TNF+ BBX**	**TNF+ UA**	**UA+ TNF**	**E35+ BBX**	**E35+ UA**	**BBX+ E35**
AVG	0.0016	0.0027	0.0011	0.0012	0.0006	0.0040	0.0032	0.0009	0.0013	0.0022	0.0015	0.0017	0.0025
SD (+/-)	0.0006	0.0005	0.0003	0.0005	0.0008	0.0007	0.0007	0.0001	0.0005	0.0002	0.0002	0.0001	0.0010

Table B.30: Corresponds to Fig 5.37

Whole (n=6)	NT	MBCD	H202	TNF	E35	BBX	UA	TNF+ BBX	TNF+ UA	UA+ TNF	E35+ BBX	E35+ UA	BBX+ E35
AVG	1.0000	0.4549	1.8819	1.4860	1.2851	0.7415	0.7329	0.8606	1.0190	0.9010	0.7596	0.7786	0.9679
SD (+/-)	0.1722	0.2256	0.2413	0.1867	0.1879	0.0421	0.1179	0.0962	0.2441	0.0404	0.0334	0.0298	0.0879

Table B.31: Corresponds to Fig A.1

SH 45-min (n=5)	NT	H202	TNF	BBX	NP	UA	BBX+ TNF	NP+ TNF	UA+ TNF	TNF+ BBX	TNF+ NP	TNF+ UA
AVG	276.88	1212.21	493.07	277.57	316.53	310.25	277.57	316.53	310.25	493.07	493.07	493.07
SD (+/-)	82.76	163.75	8.55	36.24	16.89	17.84	36.24	16.89	17.84	8.55	8.55	8.55
90-min (n=5)	NT	H202	TNF	BBX	NP	UA	BBX+ TNF	NP+ TNF	UA+ TNF	TNF+ BBX	TNF+ NP	TNF+ UA
AVG	209.11	1099.10	457.28	236.12	303.00	296.51	170.57	199.19	214.46	151.38	162.15	105.86
SD (+/-)	5.94	96.18	18.54	31.07	52.38	15.75	6.38	17.32	12.68	6.37	12.29	3.56

Table B.32: Corresponds to Fig A.2

C 45 min (n=6)	NT	H2O2	TNF	BBX	NP	UA	BBX+ TNF	NP+ TNF	UA+ TNF	TNF+ BBX	TNF+ NP	TNF+ UA
AVG	1338.08	2902.58	1869.45	729.02	1140.18	1190.33	838.77	1096.28	1172.77	1869.45	1869.45	1869.45
SD (+/-)	105.86	279.98	183.70	52.91	64.18	65.81	173.91	83.34	68.30	183.70	183.70	183.70
C 90 min (n=6)	NT	H2O2	TNF	BBX	NP	UA	BBX+ TNF	NP+ TNF	UA+ TNF	TNF+ BBX	TNF+ NP	TNF+ UA
AVG	1305.04	3965.67	2434.11	777.80	1072.74	1147.59	1441.33	1427.46	1550.98	1356.76	1244.96	1350.31
SD (+/-)	109.07	179.56	135.11	75.34	81.55	66.83	99.65	97.05	69.57	102.22	64.89	87.52

Table B.33: Corresponds to Fig A.3

S 45-min (n=6)	NT	H2O2	TNF	BBX	NP	UA	BBX+ TNF	NP+ TNF	UA+ TNF	TNF+ BBX	TNF+ NP	TNF+ UA
AVG	204.31	787.12	463.68	126.64	190.68	207.73	126.64	190.68	207.73	463.68	463.68	463.68
SD (+/-)	24.74	23.44	16.69	12.47	19.52	26.65	12.47	19.52	26.65	16.69	16.69	16.69
S 90-min (n=6)	NT	H2O2	TNF	BBX	NP	UA	BBX+ TNF	NP+ TNF	UA+ TNF	TNF+ BBX	TNF+ NP	TNF+ UA
AVG	178.38	986.44	582.40	122.98	179.34	197.71	251.86	268.73	276.64	230.85	230.96	268.14
SD (+/-)	37.21	13.17	44.17	11.93	16.80	4.32	37.64	51.42	33.88	23.12	27.85	34.65

Table B.34: Corresponds to Fig A.4

DRG 45-min (n=6)	NT	H2O2	TNF	BBX	NP	UA	BBX+ TNF	NP+ TNF	UA+ TNF	TNF+ BBX	TNF+ NP	TNF+ UA
AVG	213.71	882.70	420.57	190.16	201.99	166.92	190.16	201.99	166.92	420.57	420.57	420.57
SD (+/-)	31.96	15.94	15.71	13.97	1.76	13.34	13.97	1.76	13.34	15.71	15.71	15.71
DRG 90-min (n=6)	NT	H2O2	TNF	BBX	NP	UA	BBX+ TNF	NP+ TNF	UA+ TNF	TNF+ BBX	TNF+ NP	TNF+ UA
AVG	207.55	1006.32	582.11	181.59	202.12	156.94	290.12	276.66	297.75	253.86	253.20	276.80
SD (+/-)	26.70	75.64	19.79	16.25	4.41	10.59	18.16	3.35	25.27	3.93	4.34	29.38

Table B.35: Corresponds to Fig A.5

C (n=5)	NT	H2O2	TNF	17-E	35-E	100-E	BBX	UA	TNF+BBX	TNF+UA	BBX+TNF	UA+TNF
AVG (norm)	1.0000	4.1816	2.7157	1.9803	2.9749	2.0433	1.0687	1.4742	1.7335	1.4216	1.9723	1.8753
SD (+/-)	0.0633	0.0870	0.0477	0.1058	0.3373	0.2432	0.1156	0.1279	0.2945	0.1164	0.1805	0.1614
Cb (n=5)	**NT**	**H2O2**	**TNF**	**17-E**	**35-E**	**100-E**	**BBX**	**UA**	**TNF+BBX**	**TNF+UA**	**BBX+TNF**	**UA+TNF**
AVG (norm)	1.0000	5.3410	2.9892	2.7245	3.4715	3.2499	1.8343	1.7240	1.9654	1.5658	2.3423	2.6424
SD (+/-)	0.0912	0.2327	0.0659	0.1913	0.1380	0.1266	0.2191	0.0742	0.1741	0.0543	0.1578	0.4484
DRG (n=5)	**NT**	**H2O2**	**TNF**	**17-E**	**35-E**	**100-E**	**BBX**	**UA**	**TNF+BBX**	**TNF+UA**	**BBX+TNF**	**UA+TNF**
AVG (norm)	1.0000	3.1599	1.9420	1.3546	1.9093	1.4095	1.0057	1.0445	1.3130	1.2922	1.3345	1.4137
SD (+/-)	0.0702	0.0932	0.0239	0.1310	0.1582	0.0624	0.0703	0.0846	0.0701	0.0633	0.0833	0.1185
S (n=5)	**NT**	**H2O2**	**TNF**	**17-E**	**35-E**	**100-E**	**BBX**	**UA**	**TNF+BBX**	**TNF+UA**	**BBX+TNF**	**UA+TNF**
AVG (norm)	1.0000	3.0999	2.2527	1.6033	2.2870	1.6900	0.7405	1.0145	0.6732	0.9534	1.1921	0.8094
SD (+/-)	0.0633	0.0335	0.0548	0.1045	0.0290	0.2621	0.0446	0.0547	0.0375	0.0478	0.0270	0.0833

C (n=5)	E-17+ BBX	E-17+ UA	BBX+ E-17	UA+E-17	E-35+ BBX	E-35+ UA	BBX+ E-35	UA+ E-35	E-100+ BBX	E-100+ UA	BBX+ E-100	UA+ E-100
AVG (norm)	0.7001	0.7767	0.5011	0.7921	0.6755	1.3465	1.4976	1.3973	1.1076	1.3731	1.4988	1.9583
SD (+/-)	0.0976	0.0721	0.0310	0.1455	0.0720	0.2072	0.0777	0.0467	0.0599	0.0353	0.0684	0.3438
Cb (n=5)	**E-17+ BBX**	**E-17+ UA**	**BBX+ E-17**	**UA+E-17**	**E-35+ BBX**	**E-35+ UA**	**BBX+ E-35**	**UA+ E-35**	**E-100+ BBX**	**E-100+ UA**	**BBX+ E-100**	**UA+ E-100**
AVG (norm)	1.6206	2.0063	1.4044	2.3412	1.4007	1.9362	2.4426	2.3893	2.4386	3.1090	3.1558	3.1640
SD (+/-)	0.0923	0.1543	0.1173	0.0621	0.2847	0.1675	0.2600	0.3121	0.1510	0.1864	0.2583	0.0803
DRG (n=5)	**E-17+ BBX**	**E-17+ UA**	**BBX+ E-17**	**UA+ E-17**	**E-35+ BBX**	**E-35+ UA**	**BBX+ E-35**	**UA+ E-35**	**E-100+ BBX**	**E-100+ A**	**BBX+ E-100**	**UA+ E-100**
AVG (norm)	0.8778	1.0106	1.2123	1.2181	0.7507	1.0471	0.9241	0.9441	0.9432	0.9464	0.9340	0.9853
SD (+/-)	0.0505	0.0838	0.0794	0.1943	0.0600	0.0674	0.0638	0.1032	0.0828	0.1921	0.0928	0.2292
S (n=5)	**E-17+ BBX**	**E-17+ UA**	**BBX+ E-17**	**UA+ E-17**	**E-35+ BBX**	**E-35+ UA**	**BBX+ E-35**	**UA+ E-35**	**E-100+ BBX**	**E-100+ UA**	**BBX+ E-100**	**UA+ E-100**
AVG (norm)	0.8868	0.9618	0.8801	0.8691	0.6239	0.9661	0.9654	1.0098	0.9400	1.0279	1.0181	0.7590
SD (+/-)	0.1403	0.1167	0.1296	0.0175	0.0415	0.3537	0.0306	0.0454	0.0756	0.0675	0.0940	0.0365